METAL COATING OF OPTICAL FIBRES

PETER G. HALE

CHRIST CHURCH

A Thesis submitted for the degree of Doctor of Philosophy

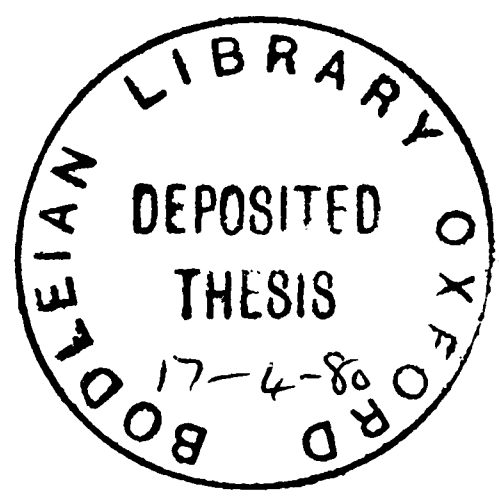
at the University of Oxford

Michaelmas Term 1979

Department of Engineering Science,

Parks Road,

Oxford



'"That's how it is", said Pooh'

A. A. Milne, 'When We Were Six'

ACKNOWLEDGEMENTS

I am greatly indebted to the late Professor R. Kompfner, who initiated the project, and whose guidance was an inspiration. My thanks are also due to Dr. D. Walsh for his supervision of the work.

I would like to acknowledge the help received from other members of the group:- J. Almeida, E. Asl Soleimani, D.K. Hamilton, P. Johnson, M.P. Jordan, J.R. Knight, P.St.J. Russell, C.J.R. Sheppard and T. Wilson. I would also like to mention B. French, J.F. Hastings, R. Sawala and many other members of the Department whose technical assistance was invaluable.

Finally I thank Lucy Brooks, whose moral support and typing ability have been greatly appreciated, and Mrs. J. Takacs for her excellent artwork.

ABSTRACT

This thesis is concerned with the production of metal-coated optical fibres, the fibres being drawn within a vacuum. Most common methods for producing optical fibres employ an oxy-gas ring burner or an inert gas resistance furnace to reach the high temperatures necessary to melt silica. These methods have the disadvantage of exposing the molten or hot silica fibre to the atmosphere before a protective coating is applied, thereby increasing the possibility of contaminants being present at the fibre surface.

A novel though more elaborate method of producing fibres is described, with preliminary experimental results. Vacuum production allows the fibre to be metal-coated, using a magnetron sputtering technique, before exposure to the atmosphere, and the methods by which this is achieved are described.

An electromagnetically operated optical fibre switch utilising a ferromagnetically-coated optical fibre is also described.

CONTENTS

Page

CHAPTER ONE

1.1 Introduction 1
1.2 Historical Background 8
1.3 Introduction to Present Work 13
1.4 Summary 20

CHAPTER TWO Design and Construction of Fibre Drawing Apparatus: Mechanical

2.1 Introduction 22
2.2 Feed Mechanism 22
2.3 Tungsten Mesh Furnace 27
2.4 The Winding Drum 33
2.5 Vacuum System 34
2.6 Support Frame 37
s.7 Fibre Off-wind Apparatus 39

CHAPTER THREE Design and Construction of the Fibre Drawing Apparatus: Electrical and Control

3.1 Introduction 40
3.2 Power Distribution 40
3.3 Drawing Motors' Controllers 40
3.4 Traverse Motor Controller 44
3.5 Furnace Controller 44
3.6 Vacuum Control 58

CHAPTER FOUR Metallic Coating by Magnetron Sputtering

4.1 Introduction 59
4.2 Derivation of Cylindrical Magnetron Sputtering for Fibre Coating 63
4.3 Design of Coating Apparatus 68

CHAPTER FIVE Properties of Metal Coated Fibres

5.1 Introduction 77
5.2 Prestressing of Fibres 78
5.3 The Effect of an Axial Load 83
5.4 Candidate Materials 86
5.5 Implications 98
100

CHAPTER SIX Experimental Procedures and Results

6.1 Introduction 102

6.2 Operation of the Fibre Drawing Apparatus 102

6.3 Performance of the Fibre Drawing Apparatus 107

CHAPTER SEVEN Conclusions and Direction of Further Work 126

CHAPTER EIGHT An Application of Metal Coated Optical Fibres; A Mechanical Optical Fibre Switch

8.1 Introduction 131

8.2 Construction of Switches 132

8.3 Performance 139

8.4 Conclusions

APPENDIX Derivation of Lamé Solution for Cylindrical Tube under Internal and External Pressure 144

REFERENCES 147

LIST OF FIGURES

Figure	Title	Page
1.1	Step Index Optical Fibre	2
1.2	Graded Index Fibre	4
1.3	Aluminium Coating of Fibre (after Arridge)	12
1.4	Fibre Strength Results (after Pinnow)	14
1.5	Basic D.C. Sputtering (modified Penning Cell)	18
2.1	Schematic View of Drawing Machine Omitting Rod Feed Mechanism	23
2.2	View of Fibre Drawing Apparatus	24
2.3	View of Fibre Drawing Apparatus with Off-wind Mechanism	25
2.4	Rod Feed Mechanism (schematic)	26
2.5	Rod 'O' Ring Seal (typical)	29
2.6	Rod Bellows Seal (schematic)	30
2.7	Section through Tungsten Mesh Furnace	32
2.8	Winding Drum Motion and Vacuum Seals	35
2.9	Penning Gauge Calibration (dry air)	38
3.1	View of Control Console	41
3.2	Schematic Power Distribution Circuit Diagram	42
3.3	Schematic Motor Controllers Circuit Diagrams	45
3.4	Furnace Controller: Pinciples	46
3.5	Control and Axis Thermocouple Outputs Versus Mesh Temperature	49
3.6	Furnace Controller System Diagram	52
3.7	Thermocouple Linearizer Calibration Curve	53
4.1	Utilization of Magnetic Field for Sputtering at Low Pressures (after Penning)	61
4.2	Cylindrical Magnetron Mode of Sputtering (after Clarke)	64
4.3	Small Section of Receiving Surface	63
4.4	Projection of Cylindrical Geometry	66
4.5	Section of Cylindrical Geometry	67
4.6	Mk.I Cylindrical Sputtering Device	69
4.7	Trial High Rate System	69
4.8	(i) On-line Magnetron Sputtering Device	71
	(ii) View of On-Line Magnetron Sputtering Device	72
4.9	M.S. Power Supply Circuit Diagram	75

5.1	Metal Coated Optical Fibre	79
5.2	Longitudinal Prestress Induced in a Hypothetical Coating as a Function of Normalised Thickness	81
5.3	Longitudinal Prestress in Fibre Versus Normalised Coating Thickness	90
5.4	Radial Prestress in Fibre Versus Normalised Coating Thickness	91
5.5	Circumferential Prestress in Metal Versus Normalised Coating Thickness	92
5.6	Longitudinal Prestress in Metal Versus Normalised Coating Thickness	93
5.7	Stresses Induced in a Silica Fibre and Nickel Coating as a Function of Normalised Thickness	95
5.8	$\frac{\sigma_{z1}}{\sigma_{\theta 2_{max}}}$ for Aluminium, Nickel, and Chromium	96
5.10	Normalised Stiffness in Tension and Bending for a Nickel Coated Fibre Versus Normalised Coating Thickness	99
6.1	Indicated Temperature and Power Versus Power Limit Setting (manual mode)	108
6.2	Indicated Furnace Power Versus Actual Power	110
6.3	Early Plot of Fibre Diameter Versus Length (exp't no.SR7)	112
6.4	Plot of Fibre Diameter Versus Length (exp't no.SR11)	113
6.5	Plot of Fibre Diameter Versus Length (exp't no.SR10)	115
6.6	Photographs of Cross-sections of (i) rod	116
	(ii) fibre drawn from rod	116
6.7	Weibull Plot of Fibre Strength Results (exp't no.FMIII)	118
6.8	Micrograph of Molybdenum Coated Fibre	122
8.1	Cross-section of a Mechanical Optical Fibre Switch	133
8.2	Insertion of Uncoated Fibres into Tube	136
8.3	Insertion of Coated Fibre into Tube	138
8.4	View of Prototype Switch	140

NOMENCLATURE

A - area

b - intermolecular spacing

c - ½ crack depth

D - deposition rate

d - distance, deposition rate

E - Young's Modulus

e - etching rate

f - flux

I - current, 2nd Moment of Area

J - current density

L,l - length

M - mass

m - material removal rate

n - refractive index

p - pressure

R,r - radius

S - speed

T - temperature

t - thickness

V - volume

Y - yield stress

A,B,C,D,F,L,M,N,P,Q,U,V - material constants (Chapter 5)

α - angle, linear coefficient of thermal expansion

β - angle

γ_s - surface energy

γ - Poisson's Ratio

σ_F - failure stress

σ - stress

ε - strain

ρ - density, relative density

η - viscosity

θ - temperature, angle

ψ - angle

Subscripts

f - fibre

m - metal

c - cylinder

r - receiving, radial

z - z-direction

θ - θ-direction

CHAPTER ONE

1.1 INTRODUCTION

Since the classic paper by Kao and Hockham[1], many investigators have studied optical fibres for their use in long-haul communications, and indeed, several trial systems are currently being evaluated[e.g. 2,3,4]. Low loss fibres (∿ 5dB/Km) have been fabricated for several years and are now available commercially in production quantities. Now that the fundamental technological difficulties of fibre production have been overcome, effective fibre packaging and cabling is being attempted, tested, and evaluated. Purely on economic grounds, packaging methods used tend to be those of the already established multicore cabling industry; indeed many of the investigators are the large communications cabling firms themselves.

Optical fibres for use in long-haul communications systems are made from multicomponent glasses with relatively low melting temperatures, or, more usually, from high purity silica. The light energy must be tightly confined within the fibre itself, and this is achieved by using two slightly differing (chemically) types of glass; the inner or 'core' material having a higher refractive index n, than the surrounding or 'cladding' material. Simply, the light energy is then contained within the core region by total internal reflection at the core-cladding interface, assuming an abrupt refractive index change - such a fibre is termed a step-index fibre (see fig.1.1). More detailed and explanatory discussions of propagation in optical fibres are readily available (e.g. references 5,6), and as this thesis is primarily concerned with the production and mechanical properties of metal coated fibres, the reader is referred to these.

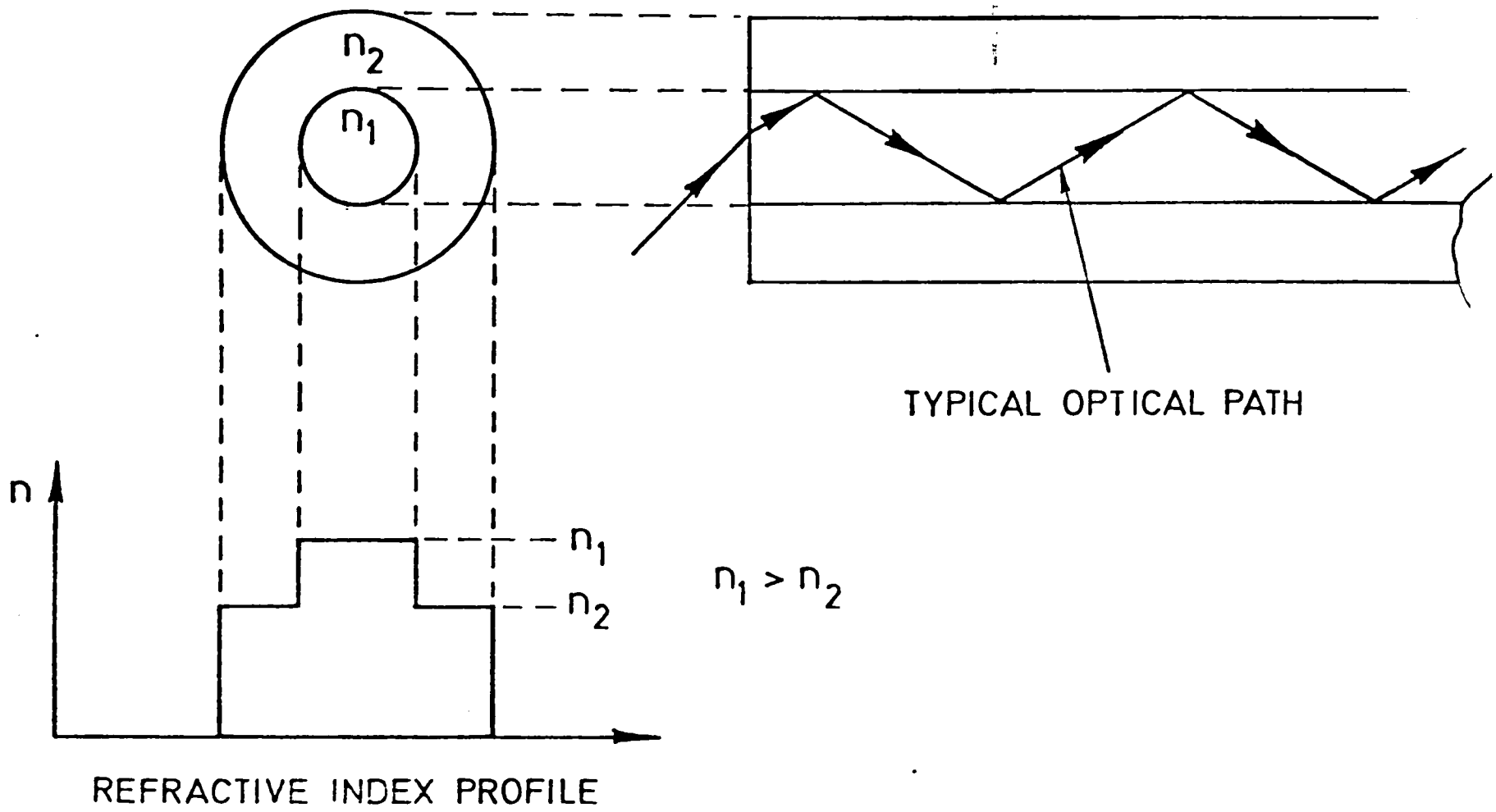


FIGURE 1-1

STEP INDEX OPTICAL FIBRE

Briefly however, there are three main classes of optical fibres. Firstly, multimode step index fibres of the type described above, which can support a large number of guided modes analogous to waveguide propagation modes. Fibres of this type have dimensions much larger than the wavelength of the source of light being used and have a core diameter of 60-80 μm (typically), an overall diameter of 100-150 μm and can support many thousands of guided modes at optical frequencies. Step-index multimode fibres suffer one large drawback - the phase velocities of higher order modes differ appreciably from those of low orders (effectively because of a difference in optical path length, higher order modes undergoing many more reflections than low order modes), and dispersion limits the upper frequency at which they can be used. Because of this, a second type of fibre has been established in which the step-index profile is replaced by a gradually changing profile, with a peak refractive index at the centre of the core (see fig.1.2). Refraction rather than total internal reflection guides the energy in this graded index type fibre, and by selecting the correct profile (approximately parabolic), all propagating modes have essentially the same phase velocity (light far away from the axis is refracted more, and has a large physical path length; the optical path length is less because material away from the axis has a lower refractive index. If the index profile is chosen correctly, the optical path lengths of all rays will be equal.) Hence dispersion is reduced and the upper frequency limit raised. The dimensions of this type of fibre are of the same order as the step-index multimode fibre.

The third optical fibre category is the single mode fibre, which, as its name implies, can support only one propagating mode, and consequently intermode dispersion is avoided. Although this appears an elegant solution for high frequency operation, practical difficulties exist in production and use of single mode fibres;

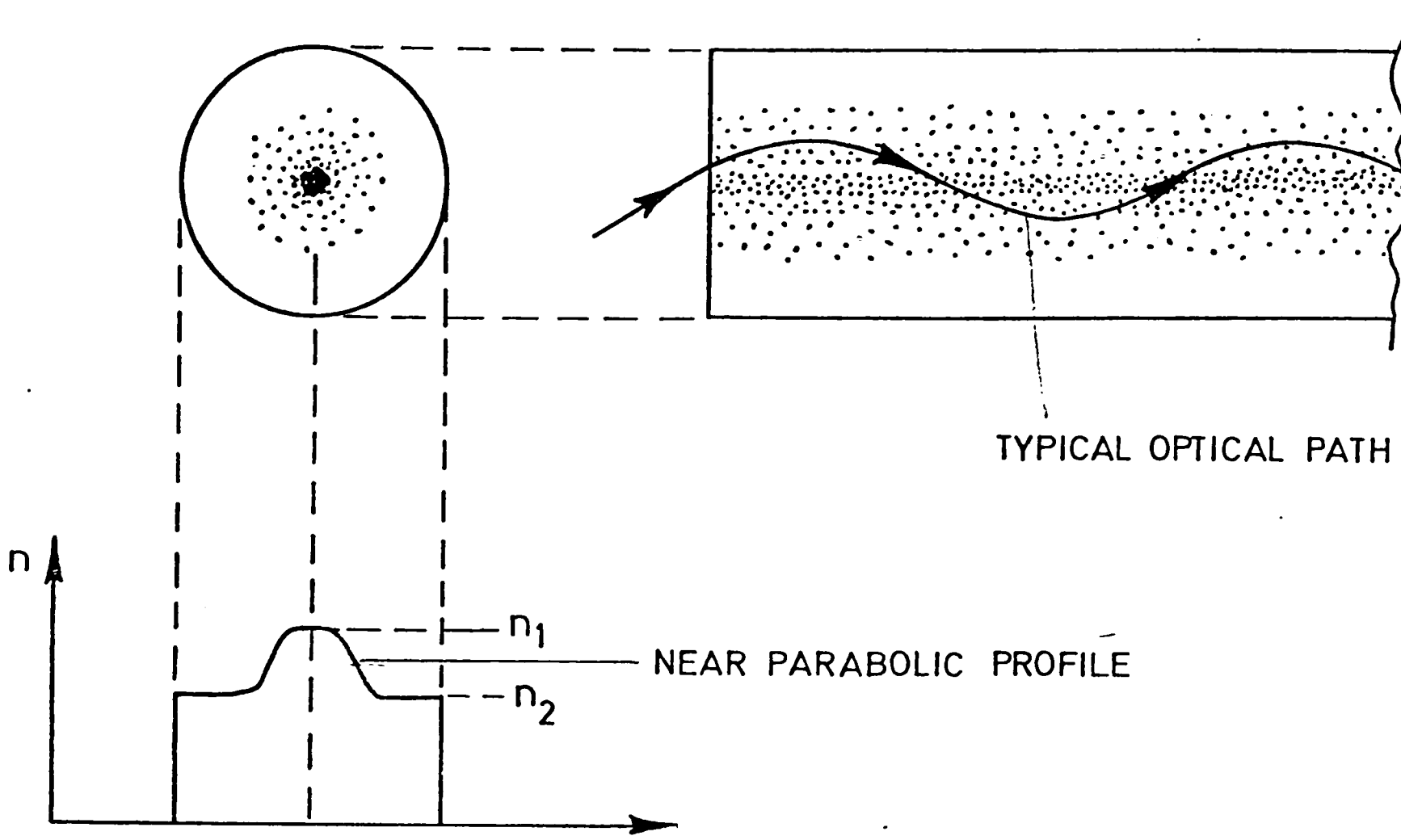


FIGURE 1-2

GRADED INDEX FIBRE

the core is very small (up to about 10 μm), and the refractive index difference between core and cladding is also small, usually less than 1 or 2%. Production techniques need to be very stringent to produce low loss fibre of this type, and fine control over fibre drawing conditions exercised. In practical use, much more care is necessary to connect single mode fibres together and to devices, as the core diameter is approximately an order of magnitude less than for multimode fibres - an error in position of even 1 μm will impair coupling efficiency dramatically[7].

Many of the technological problems of constructing a long haul optical fibre communications link have now been overcome, and several trial systems are at present in the field. As has been stated, low-loss optical fibres are available commercially, as are light sources (LEDs or solid state lasers), photodetectors (PIN or avalanche photodiodes), fibre-fibre connectors, and other components necessary for a practical fibre link, and investigators are now looking at system needs, reliability and difficulties.

Low loss optical fibres with reasonable bandwidths are generally fabricated from multicomponent glasses, by the double crucible technique[8], or from pure silica using a chemical vapour deposition (CVD) technique to produce a preform which may be subsequently heated and drawn into a fibre[9], with other techniques less commonly used (e.g. rod-in-tube and polymer clad). Although the double crucible technique has the advantage of being able to produce virtually limitless lengths of continuous fibre, the CVD method is generally preferred commercially for various reasons, not least of which is the ability to precisely control index profile. As silica is used predominantly, this thesis is primarily concerned with the metal coating of silica fibres, rather than multicomponent glass fibres.

Of fundamental importance to any optical fibre system is the need to construct fibre cables which are mechanically strong, which

can be manhandled into ducts and other operating environments, and which will have a reasonable operating life. A prerequisite of this is to produce fibre strong enough to withstand the cabling process.

Freshly drawn silica fibres are known to be intrinsically strong, but are prone to degradation on handling and exposure to the atmosphere. The property most frequently measured has been the strength in tension (or elastic limit) of fine fibres ranging from 10 μm to 1mm or more in diameter. Table 1.1 sets out collected data from various sources covering strength (σ_F) in bending and tension, and compares them to mild steel. Some values are calculated from quoted values of strain, assuming a Young's Modulus of 73.1 GN/mm^2[10]. Measurement of the tensile strength of fibres is certainly not an exhaustive method of defining the overall mechanical properties of silica fibres, but is useful in as much as any surface flaws (the major cause of failure in brittle materials) may be detected - the tensile strength drops due to stress intensifying defects on the surface.

Griffith[11] explains the mechanism of brittle failure by considering surface or internal cracks acting as stress concentrations, so that at the tip of the crack the stress is above the fracture stress when the average stress is much lower. The crack will extend if enough elastic strain energy can be released to supply the surface energy of the newly formed crack surfaces. By considering the balance between the energies, he showed that the larger crack, the smaller is the stress necessary to cause fracture. For plane stress, Griffith determined the result:

$$\sigma_F = \sqrt{\frac{2\gamma_s E}{\pi c}} \quad , \qquad (1.1.1)$$

where σ_F is the failure stress, or stress required to propagate the crack, γ_s is the surface energy of the material, E is Young's Modulus

SOURCE	DIAMETER (mm)	FAILURE STRESS σ_F (GN/m^2)	TEST METHOD
GRIFFITH (1920)[11]	< 0.5 ∿ 1.0	1.5 - 6.2 9.0 (fresh fibres)	Bending (radius measurement)
HILLING (1961)[12]	0.5 - 3.0 0.5 - 3.0	2.9 - 4.8 5.8 - 7.6 (78k)	Bending
MORLEY (1964)[13]		5.9 average falling to 2.8 over time	Tension
MORLEY ET AL. (1964)[14]	0.02 - 0.1 ∿ 1.0	1.5 - 7.0 4.5 - 4.8	Tension Bending (radius measurement)
KELLY (1973[15] (various sources)		6.0 - 10.5	Tension
MILD STEEL[10]		0.43 - 0.49	

TABLE 1.1

REPORTED FAILURE STRESS OF SILICA

of the material, and 2c is the crack length. If we compare equation (1.1.1) with an estimate of the theoretical fracture strength of a material[16]:

$$\sigma_F \simeq \sqrt{\frac{E\gamma_s}{b}} \quad , \tag{1.1.2}$$

where b is the intermolecular spacing, we see that if

$$c > \frac{2b}{\pi} \tag{1.1.3}$$

a reduction in the failure stress occurs. As b is of the order of 2×10^{-10}m for glass even minute defects of the order of a few Angstroms will cause weak fibres.

It can thus be seen that to produce fibres which are strong and which will remain strong whilst in service requires two conditions:

(i) flawless or near flawless fibre must be manufactured, and

(ii) the surface of the fibre thus produced must be protected, preferably immediately after manufacture, by a material which will not degrade the surface.

1.2 HISTORICAL BACKGROUND

Early experimental optical fibres were usually manufactured unprotected, but it was envisaged that for commercial use some kind of protective packaging would be needed to provide protection against mechanical damage, as well as to eliminate possible cross talk between adjacent fibres, and power loss due to microbends[17]. This packaging is usually achieved in three stages:

(i) on-line primary coating (individual fibres),

(ii) secondary or buffer coating (individual fibres), and,

(iii) cabling (one or more fibres).

Primary and secondary coatings are of importance to this work, and only individual fibres are considered. Microbending loss has

not been considered and the main focus has been to metal coat silica fibres whilst minimising surface damage.

Conventional (and commercial) coatings for optical fibres have generally been limited to silicone resins, plastics, nylons, rubber and other organic compounds, with one exception[18]. Broadly speaking, investigation has been on the lines suggested by Gloge[19], and results achieved generally in accordance with his expectations. Gloge considers the excess transmission loss resulting from statistical variations and lateral pressures affecting the fibre, and concludes that care and correct packaging can reduce this loss, if not effectively eliminate it. He does, however, suggest that:

> "cable forces are likely to be stronger and less uniform than those encountered on a storage drum (to which he relates his results) and may necessitate a fibre protection by the more expensive hybrid jackets or even by reinforcement".

By a 'hybrid jacket' Gloge refers to a packaging consisting of two or more protective coverings of differing elastic modulii; this is the approach taken by many investigators (primary and secondary coatings), and has been reported upon successfully in pilot systems (e.g. reference 2). Black and Cook[20] reported the optical results of coating a bare fibre with a close fitting polypropylene layer by extrusion, measuring attenuation before and after coating. The excess transmission loss was found to be 2dB/Km over the entire spectral range, the loss being attributable to 'small lateral deformations of the fibre within the plastic coating'. These results indicated that it was indeed practical to put down a protective jacket of the type described by Gloge, and this is the practice now commonly adopted.

Other authors report on the mechanical properties of coated fibres. Typically, Isomura, Yamamoto, and Yamanishi[21] have investigated the properties of various coating materials (nylon, PTMT,

EVA, PE, PTFE, phenol, polyester and plastic) and found that a plastic coating applied immediately after drawing the fibre inhibited crack propagation. A high modulus plastic was selected (to enable a thin coating to be applied with enough strength to protect against crack propagation) and achieved breaking loads of 5.35 ± 2.97 kg compared with 1.30 ± 0.52 kg for bare fibre; a significant improvement. The results also indicate that a coating applied a considerable time after drawing has a much less beneficial result; microcracks are formed before the coating application.

As mentioned previously, most primary coatings to date have consisted of silicone resins, plastics, nylons and other organic compounds. These coatings all suffer three limitations:

(i) unless the coating forms a strong chemical bond with the fibre surface, slippage and abrasion at the interface may occur. It is also likely that contaminants, especially water vapour, could eventually attack the fibre surface by seeping along the boundary from discontinuities, fibre/fibre junctions, or fibre/device junctions.

(ii) These compounds do not form a true hermetic seal around the fibre and again, water vapour may eventually seep through and attack the fibre surface. This effect would be especially serious for submarine cables.

(iii) The nature of these compounds restricts their use at elevated temperatures.

A properly applied metal coating could overcome these disadvantages and also offer other benefits such as solderability and, if a ferromagnetic material is applied, the ability to be deflected electromagnetically (see Chapter 8). Metal coatings have been applied to silica fibres prior to this work. Arridge et al.[22,23,24] experimented with aluminium coatings on silica fibres with the aim of creating a strong matrix solid by swaging together many such

coated fibres. The coating was applied by passing freshly drawn silica fibres through a molten aluminium blob (figure 1.3), a process which was termed 'freeze coating'. This proved relatively unsuccessful because of the vigorous chemical reaction at the silica-aluminium interface; the aluminium tended to oxidise, with the reaction formulated as

$$4Al + 3SiO_2 \rightarrow 2Al_2O_3 + 3Si \quad .$$

It was found that this reaction could largely be controlled by the addition of small quantities of the Group V elements Bismuth and Antimony. However, the pristine condition of the silica surface could still be easily destroyed, with corresponding fibre weakening. It was apparent that the coated fibres did have a lower mean strength and a much higher variance compared with uncoated fibres. There were three possible causes:

(i) Diameter variation in the drawn fibre, accounting for about one tenth of the total coefficient of variation of observed breaking loads.

(ii) Interfacial interaction producing Griffith cracks (chemical and oxide film effects).

(iii) Length effects. Measurements of the strength of coated fibres of different lengths in the range 38-470 mm showed a decrease in the strength of the longer fibres which was considerably greater than would be expected from diameter variation. Analysis of this length variation suggested that a flaw mechanism was operating at the interface since no comparable change of strength with length was found on uncoated fibres.

Arridge ultimately achieved mean breaking strengths of 563 Kg/mm^2 (5.52 GN/m^2) - respectable results.

Pinnow, Wysocki and Robertson[18] have applied Arridge's coating technique to optical rather than bare silica fibres and have reported

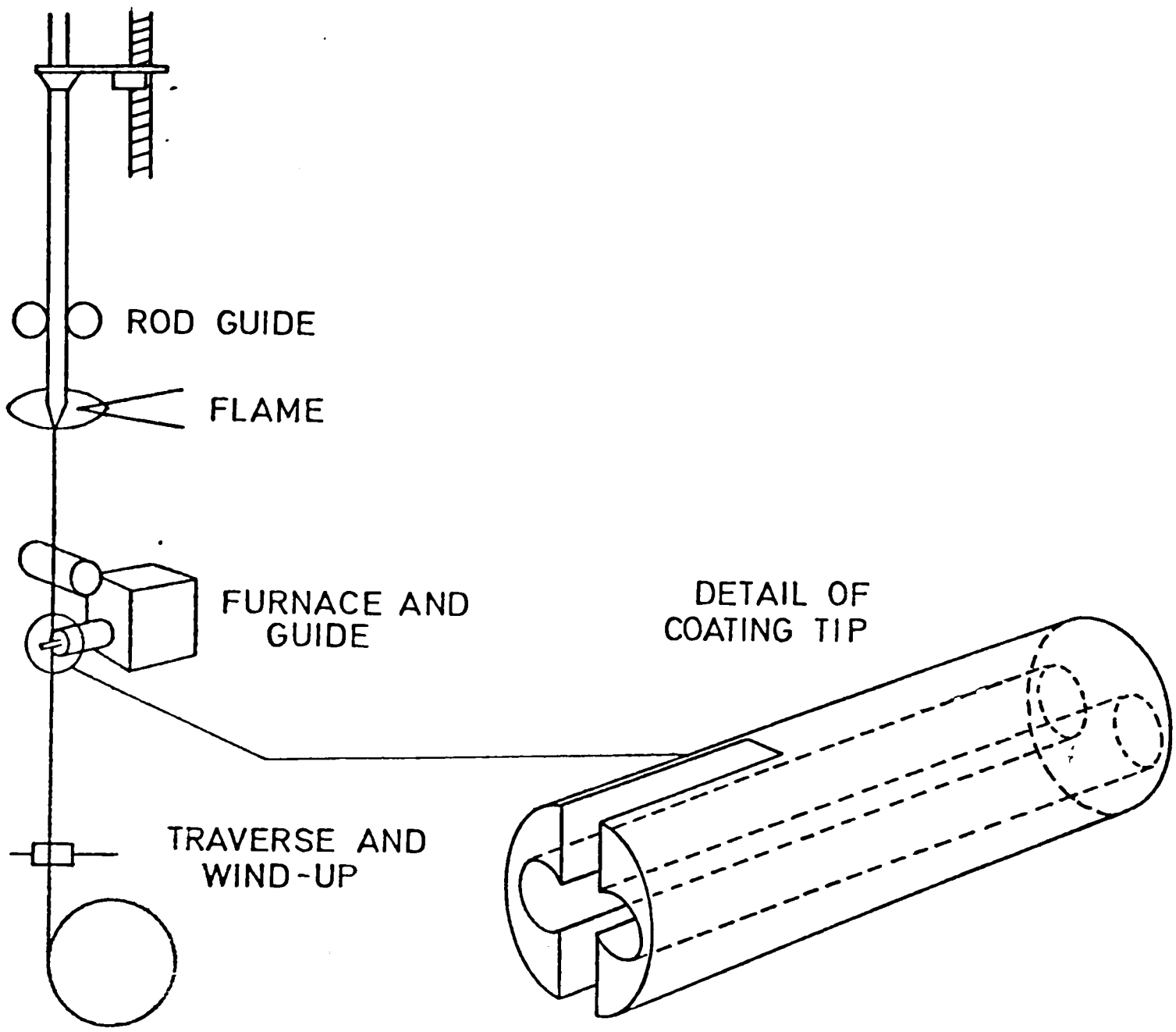


FIGURE 1-3

ALUMINIUM COATING OF FIBRE (AFTER ARRIDGE)

promising results. No flaws have been reported, and, unlike Arridge, the investigators appear to have experienced no trouble with interfacial chemical reaction. Fibre strength up to 900,000 p.s.i. ($\simeq$ 6.2 GN/m^2) and elongations up to 9% have been reported. The reported failure distribution (figure 1.4) has two distinct slopes, the lower strength failure mode believed to be due to imperfections in the coating technique. Results extrapolated to 1km fibre lengths indicate a 99.99% survival probability for elongations in excess of 2%. The aluminium coatings provided a true hermetic seal around the fibre, and were in the range 10-20μm thick on 125μm diameter fibres.

Although these results are admirable, the freeze coating technique has limitations. Firstly the method is restricted to low melting temperature materials, aluminium being the obvious candidate, but this, as will be shown later, is not an ideal material. Secondly, in alloy systems where a large liquidus-solidus temperature difference is found, freezing is not instantaneous, and surface chemical reaction may occur. Thirdly, at very high speeds of coating, the time spent in the globule is not sufficient for freezing.

1.3 INTRODUCTION TO PRESENT WORK

Various alternative coating techniques were evaluated at the outset of the project, and are listed below with a brief summary of their relative merits and drawbacks (Table 1.2 at the end of this section). Any method which may be operated at an elevated temperature is especially attractive, as the difference in temperature coefficients of expansion between most metals and silica will tend to keep the fibre in compression when reduced to ambient temperature and artificially increase the fibre's breaking strength. The effect may also inhibit microcracks.

Preliminary analysis of temperature pre-stressing of fibres has

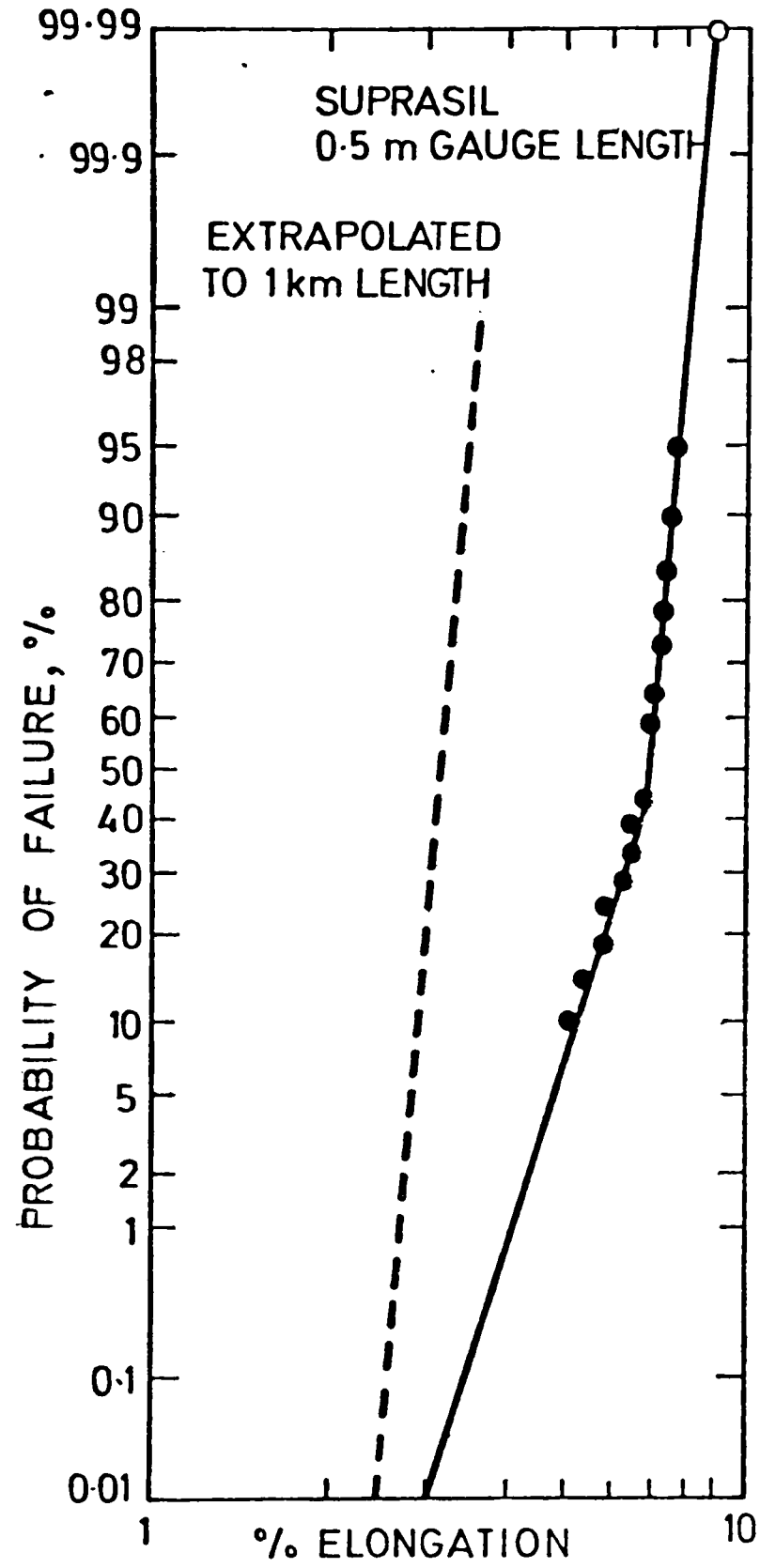


FIGURE 1-4

FIBRE STRENGTH RESULTS (AFTER PINNOW)

yielded interesting results. Firstly, the temperature difference need only be of moderate proportions (≃ 100-400°C) to produce a useful prestress within the fibre for a typical metal with a 5μm coating (higher temperature may cause the yield stress of the metal to be exceeded on coating). Secondly, a coated fibre will still be in compression across its diameter if bends of the order of 100mm radius are made.

Alternative methods of coating which were considered are:

a) Evaporation

This method of deposition was among the first to be suggested as it is a well established technique which is relatively easy to perform. Three major problems apart from cost come readily to mind.

(i) How to start the drawing operation. As a good vacuum is needed for a pure metal, as opposed to an oxide film, to be deposited, it was difficult to envisage how to initiate a pull with a fresh preform. A conventional fibre drawing machine has easy access to the hot zone, and fibre initiation is readily achieved by attaching a probe to the heated preform, and literally 'pulling' off a fibre, and attaching this immediately to the take-up (winding) drum. With an evaporation plant, the fibre must either be passed into the evacuated chamber (with vacuum sealing problems) or the complete pull/coat operation conducted within the vacuum. To the author's knowledge, silica fibre has never been drawn in vacuo prior to this work.

(ii) Film thickness. If a micron or more of metal is to be deposited in a continuous process, deposition rate is of prime importance. Conventional pullers have a fibre drawing rate of (typically) 1m/sec, and with an evaporation source of length, say 50mm, the coating must be applied in 50msec. This implies a coating rate of 20μm/min for a 1μm coating - a much higher rate than conventional evaporation sources. Two ways round the problem

were considered. Firstly to reduce the drawing speed (probably not practical for a commercial process) and secondly to have a multiple or elongated evaporation source (thus increasing the overall height of a puller).

(iii) Efficiency. One of the basic limitations of the evaporation technique when used with small targets or substrates is the extreme waste of evaporant. With a small target size as in this case of typically 100μm diameter and 50mm in length, only a small amount of evaporant will strike the target.

Consider a line source 50mm long, 25mm away from the fibre, and assume that evporant leaves the target only in a radial direction uniformly from the source. Evaporant will pass through a cylinder of surface area

$$A_c = 2\pi r_c l_c$$

$$= 2\pi.25.50 \quad mm^2$$

$$= 2{,}500\pi \quad mm^2$$

The fibre accounts for $0.1 \times 50mm^2$ (deposition will not be uniform) i.e. $\simeq 0.0601$ of this area.

For 1km of fibre, and for a coating of 1μm, the volume of the coating is

$$V_m = \pi(r_m - r_f)^2.l_f$$

$$\simeq \pi t\, d_f.l_f$$

$$= \pi.10^{-3}.10^{-1}.10^{6} \quad mm^3$$

$$= 100\pi\ mm^3$$

Typically the relative density of a coating is $\simeq$ 10gm/cc, so the mass of the evaporant needed will be

$$M_m = V_m \times \rho_m$$

$$= \frac{100\pi}{10^3} \times 10 \text{ gm}$$

$$= \pi \text{ gm}$$

$$\simeq 3 \text{ gm}$$

So, if 3gm of metal is to be put on the fibre, a mass

$$M_e = M_m \frac{A_c}{A_f}$$

$$\simeq 3 \times \frac{2,500\pi}{5} \text{ gm}$$

$$\simeq 5\text{kg}$$

of evaporant will be needed, which will be deposited inside the chamber. This may be acceptable in a research laboratory but is hardly an economic proposition.

The second two problems, although not insurmountable, do create severe practical difficulties with this method, and, indeed, the inefficiency aspect suggests that a directed or contained source of material is needed.

Experiments with the evaporation technique have been conducted successfully with short lengths of fibre.

b) Sputtering

When an electrical discharge is passed between electrodes at a low gas pressure, the cathode electrode is slowly disintegrated under the bombardment of the ionized gas molecules.

The process lends itself to a cylindrical geometry, thus containing the target (cathode) material and minimising wastage. Initially a simple D.C. sputtering system modified from the form of figure 1.5

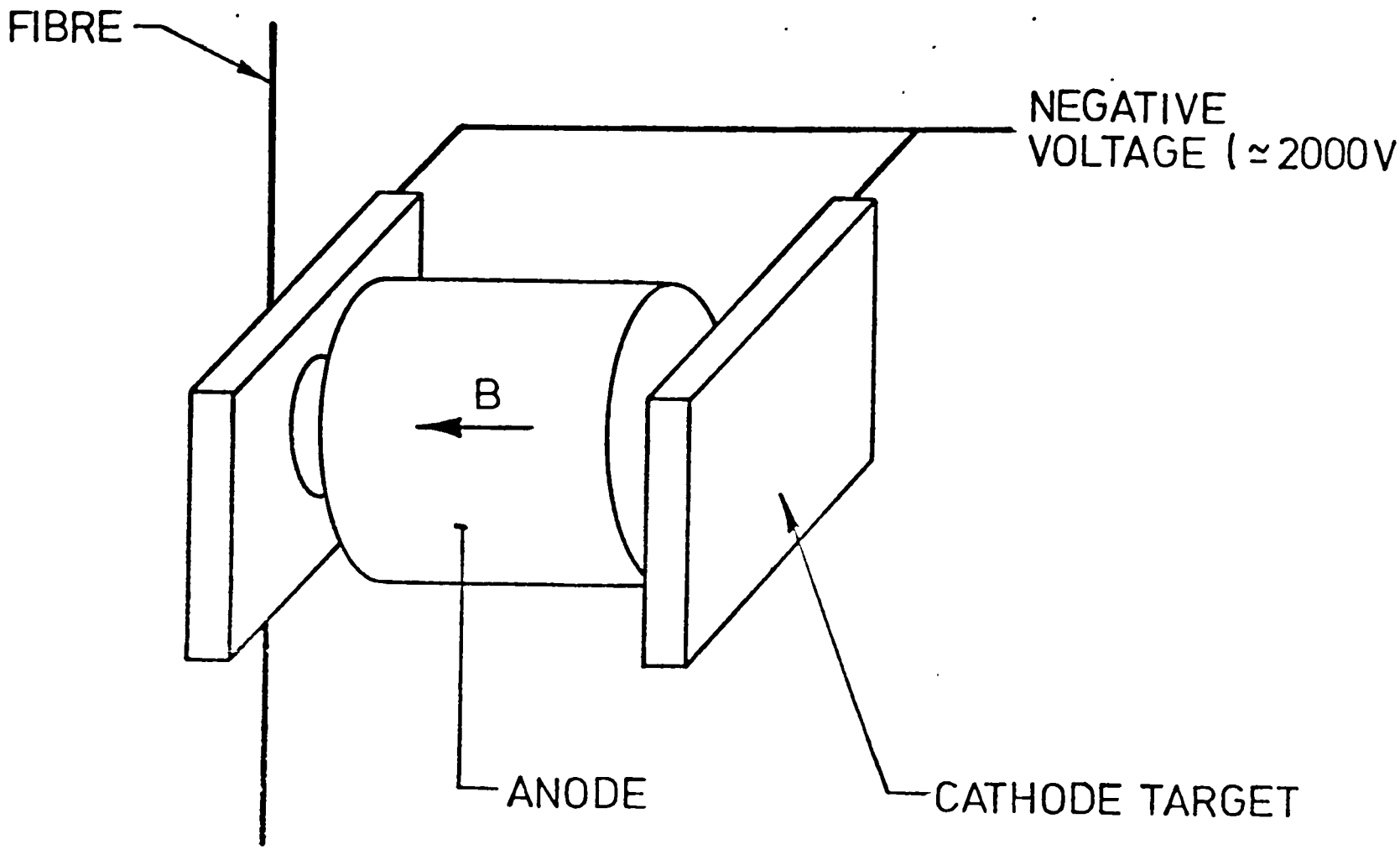


FIGURE 1.5
BASIC D.C. SPUTTERING
(MODIFIED PENNING CELL)

was envisaged, with the anode trapping unused target material. This simple system will only coat one side of the fibre and a multistage device would be needed for uniform coating.

Further investigation revealed the Planar Magnetron Sputtering technique[25] which promised very fast sputtering rates, and lent itself admirably to a cylindrical geometry. Deposition rates for commercial plant have been quoted as high as 1.5μm/min[26] for aluminium with a conventional geometry onto a flat target. The principle and derivation of cylindrical geometry is reported later (Chapter 4). Initial results in a pilot plant seem promising with good mirror-like films, good adherence, but rather low deposition rates due to an inadequate power supply.

c) Chemical decomposition

At a very early stage in the work, chemical decomposition was considered, utilising an unstable metal compound. Nickel carbonyl, $Ni(CO)_4$, was suggested as a candidate material, it being unstable, decomposing at about 60°C, giving Nickel and carbon monoxide:

$$Ni(CO)_4 \rightarrow Ni + 4CO$$

Chemists who had had some experience with the compound were consulted and suggested four basic drawbacks to the process:

- decomposition could not easily be directed (inefficient),
- carbon monoxide is toxic,
- low deposition rates,
- expensive plant.

d) Electro-deposition

This method could be a useful way for increasing the thickness of a pre-deposited thin layer. It must be used with a conducting material and as such is not a candidate for initial deposition on silica fibres. Also, to achieve good, uniform deposition the process must be conducted slowly.

e) Other methods

Various other methods of deposition were initially suggested (electron-beam evaporation, deposition of silver using Feyling's solution, etc.) but were discounted on the grounds of expense or limited use.

1.4 SUMMARY

It was decided to direct the work towards providing a facility which could be used for a variety of coating techniques and thus the fibre puller itself was designed to leave as many options open as possible.

Table 1.2 summarises the practical methods by which metal coating could be achieved. The most promising options involved the use of a vacuum or reduced atmosphere to achieve deposition and it was decided to design a fibre drawing machine that would pass the fibre through an evacuated chamber. Realistically this meant that the fibre must be drawn within the vacuum (a feat to the author's knowledge never previously attempted) which in itself might be useful for reducing loss-inducing contaminants within an optical fibre.

Preliminary work has been carried out with evaporation and sputtering sources, the latter technique looking very promising.

METHOD	SPEED	VACUUM OR INERT ATMOSPHERE?	TEMPERATURE	TOXIC BY-PRODUCTS?	TYPES OF METAL	COST/COMPLEXITY	COMMENTS
(a) EVAPORATION	LOW/MEDIUM	VACUUM	VARIABLE	NONE	VARIOUS	HIGH/HIGH	HARD TO DIRECT
(b) SPUTTERING	MEDIUM/HIGH	VACUUM	HIGHISH (VARIABLE?)	NONE	VARIOUS	HIGH/HIGH	CAN BE DIRECTED
(c) MOLTEN METAL BATH	?	POSSIBLY INERT ATMOSPHERE	MELTING TEMPERATURE OF METAL OR ABOVE	NONE	LIMITED	CHEAPISH/LOW	EFFECTIVELY LIMITED TO ALUMINIUM
(d) METAL CARBONYL	LOW	VACUUM	$\simeq 60^{o}C$	MANY	LIMITED BUT VARIOUS	MEDIUM/HIGH	
(e) ELECTRO-DEPOSITION	LOW	ATMOSPHERIC	VARIABLE	NONE	VARIOUS	MEDIUM/LOW	CANNOT BE USED DIRECTLY ONTO FIBRE
(f) CHEMICAL (Feylings Sol'n)	LOW	ATMOSPHERIC	AMBIENT+	NONE	SILVER ONLY	CHEAP/LOW	LIMITED USE

TABLE 1.2

SUMMARY OF COATING METHODS

CHAPTER TWO

DESIGN AND CONSTRUCTION OF THE FIBRE DRAWING APPARATUS: MECHANICAL

2.1 INTRODUCTION

The design of the fibre drawing apparatus (fibre 'puller') was required to be as flexible as possible. As well as drawing fibres in vacuo using a vacuum furnace, it was thought desirable to be able to use an oxy-hydrogen ring burner or an inert gas furnace as preform melting heat sources. Consequently a 'unit' approach was taken to the mechanical construction of the puller, and the vacuum enclosure can be quickly removed if necessary. A gas ring burner is available which may be substituted for the vacuum furnace enabling flame prepared fibre to be produced. Figure 2.1 shows an overall schematic diagram of the puller, omitting the rod feed mechanism, and figures 2.2 and 2.3 show photographs of the apparatus.

In operation, a silica rod or preform is fed slowly into the furnace, is melted and necks down to form a fibre which is then coated, and wound on to a storage drum. The following sections of this chapter describe the various components of the apparatus.

2.2 FEED MECHANISM

The feed mechanism (figure 2.4) enables base material in the form of rods to be fed into the furnace. If fibre is to be drawn from the furnace at constant rate of volume, i.e. constant drawing speed, input material must replace this at an equivalent volume rate. To conserve volume,

$$\pi r_p^2 . S_p = \pi r_f^2 . S_f \qquad (2.2.1)$$

or

$$Sp = \left(\frac{r_f}{r_p}\right)^2 . S_f$$

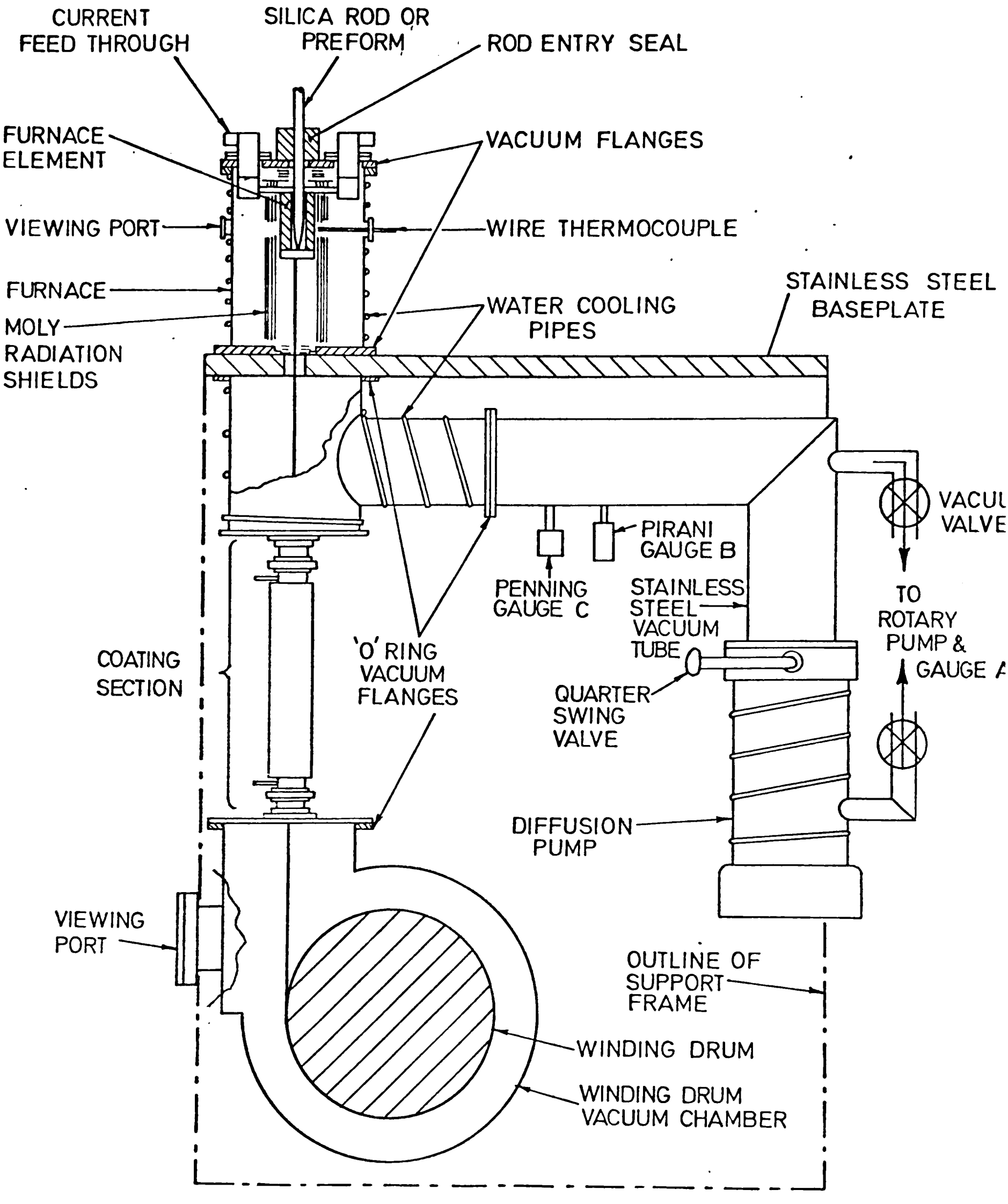


FIGURE 2-1

SCHEMATIC VIEW OF DRAWING MACHINE OMMITTING ROD FEED MECHANISM

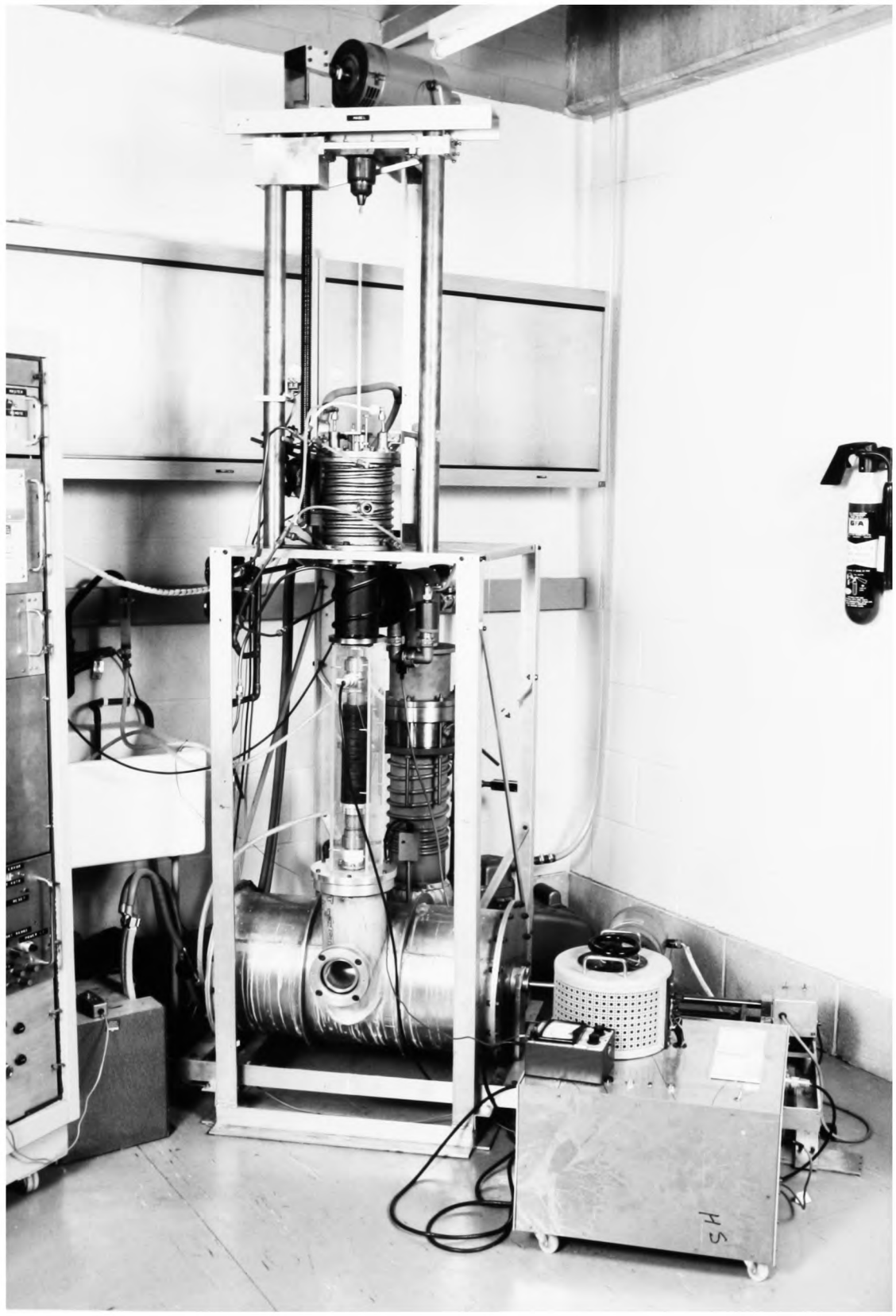


Figure 2.2 View of Fibre Drawing Apparatus



Figure 2.3 View of Fibre Drawing Apparatus with Off-wind Mechanism

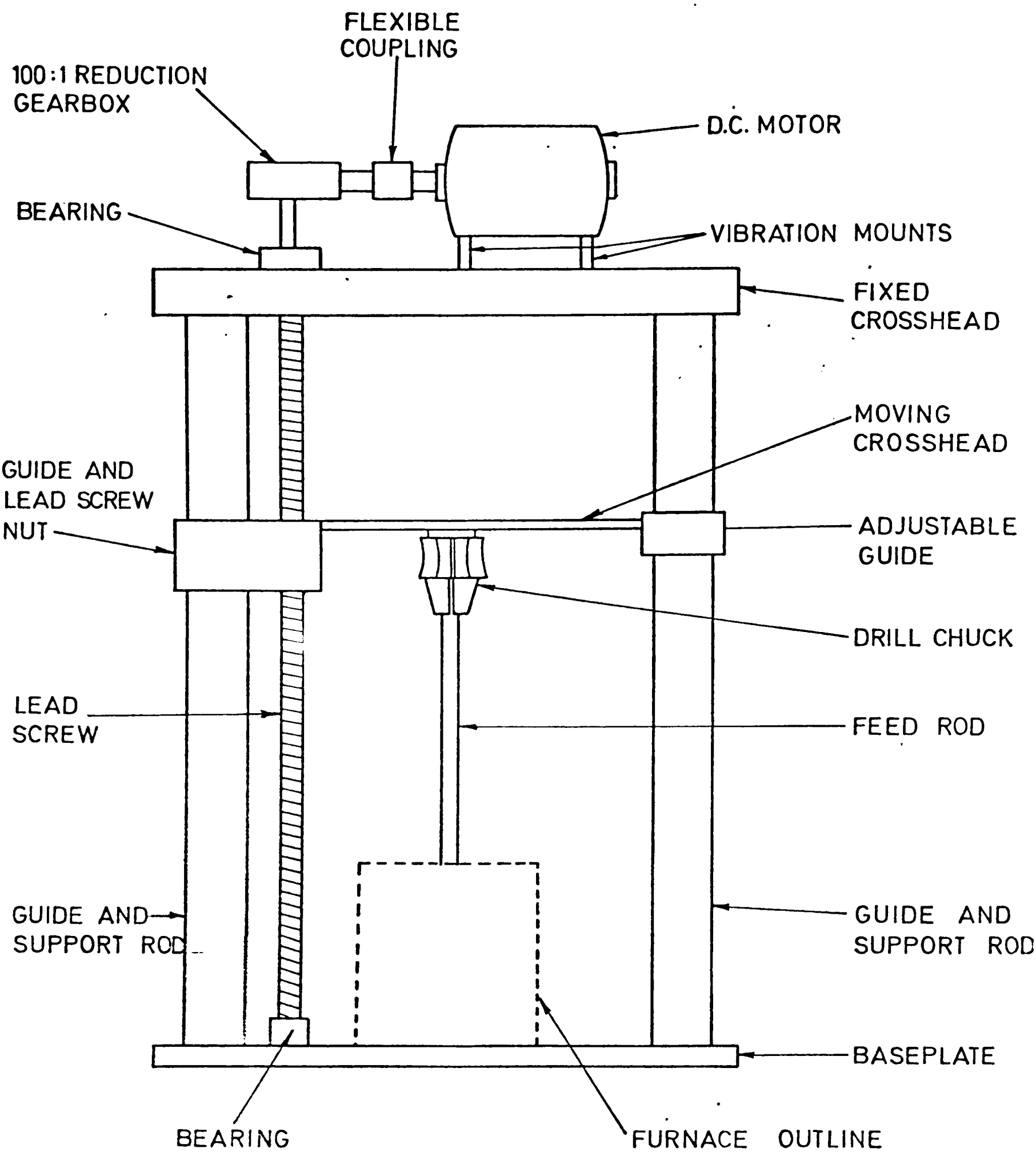


FIGURE 2-4

ROD FEED MECHANISM (SCHEMATIC)

where r_p = preform radius, S_p = preform feed speed

r_f = fibre radius, S_f = fibre take-up speed

This equation defines the feed speed for given preform or rod diameter, desired fibre diameter, and desired pulling speed, and also defines a constant feed speed for constant pulling speed. The minimum draw-down ratio $(\frac{r_f}{r_p})$ and the maximum fibre pulling speed define the maximum feed speed required.

It was decided to use a minimum rod or preform diameter of 5mm, and aim for an absolute maximum pulling speed of 80m/min for fibre with diameter 200 microns. The maximum feed speed is then ≈13m/min. This was achieved using a ½ H.P. D.C. motor with separate windings with a maximum speed of 2,000 r.p.m. feeding, via a worm reduction gearbox of ratio 1:100, a leadscrew with 5 t.p.i.. This gives a maximum attainable speed of 4 inches per minute or 0.1m/min. However, this is an extreme case; more typical figures are rod diameter 6mm, pulling speed 10m/min, fibre diameter 100 microns, giving a feed speed of about 2.8mm/min.

The motor speed is kept constant by a closed loop thyristor controller, deriving the reference speed by a tachogenerator connected directly to the motor output shaft. Desired speed is maintained ± 0.5% of desired setting. The speed is set by a digital thumbwheel switch calibrated in mm/min.

The lead screw drives a moving crosshead, guided by shafts, on which is mounted a drill chuck which grips the base material rod. Provision is made to align the drill chuck along the axis of the furnace.

2.3 TUNGSTEN MESH FURNACE

The furnace is designed to fulfill two functions. Firstly, it allows entry from the atmosphere of the silica rod, and secondly heats

the rod to a temperature at which it is sufficiently soft to be drawn.

2.3.1 Rod Entry Seal

Two alternative types of rod entry seal have been constructed. At first an 'O' ring seal was constructed, it being considered that the heating and draw down operation would remove any abrasion marks caused by friction at the rod/seal interface. There is, however, some evidence to suggest that rod/preform flaws can be detected on fibre after the drawing operation[27] and fibre produced from flame polished silica preforms have shown noticeably higher tensile strengths than unpolished. Consequently it was decided to design a bellows type seal to allow rods to be introduced to the furnace without abrasion.

(1) 'O' ring seal

The entry of the rod into the furnace is facilitated by a removable double 'O' ring vacuum seal. This unit is held down against the top of the furnace (see figure 2.5) by a top plate; easy removal is necessary as different seals are used for different rod sizes. The seal unit consists of a stainless steel body within which the 'O' rings, spacer, and compression member sit; a threaded brass ring compresses the 'O' rings, squeezing them hard against the rod and the stainless steel body. The body itself has an 'O' ring seal between it and the ground furnace top, completing the vacuum seal. This system works very well - there is no measurable leak rate.

(2) Bellows seal

In this case a stainless steel edge welded bellows unit is employed, with the entire silica rod within the evacuated volume (figure 2.6). The rod may be changed by unscrewing the threaded collett and re-inserting a new rod with a new collett. The bellows unit has a travel of 400mm between its fully-open to fully-closed position, allowing this length of rod to be used during drawing operation.

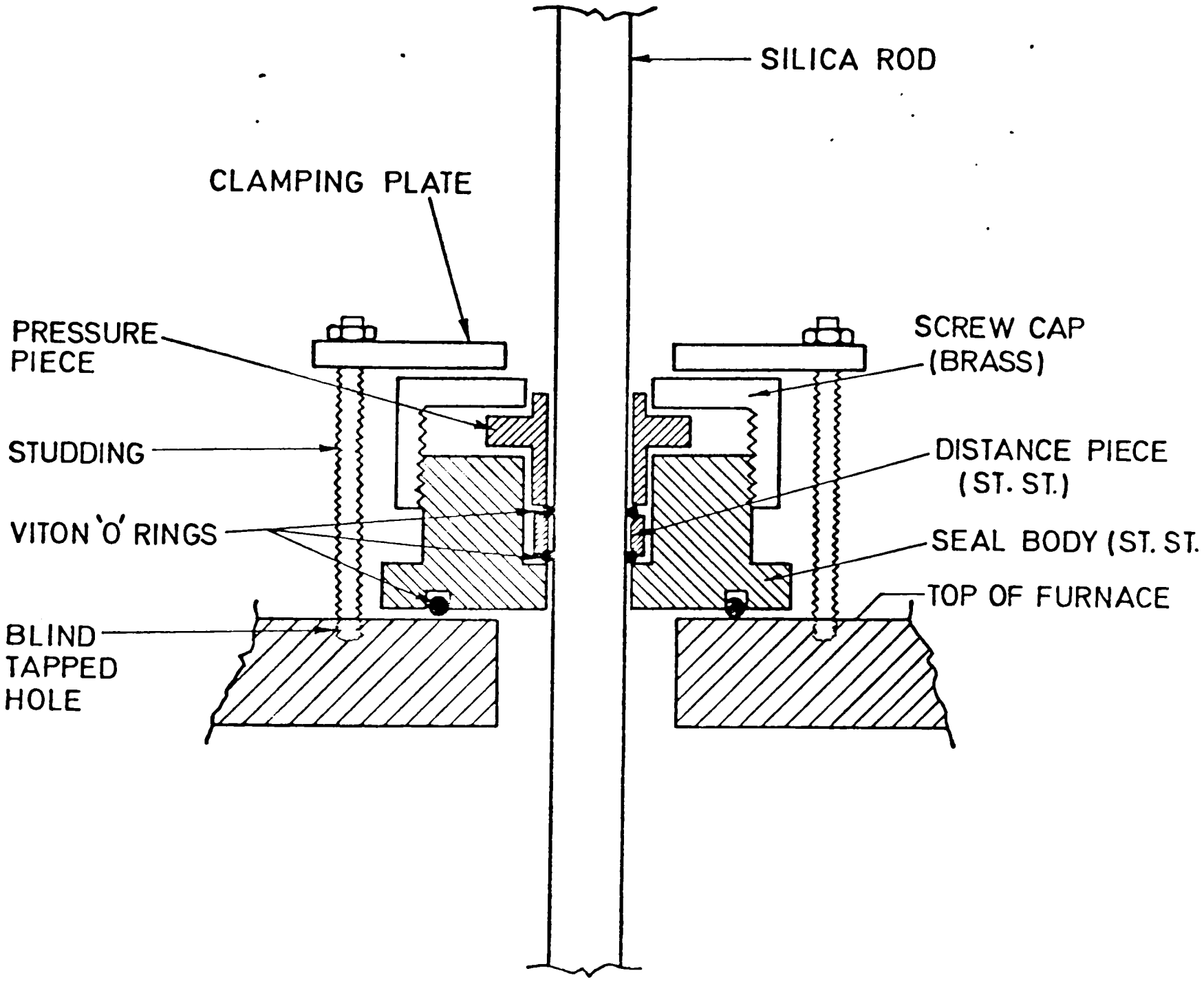


FIGURE 2-5
ROD 'O' RING SEAL (TYPICAL)

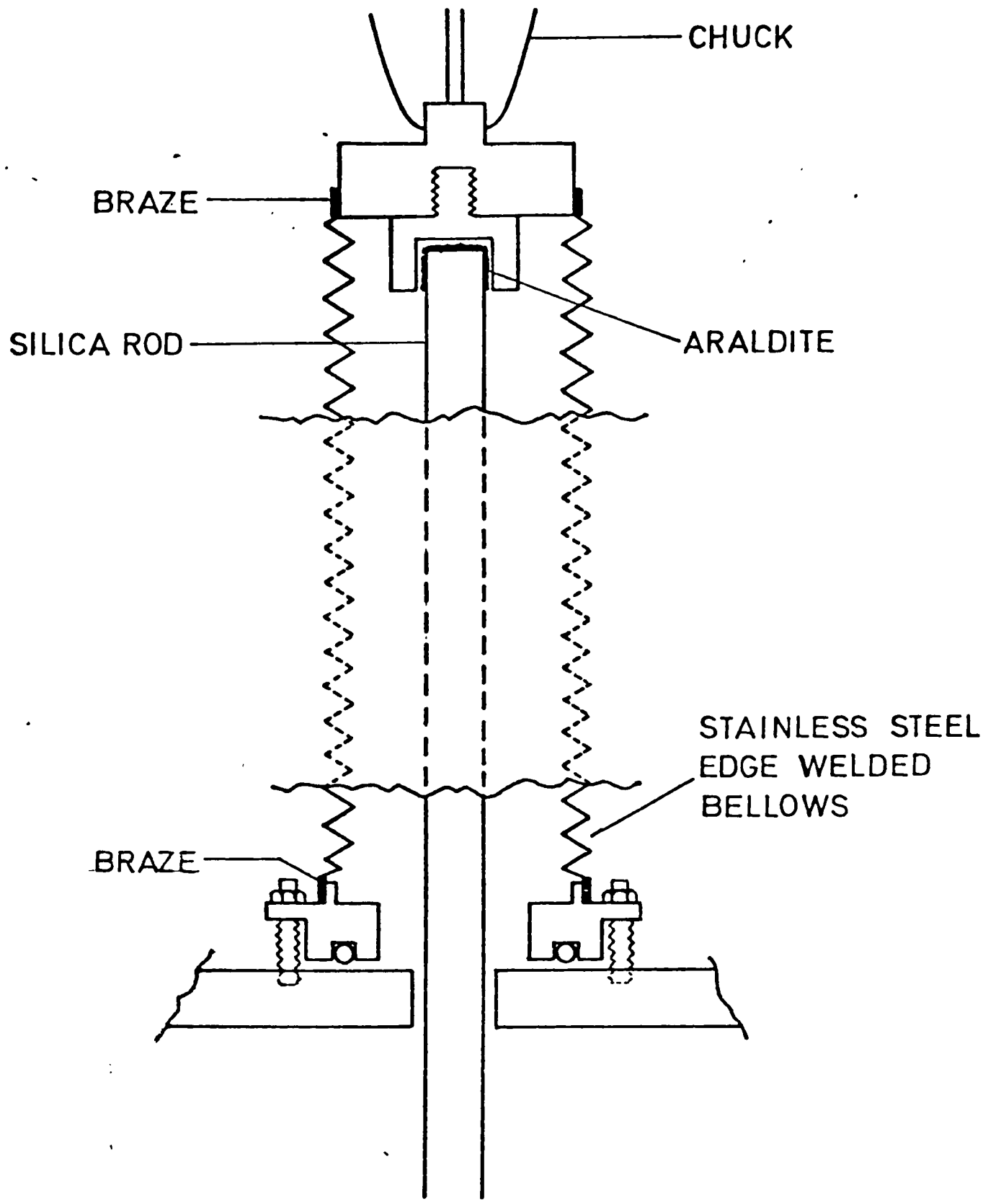


FIGURE 2-6
ROD BELLOWS SEAL (SCHEMATIC)

2.3.2 Furnace

Figure 2.7 shows a cross-section through the furnace. The heating element is a split cylindrical tungsten mesh, fed with current by two protruding tongues at the top of the mesh. At the bottom of the mesh is firmly positioned a tungsten ring; current passes down one half of the split cylinder, through the low resistance bottom ring, and up the other half of the cylinder. The overall height of the element is 105mm, with the length of the hot zone 78mm and 25mm in diameter. Compared to more conventional fibre drawing furnaces this is a long hot zone, but in this case (in vacuum) heat transfer is very inefficient by radiation alone - the temperature of the element when the silica just softens is $\simeq 1900^{\circ}C$, way above the melting point of silica ($1610^{\circ}C$).

Radiated heat is prevented from reaching the body of the furnace by five molybdenum radiation shields at $\frac{1}{4}$" spacing, and the stainless steel body itself is water-cooled by copper pipes brazed to the outer surface.

The top and bottom plates of the furnace are hollow, to allow cooling water to flow within them. A total water flow of about 3l/min at room temperature is sufficient to keep the body only a few degrees above ambient; the only appreciable hot spot is at the thermocouple entry (see below). The furnace top plate, as well as allowing the entry of the rod, has two 500A water-cooled current feed-throughs to supply the element; these also remain cool during operation.

In the furnace side walls are let two standard 1" vacuum seals, one a viewing port, the other a thermocouple entry. The viewing port looks directly at the element mesh (through slots spark-eroded in the molybdenum shields) to allow an optical pyrometer to monitor the absolute element temperature. The thermocouple entry port also has spark-eroded slots through the molybdenum shields to enable a thermocouple to be placed in the immediate vicinity of the furnace element; the thermocouple is used to control the furnace temperature.

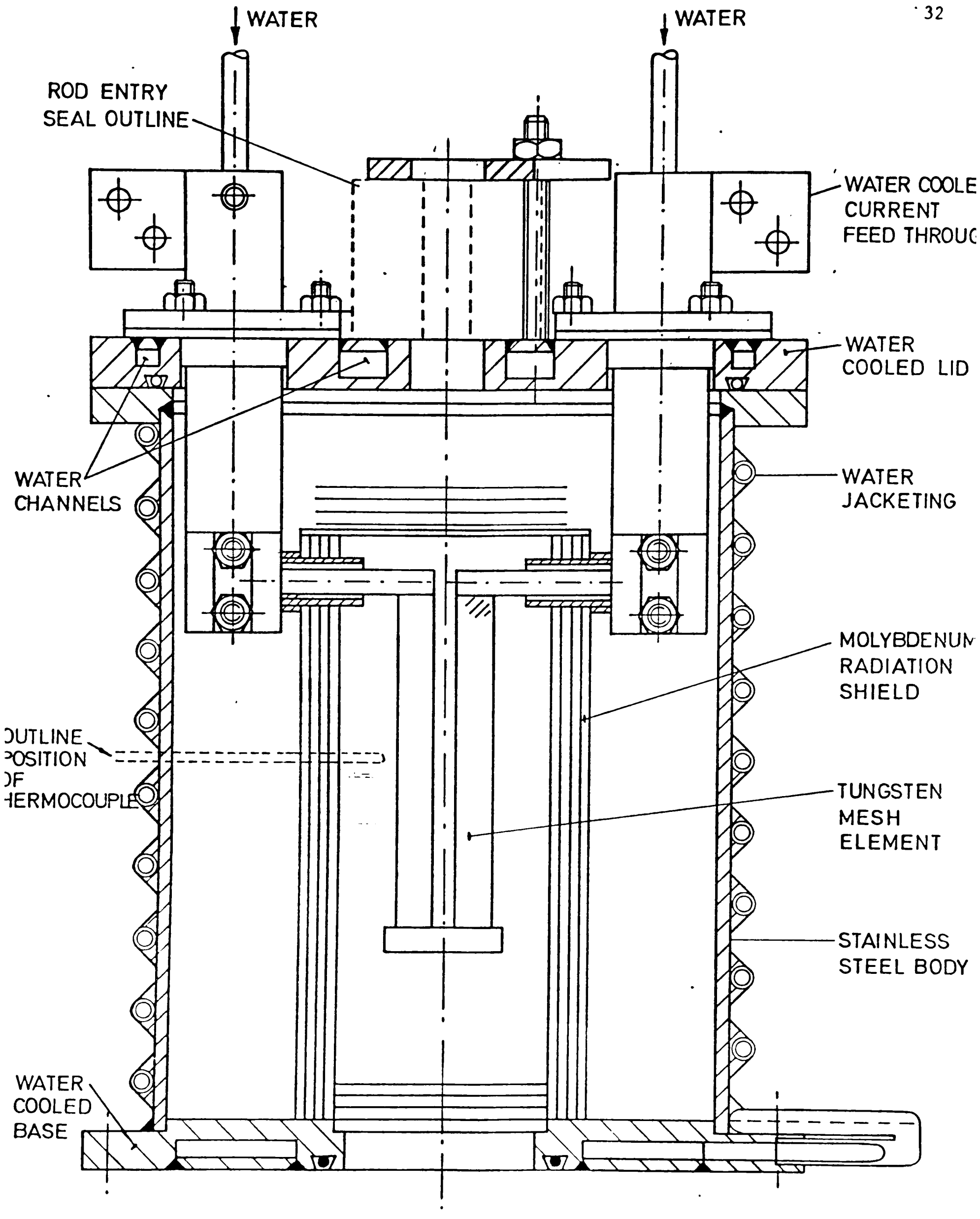


FIGURE 2-7

SECTION THROUGH TUNGSTEN MESH FURNACE

The furnace itself is bolted directly to a stainless steel plate which serves as a support for the upper half of the apparatus.

2.4 THE WINDING DRUM

The winding drum serves as a take-up spool and pull-off device for the drawn fibre, and is entirely contained within the evacuated volume. Before this choice was taken, various methods of passing the fresh fibre through a vacuum seal so that it could be wound in the atmosphere were considered, but were discounted for several reasons:

(i) if a Wilson Seal were used, the freshly drawn fibre would suffer abrasion passing through the seal;

(ii) passing the fibre through a column of mercury would increase the height of the apparatus to an impractical level, and limit the evacuated pressure to the vapour pressure of mercury;

(iii) any type of seal posed the problem of initially starting a pulling run: the drawn fibre would have to be passed through the seal. This was considered to be impractical.

The additional technical complexity of a winding drum within the evacuated volume was thus considered advisable. In practice the system as it stands works satisfactorily, with no detectable leak rate.

The drum itself has a circumference of 39.163cm, length 32cm, and was turned from a length of 12" diameter, $\frac{1}{2}$" wall seamless aluminium tubing. The variation in drum radius affects the diameter of the drawn fibre, consequently great care was taken to make the surface of the drum as smooth as possible, and to turn the drum on its true centre axis. The surface smoothness is better than 20μm and the eccentricity about the axis better than 40μm. If a constant drum angular velocity is assumed, the pulling speed is thus constant within 0.015% - insignificant compared to the error due to the drive mechanism.

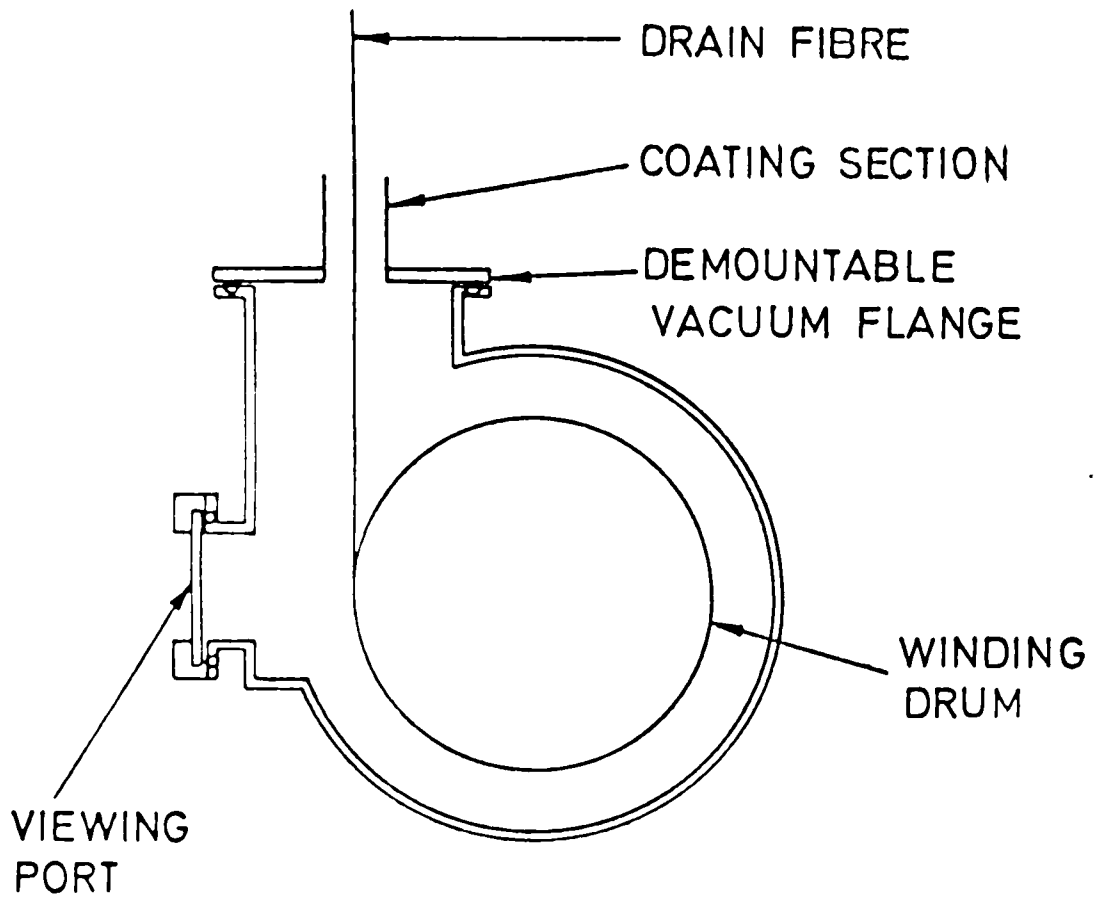
The drum is supported either end by precision spoked wheels, one of which is driven by the winding motor, the other is a sliding and rotational bearing of PTFE. As well as rotating, the drum must be translated during a pulling operation to avoid pile up of the drawn fibre over one portion of the drum and consequent diameter variation - hence the need for a translational bearing (figure 2.8).

Drive is achieved at the winding drum by means of a 12mm diameter stainless steel ground shaft which passes through the wall of the vacuum chamber by means of a standard commercial rotary and sliding vacuum seal; the driving mechanism is thus outside of the vacuum chamber. Rotary motion is achieved by a D.C. motor identical to the feed motor, via a 20:1 reduction gearbox. This gives a maximum rotation speed of 100 r.p.m., which corresponds to a pulling speed of 39m/min. Again, the motor speed is controlled using a closed loop thyristor controller with a tachogenerator coupled directly to the motor output shaft as a reference element. The motor speed regulation is ±0.5% of the desired setting.

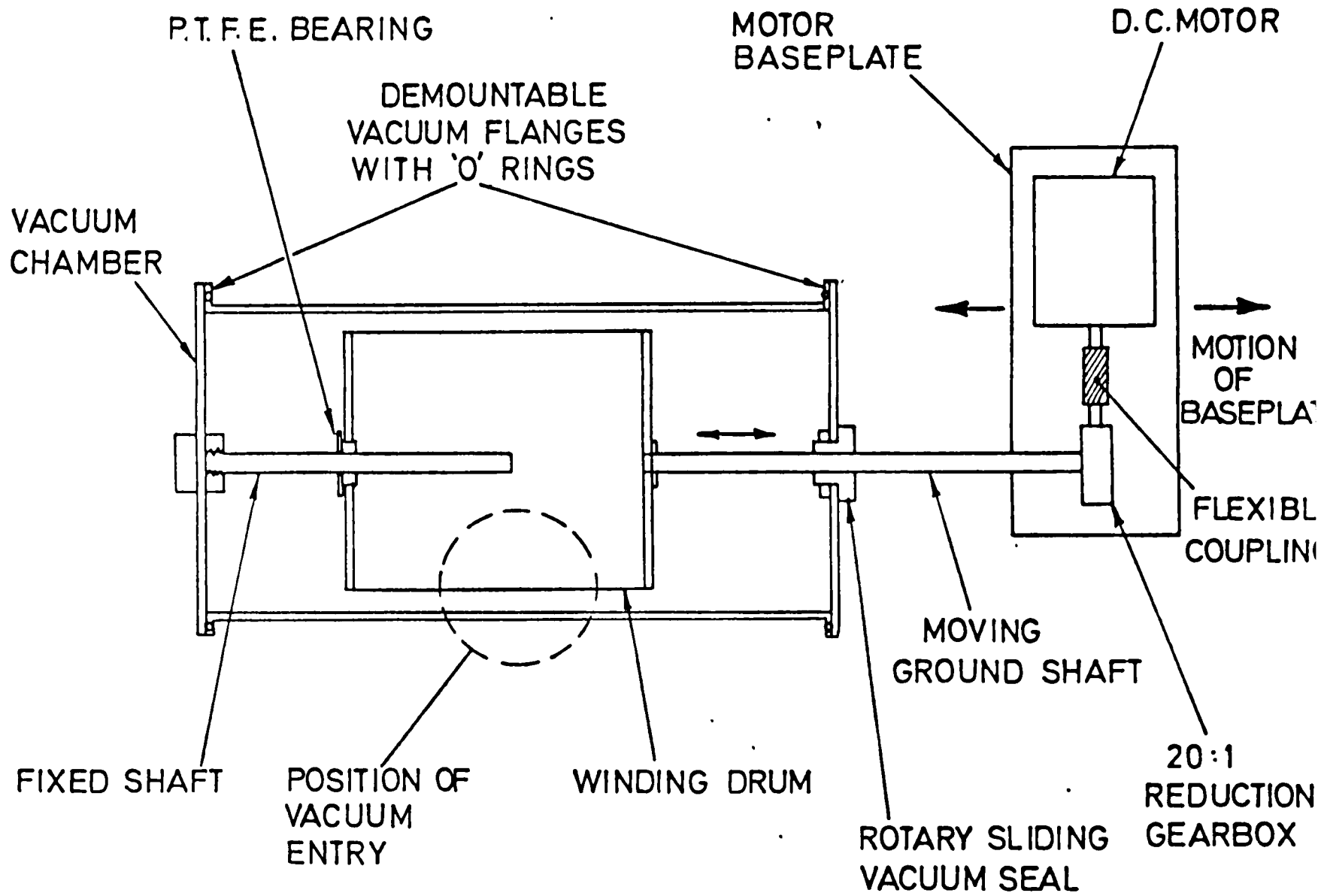
Winding drum translation is achieved by moving both drum shaft and motor drive assembly laterally. A small A.C. motor drives, via a reduction gearbox, a fine threaded leadscrew (20 t.p.i.) which moves the winding drum laterally to avoid pile-up of drawn fibre. The motor drive assembly is mounted on a plate which bears the leadscrew nut, and is guided by two parallel fixed cylindrical shafts. Sintered bronze bushes bear the weight of the plate. A simple control system relates drum translation to drum rotation (see Chapter 3.3).

2.5 THE VACUUM SYSTEM

The evacuated volume is comprised of the furnace, winding drum chamber, and a coating tube which joins the two. This tube also joins the vacuum pumps to the main evacuated volume via a six inch



SECTIONED SIDE VIEW



SECTIONED TOP VIEW

FIGURE 2-8

WINDING DRUM MOTION AND VACUUM SEALS

diameter stainless steel tube (figure 2.1). All seals, with two exceptions, are conventional elastomer 'O' ring seals, and are indicated in figure 2.1. The other seals are the rod entry seal and winding drum shaft seal, both previously described.

The total evacuated volume is quite large, consisting of:

1) Furnace - approximately $0.003m^3$
2) Coating tube - approximately $0.001m^3$
3) Winding drum - approximately $0.14m^3$
4) Piping - approximately $0.0075m^3$

In total this amounts to $0.219m^3$. The available vacuum pumps were a six inch oil vapour diffusion pump with a displacement of 650 L/sec and a two-stage rotary/backing pump of displacement 1.88L/sec at atmospheric pressure. Although this is not an ideal combination of pumps, an ultimate vacuum of 1.5×10^{-6} torr is achievable with a total pump down time of about two hours. The ultimate pressure corresponds to a mean free path of approximately 250m. It should be noted that an improvement in pumpdown pressure could be achieved by using a cooled vapour trap, but that this was not considered necessary on economic grounds; in any case backstreaming is reduced because the fibre melting and coating zones are optically baffled from the diffusion pump. If necessary a liquid nitrogen vapour trap may be added easily at a future date.

The system pressure is monitored by three gauges:

(i) a Pirani gauge in the backing/roughing line (gauge A in figure 2.1). The gauge functions as a safety device - the furnace automatically shuts down if the foreline pressure rises above a predetermined value.

(ii) A Pirani gauge in the main evacuated volume (gauge B in figure 2.1). This gauge establishes when the critical pressure for the diffusion pump has been reached and determines when to change from using the roughing system to the diffusion pumping system.

(iii) A Penning gauge in the main evacuated volume (gauge C in figure 2.1). This gauge monitors the main system pressure and establishes when a drawing operation may be started. The gauge measures a pressure somewhat remotely from the regions of interest (the furnace, from a safety point of view, or the coating tube). However a calibration curve of indicated Penning pressure versus actual furnace pressure (measured with an accurate ionisation gauge has been prepared (figure 2.9).

The 'coating tube' is described later (Chapter 4).

2.6 SUPPORT FRAME

The apparatus is split vertically by a stainless steel baseplate on which sits the furnace. The baseplate also supports the feed mechanism, mounted approximately one metre above; this allows preforms or rods of this length to be fed into the furnace.

The baseplate is supported by four braced aluminium angle sections, onto which is mounted the winding drum assembly. This consists of the winding drum, vacuum chamber, and rotational and translational motors mounted on a removable subframe which can be removed in its entirety to facilitate servicing, alignment and modifications. To facilitate removal of fibre from the winding drum, the drum and its vacuum chamber can be rotated or tipped forward about its axis, allowing access to the fibre via the drawn fibre vacuum flange.

Directly beneath the baseplate is hung the vacuum piping to the rotary and diffusion pumps. The diffusion pump is supported by the baseplate support frame, whilst the rotary pump simply rests on the laboratory floor. Vibrations from the rotary pump are eliminated from the apparatus by a flexible vacuum bellows; the apparatus does not shake significantly when the rotary pump is in operation. All

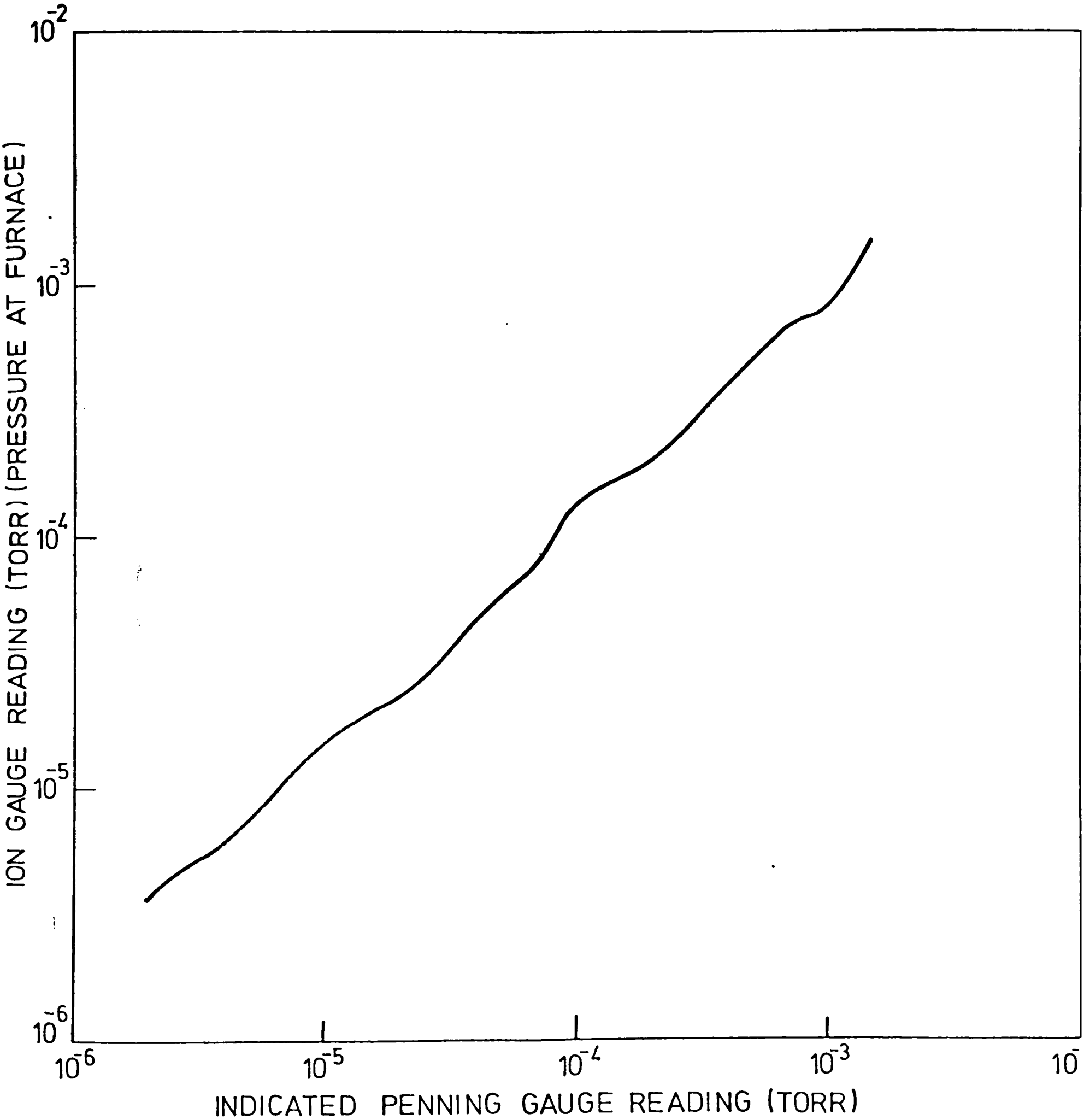


FIGURE 2-9

PENNING GAUGE CALIBRATION (DRY AIR)

electrical drive motors are also isolated against vibration by resilient mountings and flexible shaft couplings.

2.7 FIBRE OFF-WIND APPARATUS

Unlike conventional fibre drawing machines, the fibre winding or take-up drum cannot easily be removed from the apparatus, and it is thus necessary to unwind the produced fibre rather than simply replacing a full winding drum with one that is empty.

Figure 2.3 illustrates the solution to this problem. To remove fibre from the winding drum, the apparatus is let up to atmospheric pressure, the winding drum vacuum flange released and the chamber tipped forward. A secondary storage drum is positioned as illustrated, the fibre attached to it with tape, and the winding drum set in reverse motion, at constant speed. The secondary drum is rotated by a small A.C. motor via an elastic band which can slip on the storage drum shaft pulley. Thus, as the winding drum releases its fibre, the storage drum turns accordingly, but is effectively torque limited (the torque limit can be varied by altering the power supplied to the A.C. motor, and by lubricating the elastic band).

Although this seems a crude system, it is very simple and effective, allowing unwinding at approximately 150-200m/hr, with little stress applied to the fibre.

CHAPTER THREE

DESIGN AND CONSTRUCTION OF THE FIBRE DRAWING APPARATUS: ELECTRICAL AND CONTROL

3.1 INTRODUCTION

This chapter describes the control console, photographed in figure 3.1, and the methods used to define the conditions during a fibre drawing experiment. The control console is divided into separate racks, each individually powered via a power distribution rack, which control and measure the various functions of the system.

3.2 POWER DISTRIBUTION

The power distribution rack (schematic circuit diagram figure 3.2) accepts incoming mains power (250V AC, single phase), distributes the power to other racks and provides fusing. Considerable current is used during a drawing operation (approximately 25A), the furnace in particular consuming 5kW. Because of the fragility and cost of the furnace element, power is applied to the element via a contactor, which avoids the need for the protection circuits used to shut down the furnace should a major fault occur to handle the full furnace current. These protection circuits are more fully described in the following sections.

3.3 DRAWING MOTORS' CONTROLLERS

The feed and winding drum rotation motors are identical ½H.P. D.C. motors with integral tachogenerators. Commercial closed loop speed controllers are used for each motor, with variable armature current delivered by a phase controlled thyristor bridge; field current is fixed, being full wave rectified mains voltage.

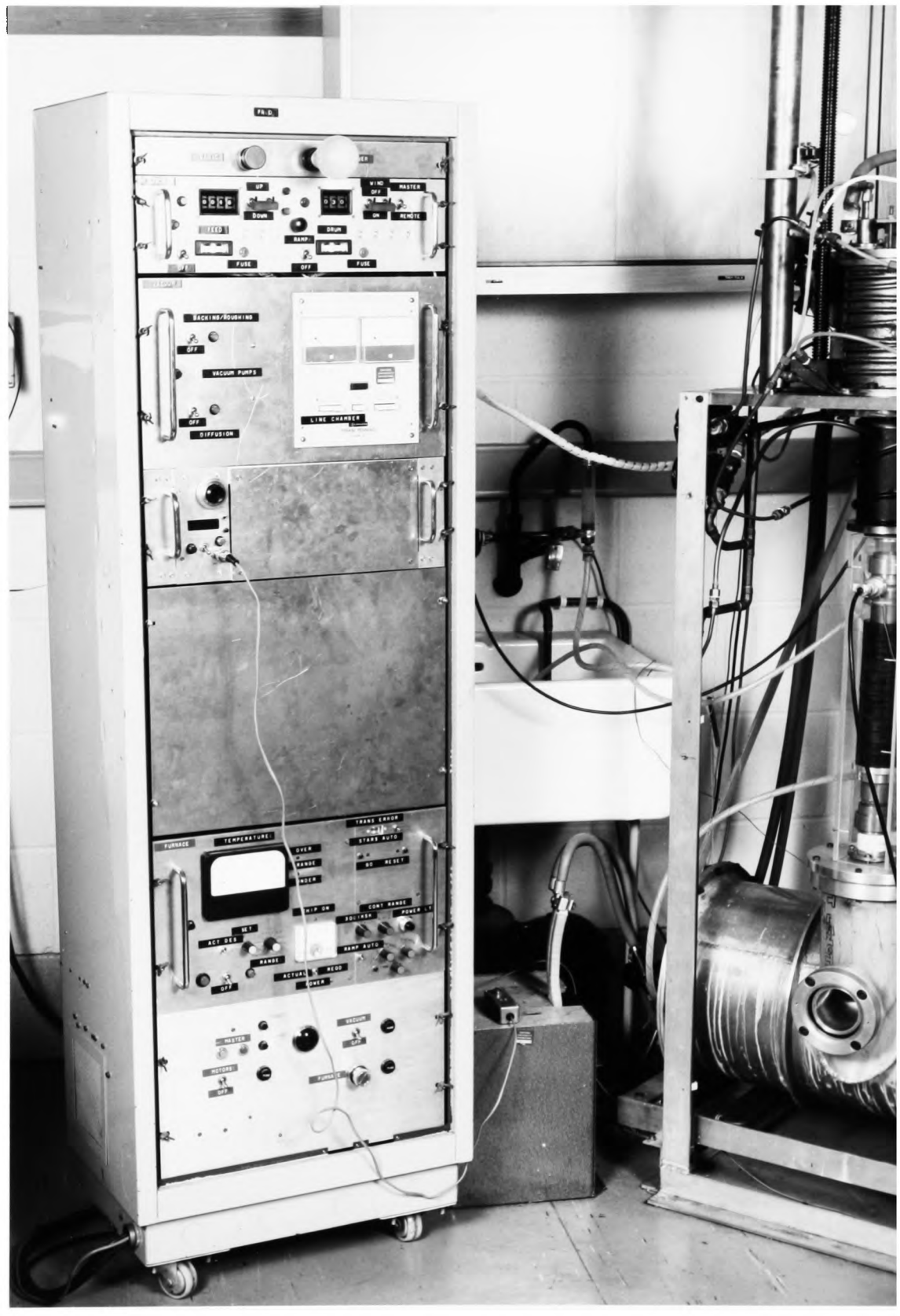


Figure 3.1 View of Control Console

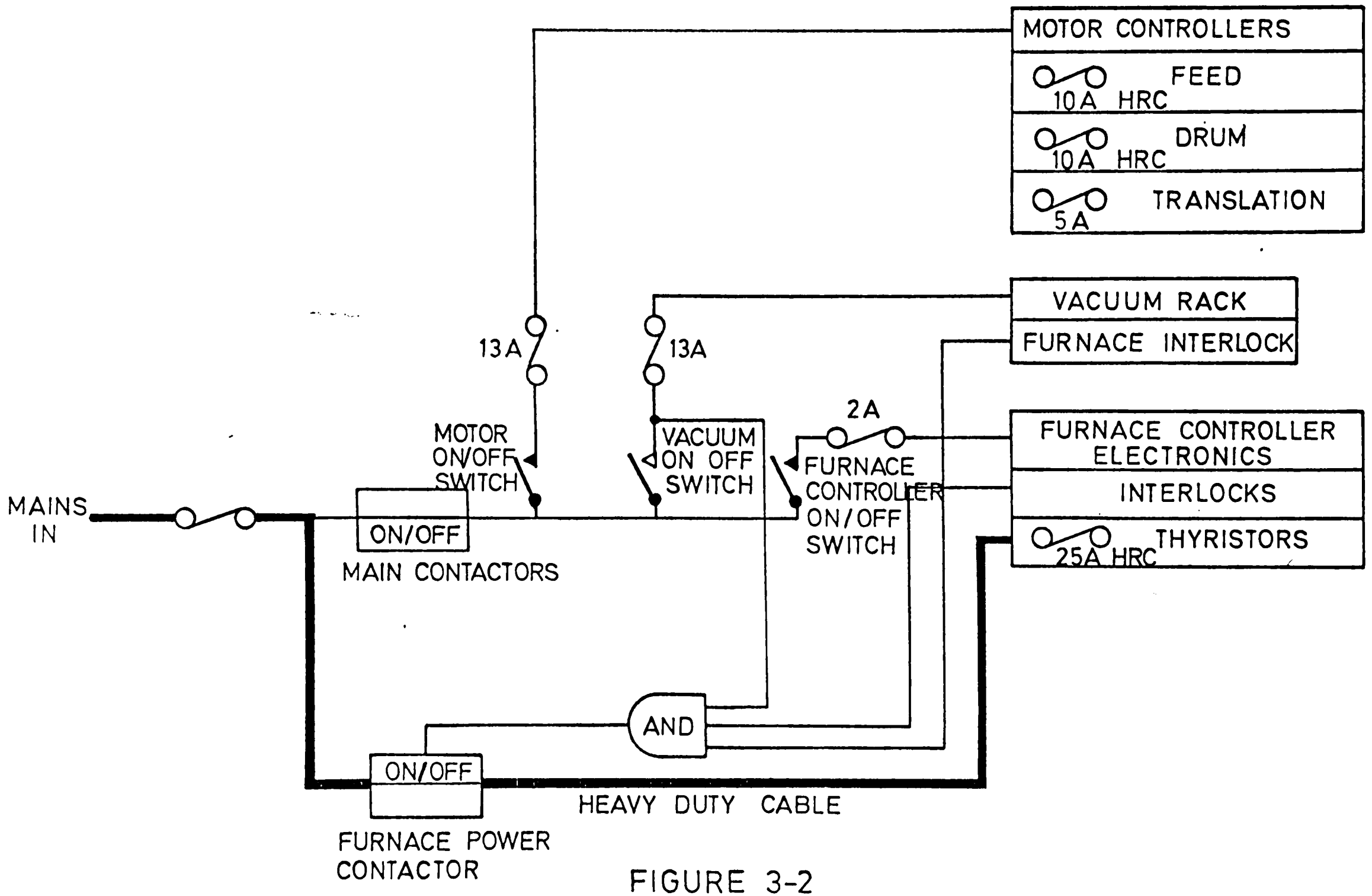


FIGURE 3-2

SCHEMATIC POWER DISTRIBUTION CIRCUIT DIAGRAM

The feed motor speed is controlled by a four digit thumbwheel switch, calibrated in rod feed rate, mm/min, which taps a reference voltage derived from a zener stabilised supply. This voltage, representing the desired feed rate, is compared with the output from the feed motor tachogenerator, and the error fed into a two term proportional-plus-integral controller which determines the required armature current for any desired speed. A deviation meter is provided which indicates error in desired speed with full scale readings ±10%. The accuracy of the unit is ±0.5% of desired setting. A ramp function generator is also provided within the unit, providing ramp acceleration and deceleration to limit switch-on surges and enabling smooth speed changes to be made. The ramp rate is varied via a front panel potentiometer and is adjustable between 2-20 seconds to full desired speed. Also on the front panel are mounted pre-set potentiometers to vary gain control for optimal response, calibration trim and torque limit. The feed motor is automatically shut down when the moving crosshead reaches the extremes of its travel by means of limit microswitches.

The winding drum rotation motor controller is identical to the feed motor controller except for two points:

(i) it has no ramp function generator (but see (ii))

(ii) it derives its reference (desired speed) voltage from either the desired feed speed voltage or a separate stabilised supply. This arrangement allows the winding drum motor to run at a speed proportional to the feed speed, or remotely. We have seen in section 2.2 that

$$\frac{S_p}{S_f} = \left(\frac{r_f}{r_p}\right)^2$$

so that this arrangement allows the pulling speed to be changed by one adjustment, the fibre diameter remaining constant, and both motors changing speed smoothly and at the same rate because

of the ramp generator. In the 'remote' position, the winding drum motor can be operated separately from the feed motor; this is useful for removing produced fibre from the drum, when no feed motion is necessary. The thumbwheel speed selection switch for this motor is calibrated in percentage of feed speed x 1000 in the 'slave position', and in m/min in the 'remote' position. Figure 3.3 shows a schematic diagram of the controller.

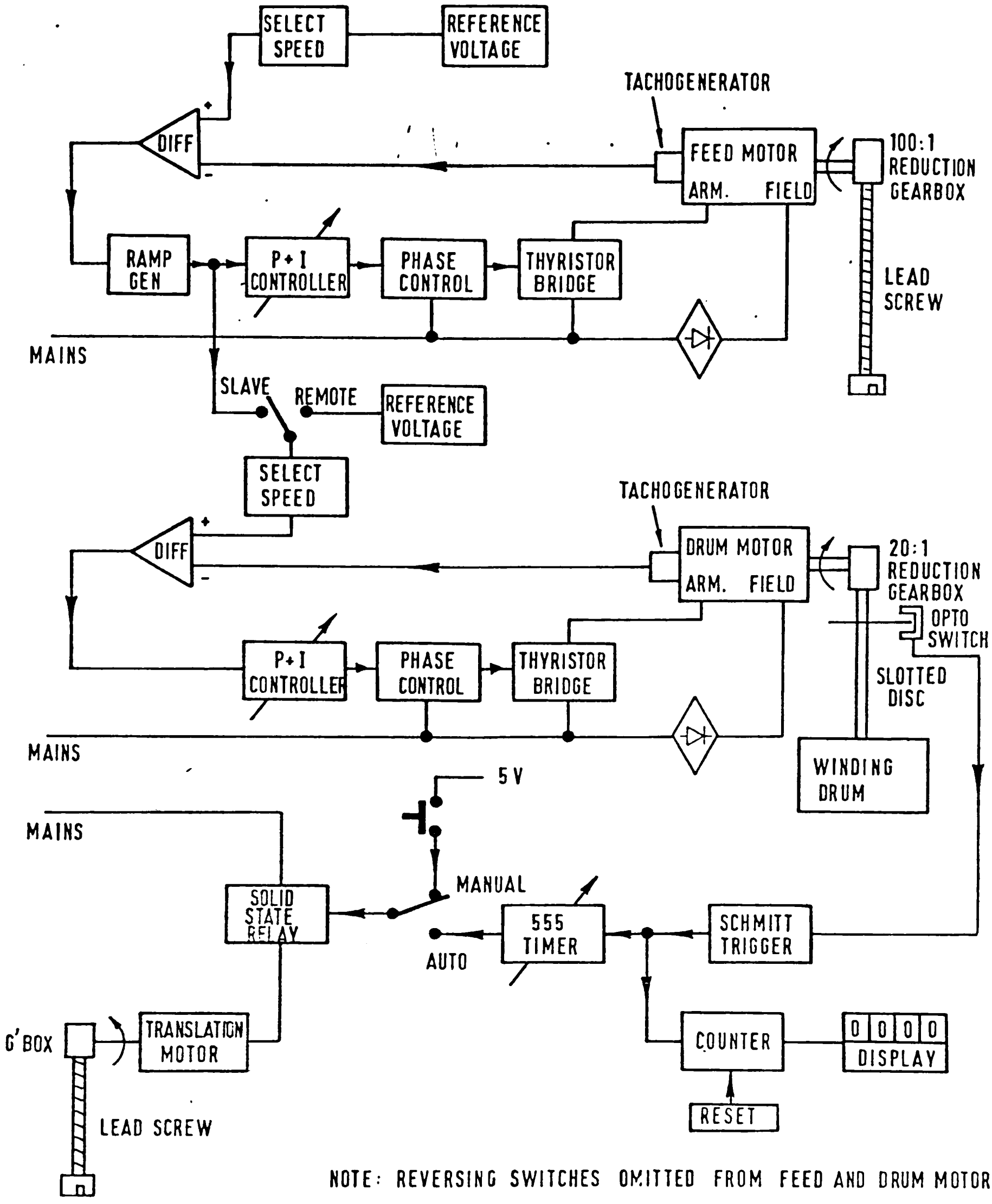
3.4 TRAVERSE MOTOR CONTROLLER

The linear motion of the winding drum is linked to the rotation. An arm attached to the winding drum motion shaft breaks the path of light between an L.E.D. and an optical detector once every drum revolution. The output from the detector is used to 'fire' an integrated circuit timer whose output is connected to the traverse motor via a solid state relay. Thus, once every drum revolution, the drum is traversed a distance determined by the timing constant of the timer, which is adjustable by a ten-turn potentiometer mounted on the front panel. The input to the solid state relay can be overridden by a hand-held push button to enable continuous motion.

The output from the optical detector also drives a digital display indicating the number of turns the winding drum has made, indirectly showing the length of fibre produced.

3.5 FURNACE CONTROLLER

The furnace controller is shown schematically in figure 3.4, the functions of each block being described separately below. The controller was built within the Department, partly by a third year undergraduate as a project, and partly by the author. It was decided to build the controller in-house as it was desired to incorporate a



NOTE: REVERSING SWITCHES OMITTED FROM FEED AND DRUM MOTORS.

FIGURE 3-3

SCHEMATIC MOTOR CONTROLLER CIRCUIT DIAGRAMS

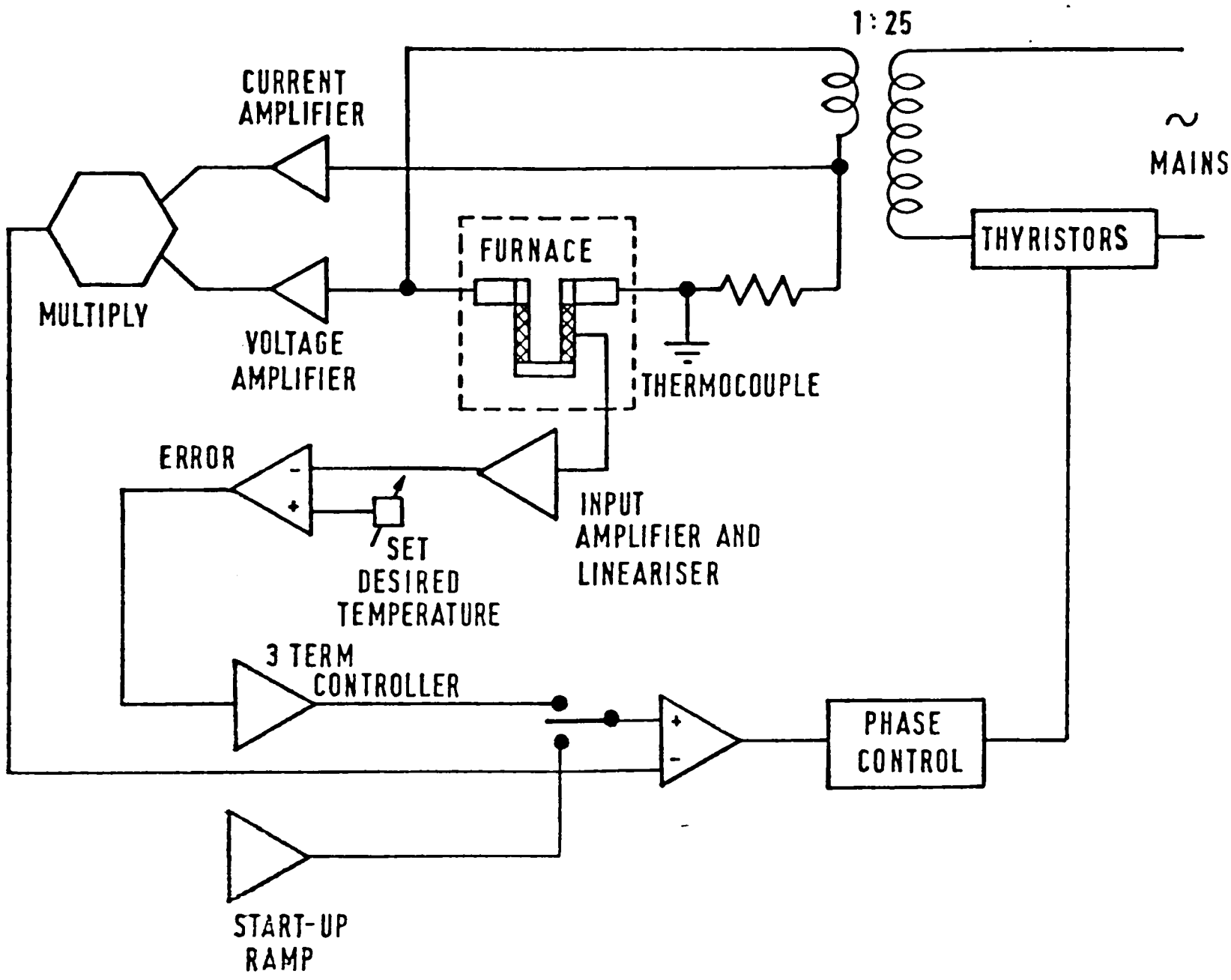


FIGURE 3-4

FURNACE CONTROLLER: PRINCIPLES

number of protection circuits for the element, which is rather sensitive to thermal shock.

3.5.1 General Description

The requirement of the controller was for a system that could control the temperature of the 5kW woven tungsten element used in the vacuum furnace, at temperatures up to approximately 2,200°C. The exact upper limit of temperature that the furnace would be called upon to produce was uncertain at the outset of the design as, although silica begins to soften at around 1200°C, the required viscosity for pulling and thus pulling temperature, could only be estimated (see table 3.1 and comments below). Also, within the vacuum, the only mechanism for heat transfer between the element and the preform rod is by radiation; consequently the element is at a considerably higher temperature than the preform during a pulling operation. However, the absolute temperature attained is not very important and more emphasis was placed on the stability of the temperature (making experiments easily repeatable) than on determining its value.

Initially great difficulty was envisaged with the temperature sensor itself; transducers for temperatures over 2,000°C tend to be expensive, unreliable and fragile. Various means were considered; most obvious is a thermocouple, which is in fact what is used. Also considered were:

(i) using a slave furnace with some form of proportional heating, so that a lower temperature can be measured. This was disregarded as both costly and difficult to construct.

(ii) Using an optical pyrometer with electrical readout. This was disregarded as too costly.

(iii) Using a photo diode array with known calibration curves. This would be a project in itself and suffers from the same drawback as (ii), as it is an optical method.

(iv) Measuring the resistance of the element itself in real-time, and, with the help of a table, a calibration curve can be worked out for its temperature. This last method is quite elegant, and could be easily adapted into the existing controller, but a thermocouple was chosen for simplicity.

The thermocouple chosen is a commercial tungsten 5% rhenium/tungsten 26% rhenium, molybdenum sheathed, insulated type which is situated ¼" away from the tungsten mesh (see figure 2.7). It was a little doubtful what meaning the reading of the thermocouple would have; thermocouple output versus mesh temperature (as measured by an optical pyrometer and furnace axis temperature (as measured by a second thermocouple) is plotted in figure 3.5. It can be seen that the control thermocouple output bears little relationship to either of the other two variables. However, as mentioned before the absolute temperature of little importance, and variations in temperature are reproduced by the thermocouple at the temperatures of interest ($\simeq 1700^{o}C$).

The element itself also presented a major problem. The cold resistance is around 1mΩ; this increases to about 20mΩ when hot. Thus, initially if a constant voltage were used the 'start up' current would be 20 times the running current and the element could be subjected to a serious thermal shock. During warm-up, care must be taken to ensure that the current drawn is not excessive in order to protect the element.

Due to the variation in resistance with respect to temperature and the need for careful monitoring of the power delivered to the element, it was decided that a separate control system would be needed for the power into the element. As this power is obtained from the secondary of a 250:10 volt transformer (with 500A at 10V AC capability), no problems of isolation occur if the voltage across, and the current through the element are measured directly.

In order to measure the current through the element, the voltage

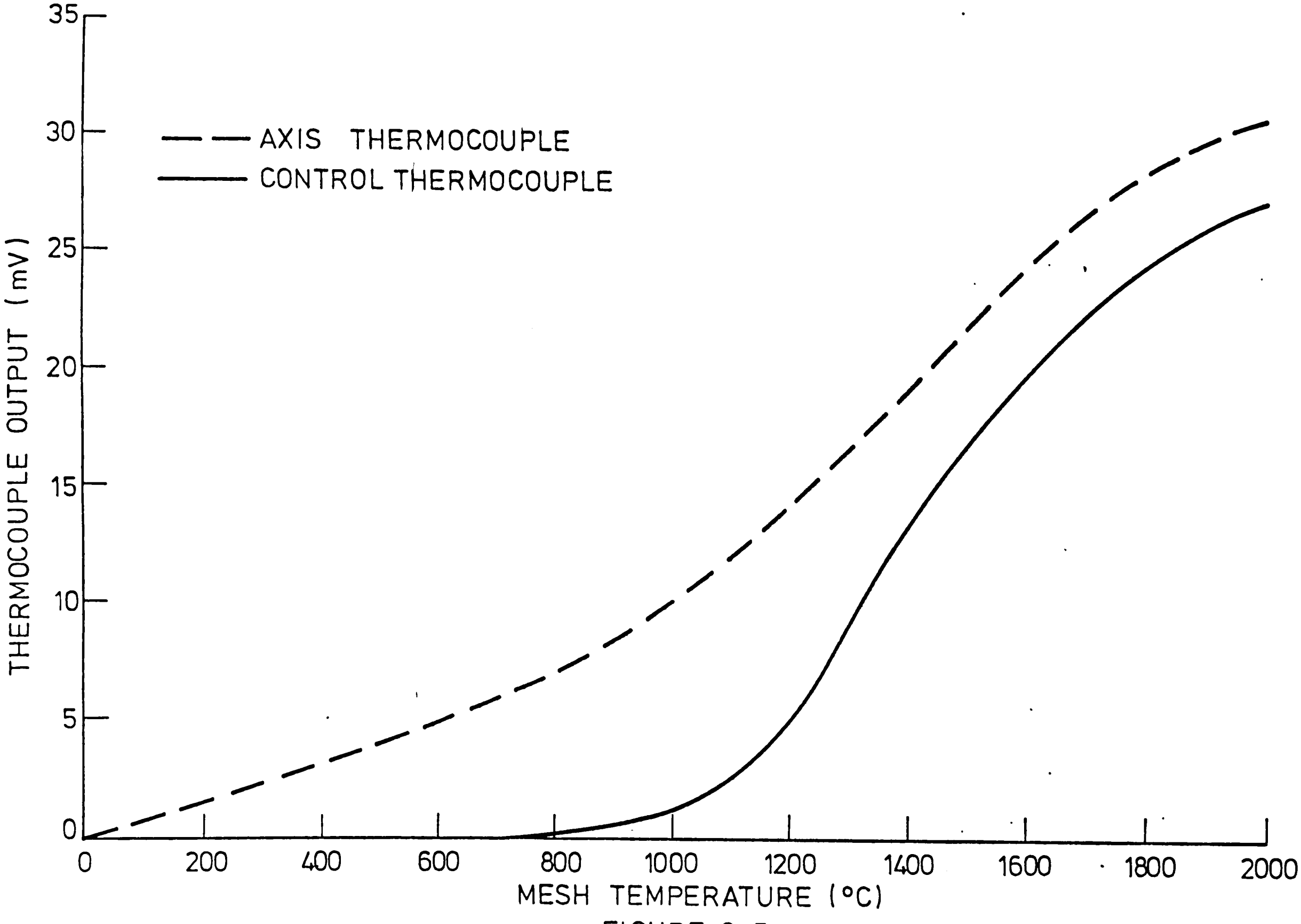


FIGURE 3-5

CONTROL AND AXIS THERMOCOUPLE. OUTPUTS VERSUS MESH TEMPERATURE (OPTICAL PYROMETER MEASUREMENT)

across a known resistance in series with the element could be measured, or a current transformer wound round the cable to the element could be used. The latter method was initially preferred as a resistor capable of taking 500A without change in resistance was thought too difficult to construct. However, the calibration of a current transformer and its initial construction dissuaded us from this course and so a resistor of nominal value 0.2mΩ using the '4 terminal' principal was designed and constructed. The main current-carrying cable is bolted on to the ends of the resistance and light sensing wires soldered directly in place along the device to obtain the required resistance exactly. Brass rather than copper was used as this has a lower temperature coefficient of resistance. The actual value of the resistance is 0.178mΩ and in practice its temperature does not rise above 50°C in free air; this represents a change of about 5% in resistance - sufficient accuracy for our needs.

Notes on the viscosity of silica

The kinematic viscosity of silica at various temperatures is as follows (Ref: Kaye & Laby):

T:	1100	1200	1300	1400	1600	1800	2000	°C
η:	14.6	12.7	11.8	9.7	8.2	4.7	3.5	$\log_{10}\eta$ in Nsm^{-2}

It is difficult to accurately work out a theoretical viscosity for optimum pulling conditions, but if we compare these values with that of ordinary glass at about 900°C, (the temperature reached in a Bunsen flame), a rough order of magnitude can be estimated. At 900°C flint glass has a $\eta(\log_{10})$ of 3.9 Nsm^{-2}. At this temperature it is possible to pull the glass quite effectively. Note also that between 1600°C to 1800°C silica undergoes a rapid drop in kinematic viscosity, and it is reasonable to assume a required temperature of at least 1800°C and probably 2000°C. (Thus a maximum of 2,500°C is reasonable for the furnace.)

The following sections refer to figure 3.6.

3.5.2 Thermocouple, Input Amplifier and Linearizer

The thermocouple output voltage is amplified by IC1, an instrumentation operational amplifier Type μA725 with a gain of about 200 giving an output voltage of about +10V at 2300°C (adjustable). The input circuit also incorporates a noise filter to remove interference, and an offset circuit to remove any error due to the reference junction of the thermocouple not being at the same temperature as that required by the given calibration curve. The output of the input amplifier also goes to a logic circuit which senses whether the thermocouple has become open circuit and shuts down power to the element.

After being amplified, the thermocouple output voltage is linearized by IC2 - 3 and TR1-6 which adjusts the output of IC1 so as to represent a linear function of input temperature. This is a conventional circuit, the transistors switching the gain of the circuit at selectable voltages. The input can thus be approximately linearized by a straight line fit of seven segments over the thermocouple output range. This system works quite well and good linearity is achieved above 1000°C (within 1%, see figure 3.7). The output is scaled such that

$$-6.66V \equiv 0^{\circ}C$$

$$0V \equiv 1000^{\circ}C$$

$$+10V \equiv 2500^{\circ}C$$

This enables desired voltage to be selected by a simple 10 turn potentiometer with resistance extremities at 0V and +10V.

3.5.3 Temperature Indication

A front panel switch selects either desired or actual temperatures. IC7 subtracts the voltage corresponding to temperature from a switchable reference voltage derived from a chain of matched resistors, the voltages

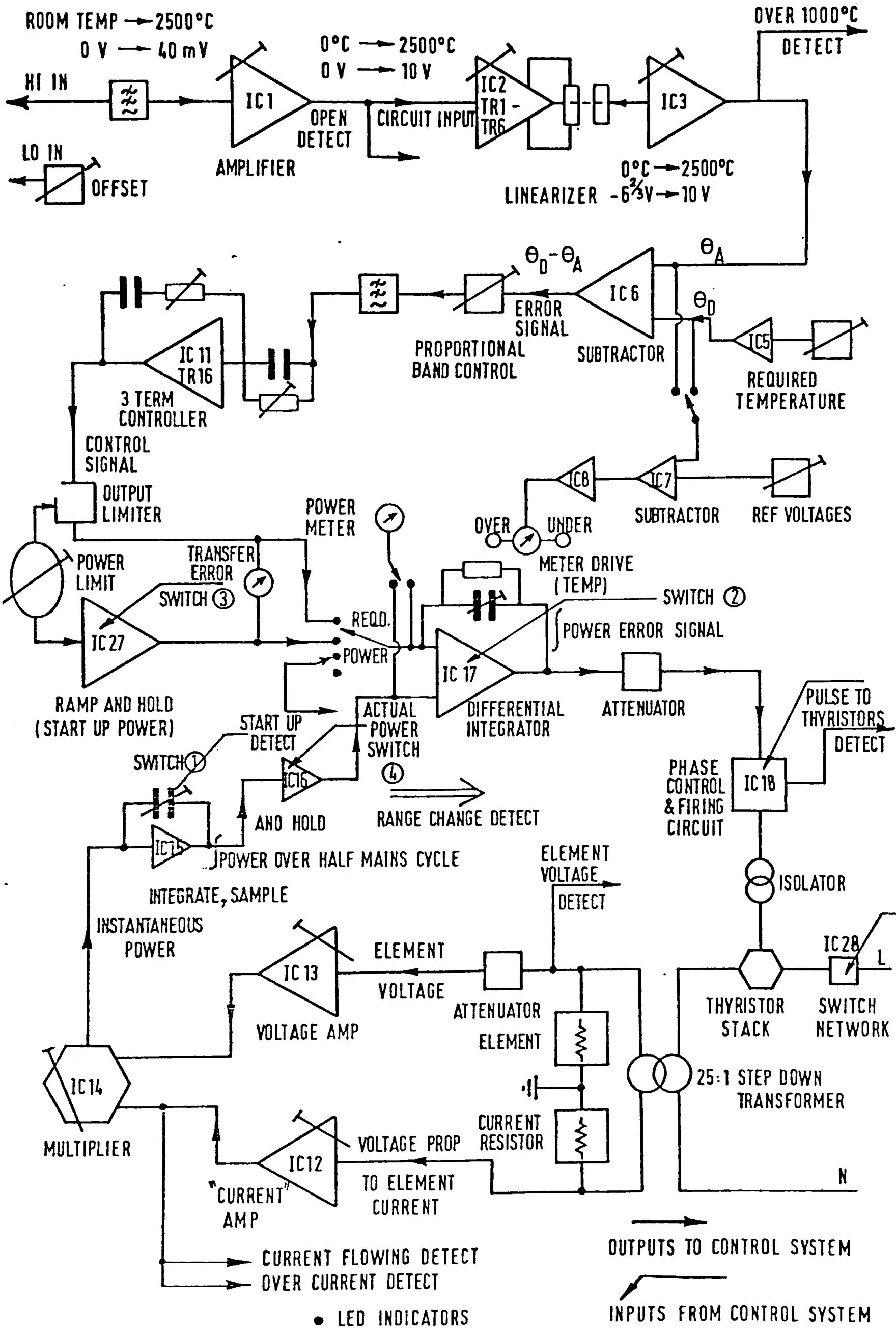


FIGURE 3-6
FURNACE CONTROLLER SYSTEM DIAGRAM

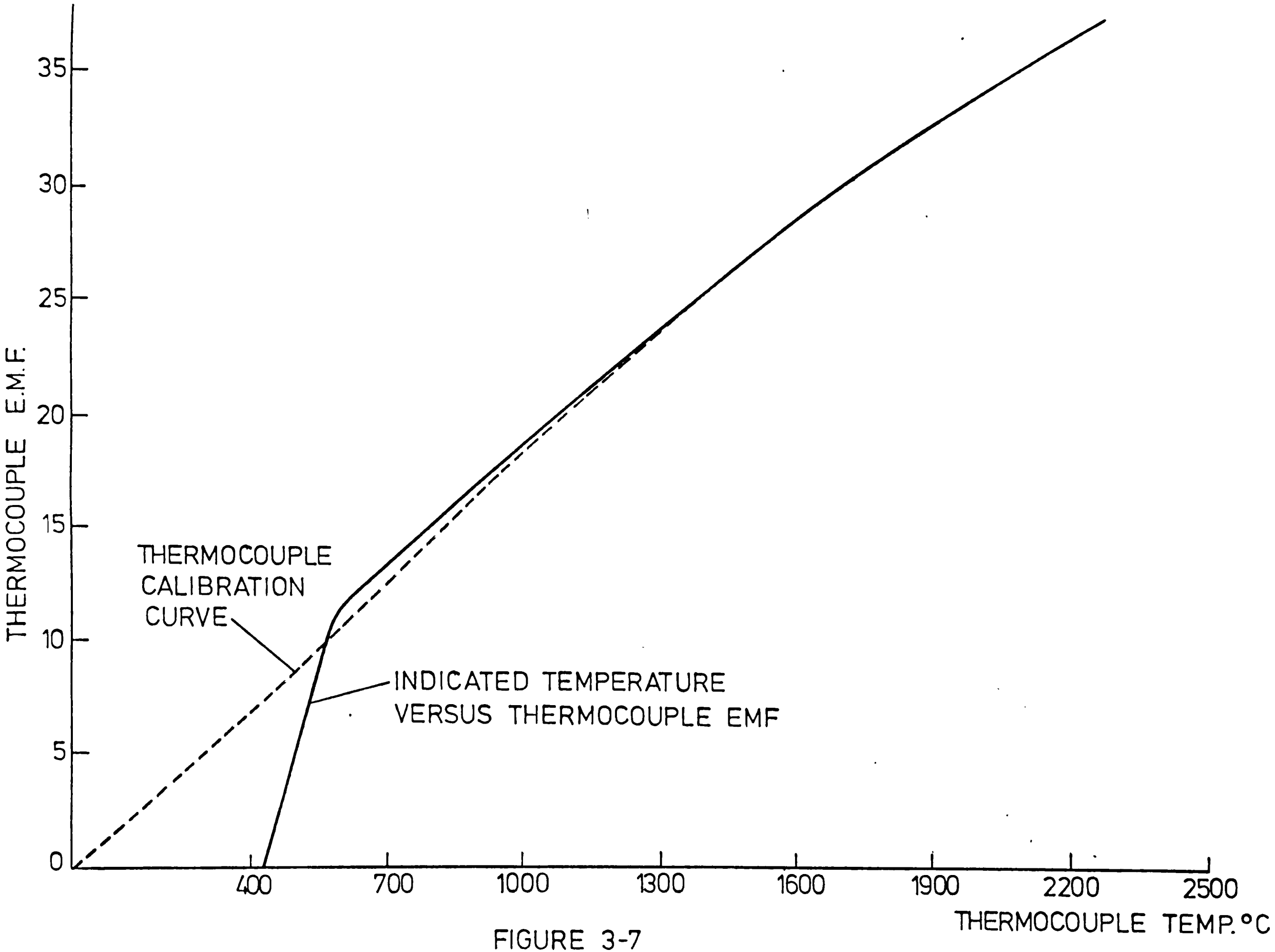


FIGURE 3-7
THERMOCOUPLE LINEARIZER CALIBRATION CURVE

at each switch position corresponding to the bottom end of the temperature range associated with each switch position. IC7 thus supplies a signal proportional to the amount the input signal is from the bottom end of the temperature range selected. This signal is buffered by IC8 which drives the temperature indication meter. Light emitting diodes indicate whether the temperature range selected is either under-range or over-range.

3.5.4 3-Term Controller

The error signal output from IC6 is fed to a simple 3-term controller with variable transfer functions of the form:

$$\frac{V_o(s)}{V_i(s)} = K_1 + \frac{K_2}{s} + K_3 s. \qquad (3.5.1)$$

The controller is built round a quad operational amplifier type LM324, 3 amplifiers performing the proportioning, differentiating and integrating functions of equation (3.5.1) and the fourth summing the output. The gain and time constants of the controller are variable as the characteristics of the furnace were not known at the time of construction. The range of adjustable parameters is listed below:

proportional band: $25^{o}C \rightarrow 1000^{o}C$

integral time constant: $1sec \rightarrow \infty$

differential time constant: $0 \rightarrow 2sec$

The output from the controller is negative going for increase in error and is prevented from going positive by a diode. The output of the controller can be limited to any desired value by sinking the output current in a transistor, the base voltage of which is variable. This is useful for preventing any power surges.

3.5.5 Start-up Ramp and Comparator

Initially, when the controller is switched on, the required temperature will be so much higher than the actual temperature that

the 3-term controller will attempt to deliver full power to the element. This, as has been said before, would very quickly burn out the element and so a very slowly rising ramp is generated as an alternative to the controller output, and is used to gradually warm up the furnace. The ramp is generated by integrating a small voltage difference (0.1 volt) with a long time constant RC circuit; the resultant ramp has a slope of about 1 volt per 5 minutes. The power limit circuit also operates on the ramp, in order that the furnace can be run up to a constant power level.

The difference in required power between the start-up ramp and controller can be compared by a simple centre zero meter. When the furnace has warmed up to (say) 1250°C, the controller gain potentiometer can then be adjusted so that the required controller power level can be 'matched' to the ramp power level and transfer between start-up mode to automatic mode is then bumpless. The change between start-up/automatic mode is made by a simple changeover toggle switch. This switch is also ganged so as to provide information to the logic circuits as to its position.

3.5.6 Power Measurement

The voltage representing the actual power in the element is derived by attenuating the actual voltage across the element (IC13), amplifying the voltage across the series current measuring resistance IC12, and multiplying the two together by means of a four quadrant multiplier IC14 (type AD533). The two signals are always of opposite polarity as the common point between the element and series resistor is grounded, and hence a negative voltage proportional to the instantaneous power in the element is obtained. This is then integrated by IC15 over 10ms or half a mains cycle, the integrator being reset just after the beginning of a new half cycle, because, except when full power is being delivered ot the element, there should be no signal

at this time. The voltage reached at the end of each half cycle is sampled and held by IC16, and represents the average power being delivered to the element. IC12-15 have complex switching circuits associated with them in order to change gains with differing conditions - differing power levels, and differing temperatures (change in element resistance).

The output from IC16 (average power) is metered (by means of a switch 'required power' can also be metered).

3.5.7 Output Circuit

The required power level and actual power level is compared by IC17, and the voltage proportional to their difference fed into the thyristor firing circuit IC18. This integrated circuit (type L120) is a self-contained phase angle firing IC which, for a variable DC input voltage, produces output pulses during each half of a mains cycle. Effectively the IC generates a voltage ramp commencing at the start of each mains cycle. When this ramp voltage reaches the level of the incoming signal, a pulse is produced of the same polarity as that of the mains half-cycle. As the ramp is linear, the time taken to reach the required switching voltage is a linear function of this voltage, and so the phase angle at which the thyristors are triggered is linearly dependent on the input voltage.*

The output pulses from the firing circuit are then steered by two diodes into two isolating pulse transformers, the secondaries of which are used to fire SCR1 and SCR2 during their appropriate conduction periods. The thyristors are in bridge configuration with series diodes in order to hold off reverse voltage. This is necessary as the two thyristors are rated at 400 PIV and reverse break over is undesirable.

---

* Within the L120, the input signal is inverted and level shifted otherwise OV input corresponds to full output.

The thyristors are protected by a high speed semiconductor fuse.

3.5.8 Protection Circuits

A number of furnace element protection circuits are incorporated within the controller. These are:

- thermocouple open circuit. This, via a relay, pulls out the furnace supply contactor.
- overcurrent. An alarm light emitting diode illuminates at about 400A, and at 500A the furnace supply contactor pulls out.
- auto / start-up switch. To enable the controller, the auto/ start-up switch must be in the start-up mode. Auto. mode can be selected only above 1200^{o}C to avoid thermal shock. The logic in this case inhibits the L120 firing circuit.
- operating range and indicated power. These switches must be in the 'low' (low element resistance) and 300 Watt ranges, i.e. a start-up mode. The logic in this case inhibits a 'GO' button which executes the start-up ramp.
- mains pulse missing. A monostable fired in synchronism with the mains supply inhibits the L120 firing chip if a pulse is missing.
- switches being operated. If any switch within the control loop is operated, the L120 is momentarily inhibited to prevent any contact bounce inadvertently switching the furnace full on.
- thyristors. The two driving thyristors are comprehensively fused.
- vacuum failure. Should the vacuum rise above a predetermined pressure, the furnace supply contactor pulls out. This is achieved by comparing the output voltage produced by the Pirani gauge in the diffusion pump backing line with a variable reference voltage, and using this output to open a relay in the furnace supply contactor's hold-on coil circuit.

3.5.9 Power Supplies

Five main isolated supplies provide power for the controller:

(i) -15V - 0 - +15V D.C. regulated for the operational amplifier supplies.

(ii) +5V DC regulated for the TTL integrated circuits.

(iii) -10V - 0 - +10V D.C. precision regulated for the temperature measurement circuits.

(iv) +20V D.C. smoothed for operating relays.

(v) 250V A.C. for the L120 phase firing circuit.

3.6 VACUUM CONTROL

The vacuum control rack provides switched mains power to both rotary and diffusion pumps, and incorporates a commercial Penning and Pirani gauge control unit. The rotary pump is provided with an electrically operated automatic air admittance valve which operates when the pump is switched off to avoid oil suck-back. The diffusion pump incorporates a thermal switch which shuts down the pump should the cooling water flow stop or rise above $40^{o}C$.

Pressure within the system is regulated by a precision needle valve mounted on the winding drum vacuum chamber. This allows a desired system pressure to be set by leaking in gas (generally argon for sputtering) from a cylinder at a precise rate whilst pumping is continued. The valve is situated such that a flow of argon through the coating device to the vacuum pumps is maintained.

CHAPTER FOUR

METALLIC COATING BY MAGNETRON SPUTTERING

4.1 INTRODUCTION

As briefly described in Chapter One, magnetron sputtering (M.S.) as a metal coating technique was chosen as the most promising method from a number of possible techniques. M.S. in commercial plants has proved a valuable and efficient method for metal coating in a number of fields, notably in the semiconductor industry for depositing metal contacts. For our application, M.S. offered the following features:

(i) of the vacuum techniques, it is capable of a very high deposition rate.

(ii) It is a directed technique and in the cylindrical form metal atoms not striking the substrate (fibre) strike the target and are available for resputtering.

(iii) A cylindrical high rate of M.S. device is readily constructed.

(iv) It may be used with a number of metals and alloys.

(v) Low substrate damage is reported for commercial devices.

The basis of a sputtering technique is an electrical discharge which is passed between electrodes at low gas pressure. The cathode electrode is slowly disintegrated under the bombardment of the ionized gas molecules, and the disintegrated material leaves the electrode surface (either as free atoms or in chemical combination with the residual gas molecules) and is condensed on surfaces surrounding the cathode unless returned to the cathode by collision with gas molecules.

Güntherschulze[28] has shown that the amount of silver Q_1 sputtered in hydrogen in unit time and at constant current density on to a receiver placed under a plane cathode was, for cathode falls below 1kV, inversely proportional to the gas pressure p and the cathode-

receiver distance, d, i.e.

$$Q_1 = \frac{k_o}{dp} \quad , \tag{4.1.1}$$

where k_o is a constant. Such a relationship would be expected to apply where the sputtered atoms, considered as a gas, reach the receiver by diffusing through the discharge gas. At cathode falls of greater than 1kV the sputtered atoms leave the cathode with considerable velocity and normal diffusion may only occur at large distances from the cathode. Equation 4.1.1 may be rewritten

$$Q_1 = \frac{K_1 Q_o}{dp} \tag{4.1.2}$$

where Q_o is the amount of sputtered material leaving the cathode, and K_1 is a constant. Penning and Moubis[29] have shown that $Q_1 = Q_o$, that is that all of the atoms liberated reach the receiver, when for many gas-metal pairs the value of dp is less than 0.01, where d is in cm. and p is in Torr. For values of $dp < 0.01$ the mean free path of the sputtered atoms have generally become comparable to or greater than the cathode receiver distance d.

Under normal depositions conditions dp is of the order of 0.1 - 0.4 and it is not possible to reduce this value without unduly increasing both the duration of the sputtering period and the size of the sputtering apparatus. When the pressure is decreased the cathode dark space, and thus the cathode to receiver distance, increase accordingly. Also, the current density at constant cathode fall is proportional to p^2 so that unless very high potentials are used, the current density is so small at low gas pressures that the sputtering period becomes excessive.

To overcome this difficulty, Penning and Moubis utilised a magnetic field to increase the path lengths of electrons, and consequently the amount of ionization (figure 4.1). At low gas pressures ($\sim 10^{-2} - 10^{-3}$ Torr) the electrons follow spiral paths under the

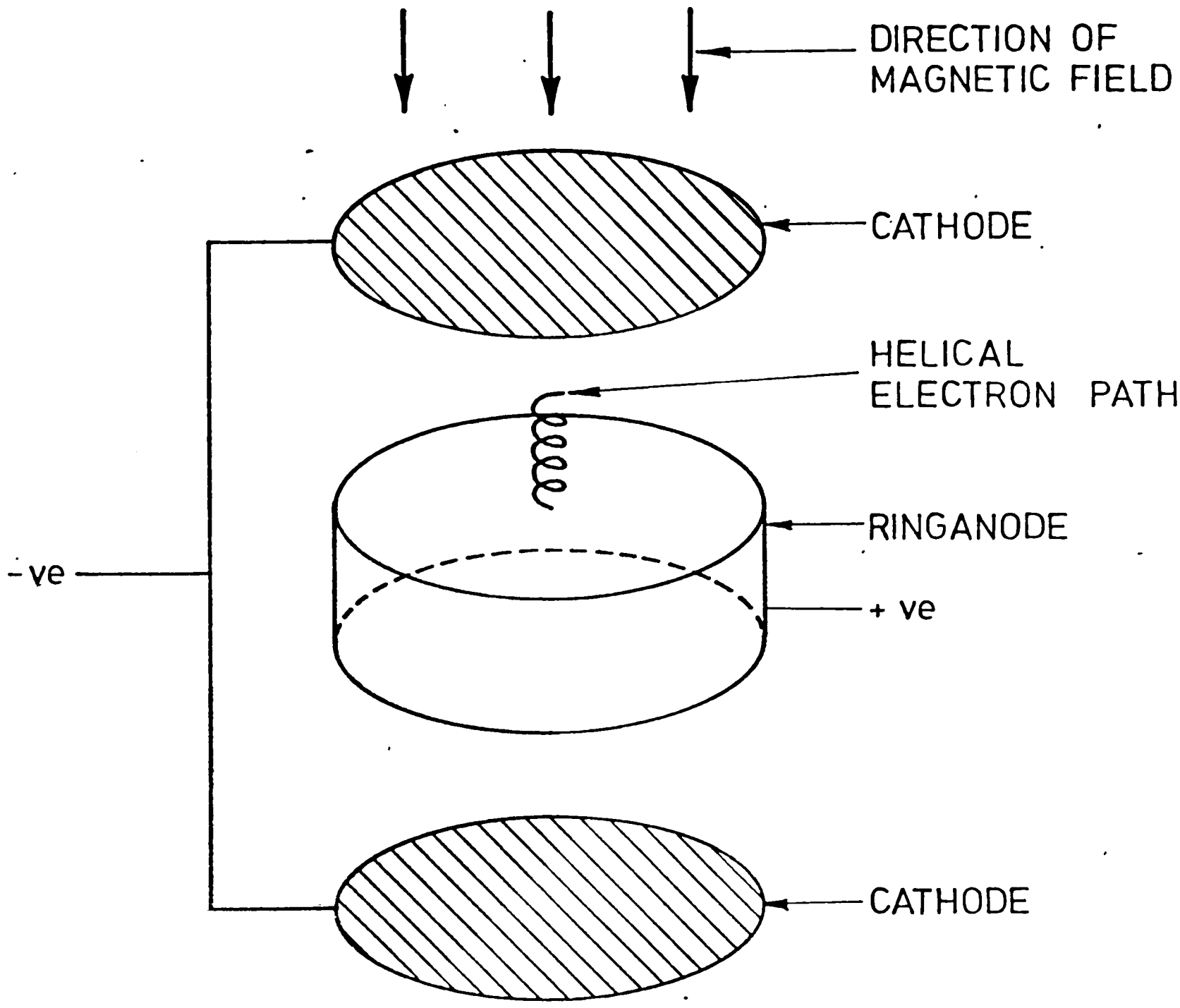


FIGURE 4-1

UTILIZATION OF MAGNETIC FIELD FOR SPUTTERING AT LOW PRESSURES (AFTER PENNING)

influence of the electric and magnetic fields, instead of travelling 'straight' between cathode and anode, and the probability of an ionizing electron-gas molecule collision is increased. The electrons are reflected at each cathode surface until they make an ionizing collision with a gas molecule and are 'bumped' off the magnetic field line on to the anode surface. Effectively the cathode dark space is not extended by pressure reduction and the size of the apparatus can be made compact. It should be noted that this form of apparatus is similar to that of the Penning vacuum gauge used extensively for the measurement of low pressures.

In the form of figure 4.1, the arrangement is not particularly suitable for deposition purposes. To obtain a coating on a plane surface, the object must be rested on the surface of one of the cathodes, where it is subjected to considerable electrical stress due to positive ions bombarding its outer surfaces resting on the negative electrodes (glass plates several millimetres thick may be punctured by the discharge). Holland partially overcame this defect by removing the central portion of one cathode and placing the substrate to be coated behind this annular cathode (see figure 1.5). However, much sputtered material is collected on the inside wall of the cylindrical anode.

Because the electrons must undergo ionizing collisions before escaping, the gas discharge may be sustained at very low gas pressures, and very high current densities may be obtained. The current density in a Penning device may be so high that such devices are often referred to as operating in the arc mode.

The large circular average motion of the electron in the Penning cylinder is termed the Hall drift. If a magnetic field is applied parallel to a finite plane, the Hall drift carries the electrons off to one side. The magnetron mode of operation is characterised by the magnetic field <u>emerging</u> from the cathode, becoming nearly parallel to

the surface, and returning into the cathode, with a closed magnetic field loop. By this means (referring to figure 4.2) electrons are trapped, as in the Penning device, by the magnetic field, and the probability of an ionizing collision is high, and high current densities are obtained. In this case, the substrate may be placed well away from the cathode, and substrate damage due to ion bombardment is minimised.

Much literature is available on the subject of M.S.; the reader is referred to references 26, 31, 32 and 33 for a more concise explanation.

4.2 DERIVATION OF CYLINDRICAL MAGNETRON SPUTTERING FOR FIBRE COATING

In order to design an effective cylindrical sputtering device, we need an estimate of deposition rate onto a fibre substrate. Figure 4.3 represents a small section dA_r of the receiving surface.

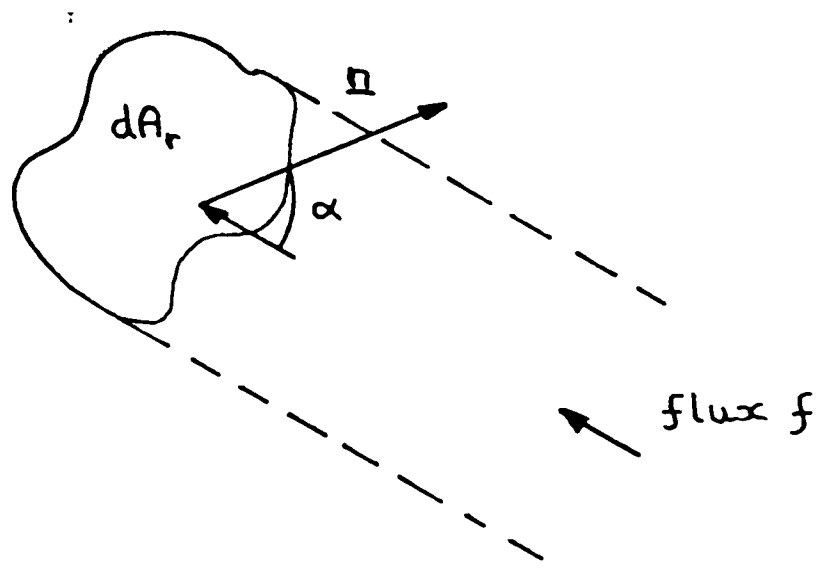


Figure 4.3

A flux f kg m^{-2} s^{-1} of material arrives at the receiving surface at an incident angle α to the normal $\underline{n}$ to the surface. The deposition rate d ms^{-1} is

$$d = \frac{f \cos \alpha}{\rho} \qquad (4.2.1)$$

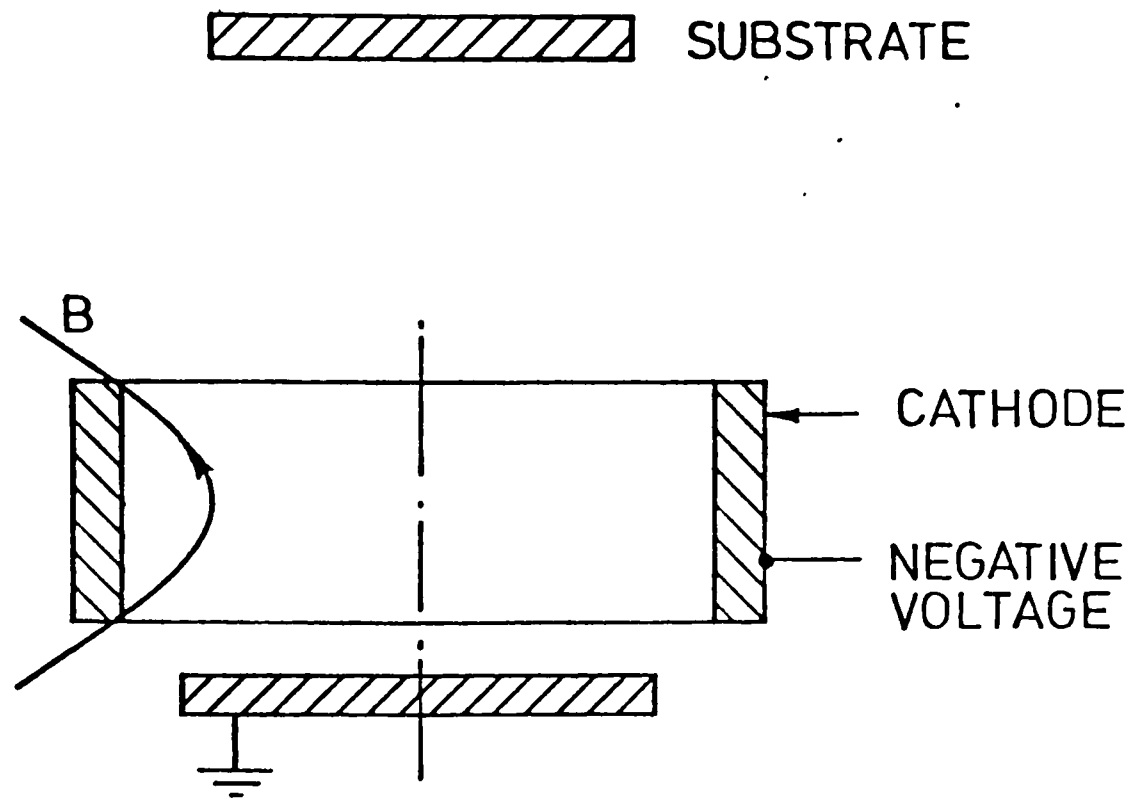


FIGURE 4-2

CYLINDRICAL MAGNETRON MODE OF SPUTTERING (after Clarke)

where $\rho kg\ m^{-3}$ is the density of the material being deposited. We wish to find the relation between flux and etching rate. Define $m\ kg\ m^{-2}\ s^{-1}$ as the material removal rate

$$m = \rho e \tag{4.2.2}$$

where e is the etching rate (ms^{-1}). The amount of material sputtered in any given direction is a function of the angle this direction makes with the normal to the source surface. It has been shown[33] that this function is essentially cosine in nature and of the form C cos β, where β is the sending angle, and C is an unknown. This function must also satisfy the condition that all the material sent in all directions of a hemisphere is m, i.e.

$$\begin{aligned} m &= \int C \cos \beta \, d\Omega \\ &= 2\pi C \int_0^{\pi/2} \sin \beta \cos \beta \, d\beta \\ &= \pi C \end{aligned} \tag{4.2.3}$$

Thus the amount of material removed within a solid angle dΩ centred around a direction that makes an angle β with the normal to the surface is

$$F = \frac{m}{\pi} \cos \beta \, d\Omega \tag{4.2.4}$$

The solid angle by which an element of receiving area dA_r is seen from a point source is

$$d\Omega = \frac{dA_r}{d^2} \tag{4.2.5}$$

where d is the separating distance (m). The amount of material received by the area dA_r is therefore

$$r = \frac{m}{\pi} \cos \beta \frac{dA_r}{d^2} \tag{4.2.6}$$

Referring to equation (4.2.4), and reducing the area dA_r to a

single point ($d\Omega \to 0$) we get the unidirectional flux, f:

$$f = \frac{m}{\pi} \cos \beta \qquad (4.2.7)$$

Equation (4.2.7) and equation (4.2.1) give

$$d = \frac{m \cos \alpha \cos \beta}{\pi \rho} \qquad (4.2.8)$$

or $$d = \frac{e \cos \alpha \cos \beta}{\pi} \qquad (4.2.9)$$

Equation (4.2.9) defines the deposition rate for a unidirectional flux. In the more general case of material coming from many directions, the elementary deposition rate is

$$dD = \frac{e \cos \alpha \cos \beta}{\pi} d\Omega_1 \qquad (4.2.10)$$

An elementary source area dA_s subtends a solid angle $d\Omega_1$, defined by

$$d\Omega_1 = \frac{dA_s}{d^2} \qquad (4.2.11)$$

and so,

$$dD = \frac{e \cos \alpha \cos \beta}{\pi d^2} dA_s \qquad (4.2.12)$$

Our case is the limit of a cylinder sputtering inwards onto a smaller, coaxial cylinder, when the diameter of the receiving cylinder is reduced almost to zero. Figure 4.4 is a projection of these cases

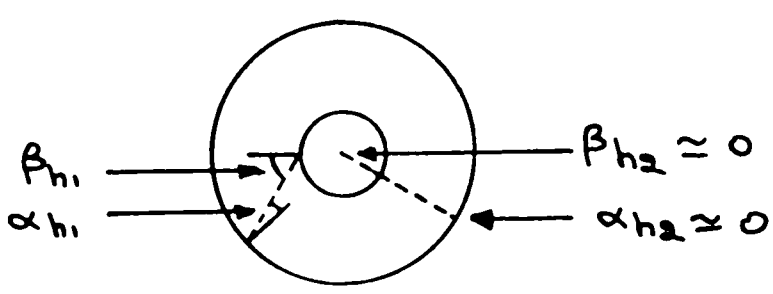


Figure 4.4

It can be seen that the horizontal components of angles α and β tend to 0 as the diameter of the receiving cylinder becomes smaller, and as α and β have only vertical components, α_v and β_v where $\alpha_v = \beta_v$. Equation (4.2.12) can now be simplified:

$$dD = \frac{e \cos^2 \alpha}{\pi d^2} dA_s \qquad (4.2.13)$$

For the case of the receiving point R (Figure 4.5)

$$\cos \alpha = \sin \theta$$

$$dA_s = d^2 \sin\theta d\theta d\psi$$

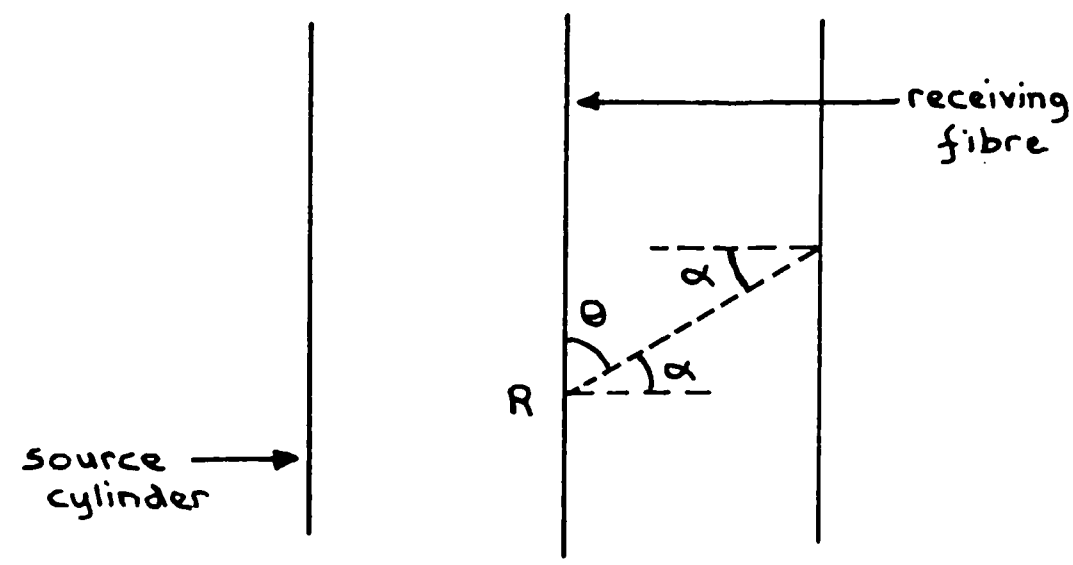


Figure 4.5

where ψ is the horizontal angle of the spherical co-ordinates centred on the receiving point R.

$$\text{Now} \quad D = \int \frac{e \cos^2 \alpha}{\pi d^2} dA_s$$

$$= \int \frac{e \sin^3 \theta}{\pi} d\theta d\psi \qquad (4.2.14)$$

As only half the target cylinder is relevant as a source area, the limits of ψ are 0 and π. Therefore

$$D = \frac{e}{\pi} \int_0^{\pi} d\psi \int_0^{\pi} \sin^3\theta d\theta$$

$$= e \int_0^{\pi} \sin^3\theta d\theta \qquad (4.2.15)$$

$$= \frac{4e}{3}$$

Thus the deposition rate is proportional to the etching rate, and, as etching rate is proportional to target current density, the limiting

deposition rate for a given target is essentially determined by the current capacity of the power supply, assuming that the target can be effectively cooled.

4.3 DESIGN OF COATING APPARATUS

Figure 4.6 shows the geometry of our trial sputtering device. An annular ferrite permanent magnet polarised North on one face and South on the other provides, via pole pieces, the emerging and returning magnetic field trap, the peak field strength being about 50mTesla. The cathode target is simply a sheet of the required metal rolled into a cylinder of diameter 40mm and sprung against the polepieces. Six wire anodes 5mm away from the target, mounted on PTFE insulators, complete the apparatus. With an argon atmosphere of 5mTorr, the design was capable of a sputtering rate of 0.1μm/min of nickel on to a silica fibre situated on the cylinder axis, with a current of 100mA, the current being limited by the cathode heating due to ion bombardment. The cathode erosion zone is closely confined within the area where the magnetic field is parallel to the cathode surface, showing elegantly that the device operates in the magnetron mode. Also the plasma ring is very near the erosion zone, and the device is very stable. It is difficult to define a precise sputtering rate as the sputtered metal atoms may not necessarily emerge perpendicularly to the cathode target; many atoms will then either not hit the fibre or will strike the fibre some axial distance away from the erosion zone (the emission characteristic is cosine in nature[33]).

As mentioned, high plasma currents were unattainable with this preliminary device as no provision was made for force cooling the cathode target. To prove a high rate device was feasible, a water-cooled cathode model was constructed.

The trial high rate system (figure 4.7), whilst having approximately

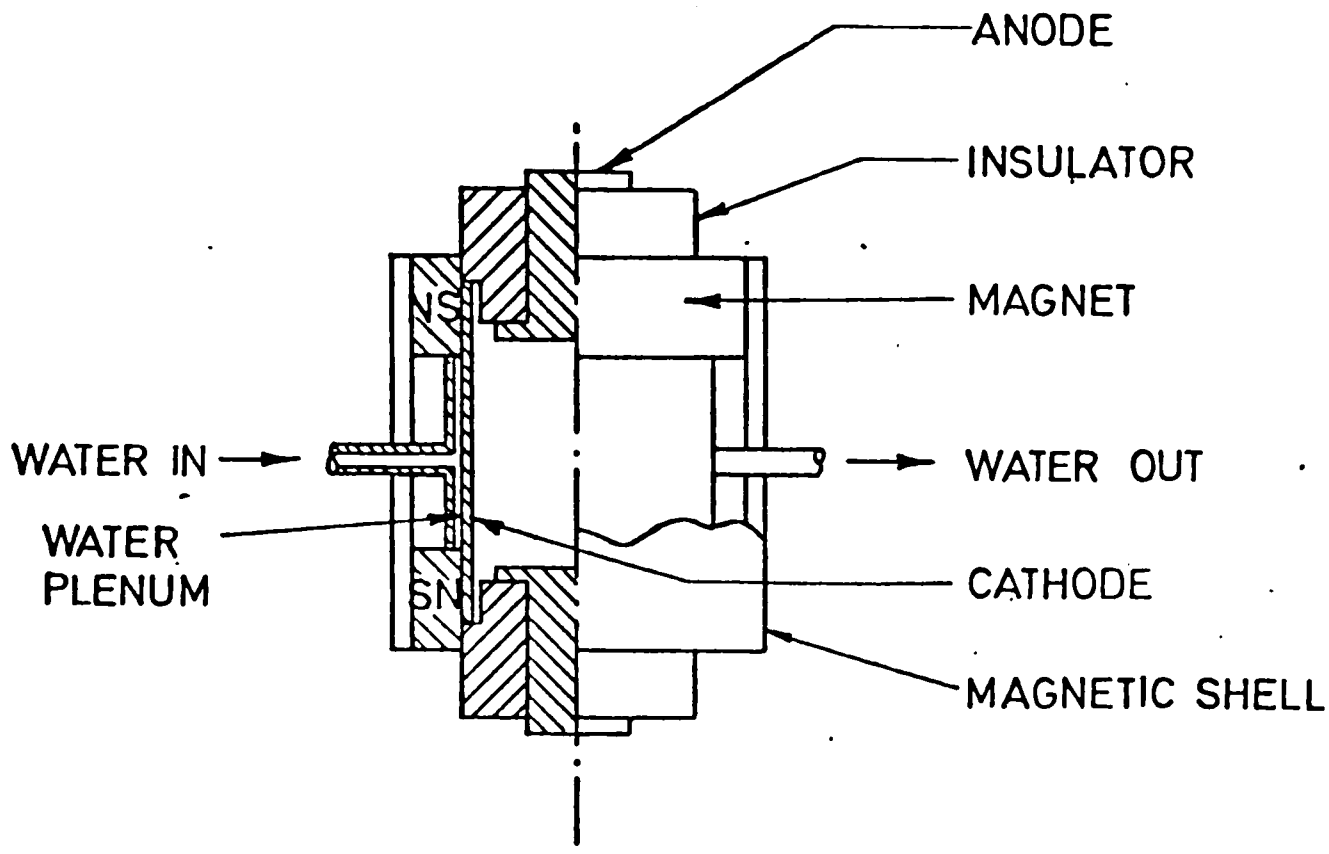


FIGURE 4-7
TRIAL HIGH RATE SYSTEM

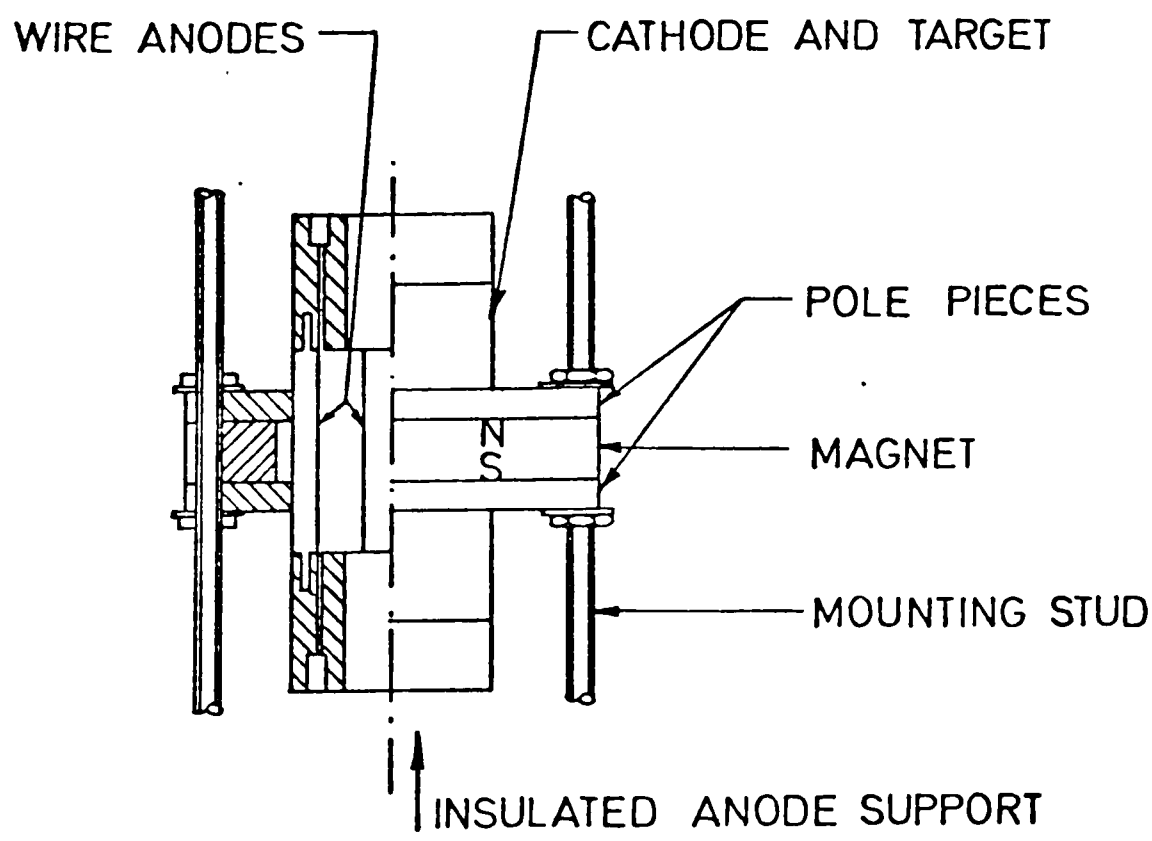


FIGURE 4-6
MKI CYLINDRICAL SPUTTERING DEVICE

the same target area as the first device, was designed to have a higher current density capability, and could withstand 1.5A of plasma current before temperature became a problem. Indeed, other instabilities within the system tended to mask heating problems. With a current of 1.5A, the cooling water rose 10°C, and there was no evidence of the nickel target melting.

During performance tests of the high rate design, it became apparent that ion leakage from the device boundary was causing arcing to other metallic parts of the vacuum system; this problem has been resolved on the final design by isolating the cathode, which is now the only live metallic part (the remainder of the apparatus is electrically connected to the anode, which is grounded).

The final on-line coating system, which is now installed in the apparatus, was thus designed with the following main points:

- live cathode and grounded anode
- water cooled target
- permanent magnets and water ducts exterior to the vacuum chamber to minimise outgassing and leakage problems
- future modification of the magnetron magnetic field easily facilitated.

Figure 4.8 shows a half section and detail of the on-line sputtering device. The sputtering system consists of two co-axial cylinders, the inner one of which forms the wall of the vacuum chamber, and is also the cathode. The cooling water flows between these cylinders and is thus directly in contact with the cathode. Exterior to the two cylinders are annular permanent magnets (arranged as shown in the figure) which create the closed magnetic path loops. Demountable vacuum couplings connect the device to the rest of the vacuum system, and glass spacers isolate the cathode from the rest of the apparatus. The spacers and vacuum couplings also provide mechanical support for the device. A single 4mm rod anode runs down the device, 3mm away

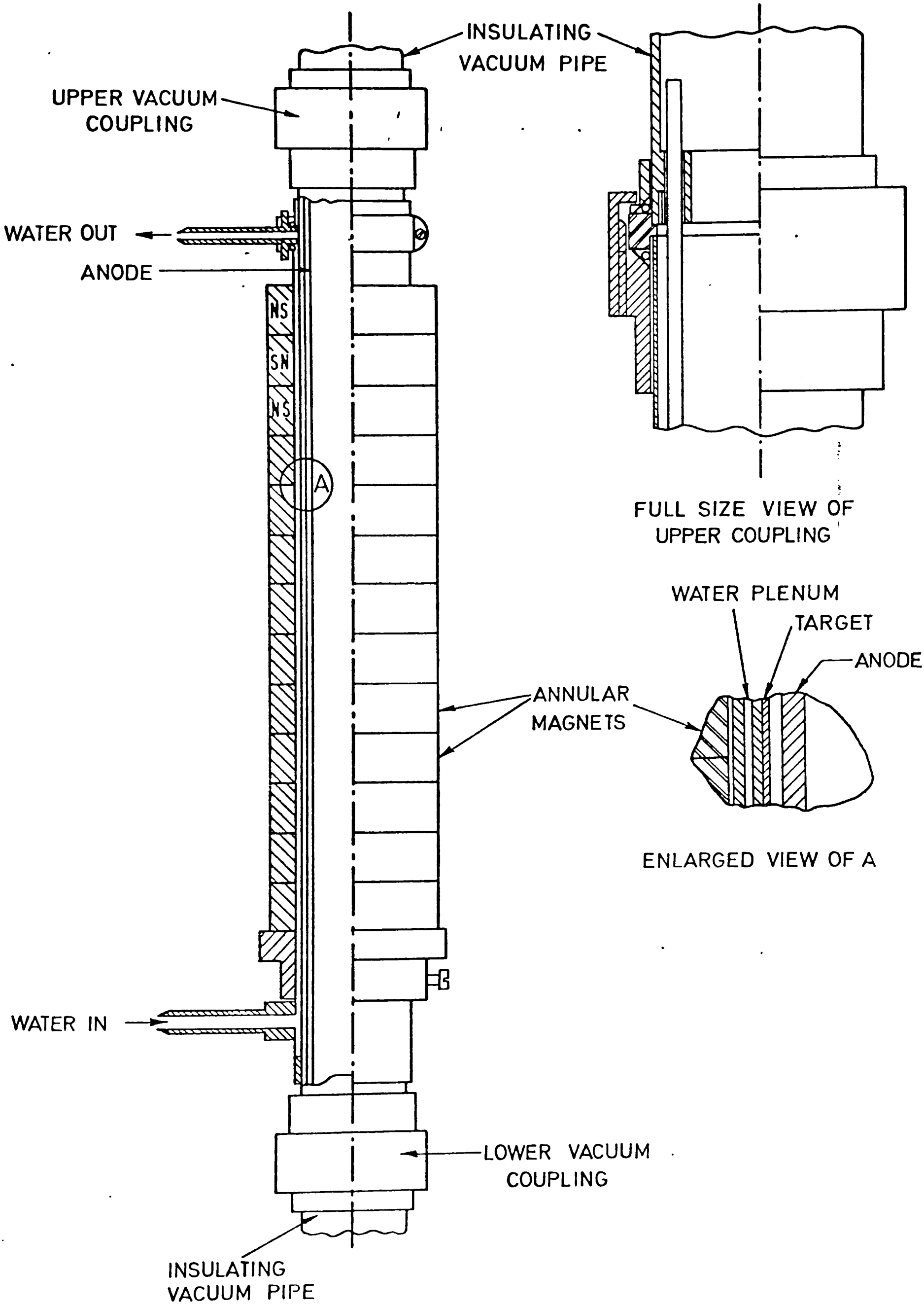


FIGURE 4-8(i)
ON-LINE MAGNETRON SPUTTERING DEVICE



Figure 4.8(ii) On-line Magnetron Sputtering Device

from the inner wall, and is maintained in position by holes in the insulating spacers, and is electrically connected to the rest of the apparatus.

By removing the upper vacuum and water couplings, the permanent magnets may be removed and replaced by an alternative magnetic system (for example a solenoid), and thus the geometry of the magnetic field and consequently the target etching pattern may be altered. The target material itself is made of thin sheet and rolled into a cylinder slightly larger than the cathode. On insertion to the cathode cylinder it maintains its shape by springing against the cathode wall. It has been found that this method of target insertion is not ideal, intimate contact between cathode and target not being maintained. For target materials with low melting points some form of bonding between cathode and target is provided, commercial heat sink compound proving satisfactory.

The system has been tried and performs effectively with currents up to 3A. The etching pattern produced by the permanent magnet stack is not particularly efficient, as less than 50% of the target area is etched, but moving the stack axially between pulling operations overcomes this drawback simply and economically. At some sacrifice to simplicity, replacing the magnets with a long solenoid would overcome this problem entirely.

The power supply for the on-line sputtering head was designed to fulfill two criteria:

(i) to provide ≈ 1kV to initiate the plasma, and

(ii) to provide sufficient current to produce a sufficient deposition rate onto a fibre whilst being drawn.

This current was calculated as follows. Space constraints of the puller design limited the overall length of the sputtering device to approximately 300mm. Thus the length of fibre which can be coated at any one instant is 300mm. Assuming a drawing speed of 1m/min, an

optimistic estimate, any one point on the fibre will be within the sputtering cylinder for 20 secs. Our initial aim was to coat the fibre with 0.1μm of material, so the deposition rate must be 0.3μm/min. Now as $D = \frac{4e}{3}$, and e for say, copper, is 1.66×10^{-10} $J^{(32)}$, where J is the current density. For a target of length L and radius R:

$$J = \frac{I}{2\pi RL} \qquad (4.3.1)$$

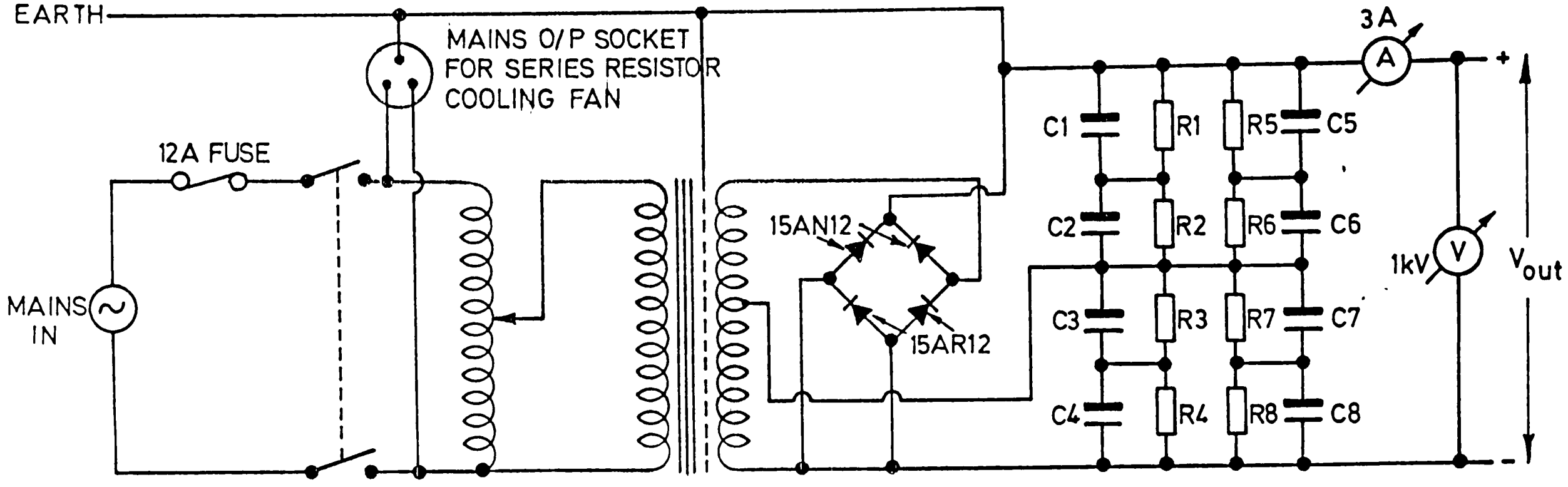
where I is the total current. This gives

$$D = \frac{4}{3} \times 1.66 \times 10^{-10} \frac{I}{2\pi RL} \qquad (4.3.2)$$

Note from equation (4.3.2) that for a given current, the deposition rate is inversely proportional to both radius and length, implying that these should both be as small as possible. However, as the length of the device is reduced in an on-line coating system, the time in which a given length of fibre is within the sputtering region is reduced proportionally and thus the length has no real effect - the length of our device was chosen to facilitate target cooling. The radius of the device, however, is important (no time restraint applies) and in the system is reduced to a practical minimum of 20mm. This allows the silica blob formed when a drawing run is initiated to pass through the system unhindered.

With these dimensions, and assuming a copper target, the required current is 0.85A. The completed power supply has a maximum output voltage in excess of 1kV and a current output of 3A, the output voltage being continuously variable. Ideally a constant current supply would have been preferred to ease operation and to cope with flashover between electrodes, but cost dictated a simple power supply.

The power supply (circuit diagram, figure 4.9) consists of a 'Variac' feeding a 250V.A.C. to 350V-0-350V RMS isolating transformer. The output voltage is bridge-rectified and smoothed with an electrolytic capacitor bank. The ripple at full output voltage and current



C1 — C8 3300 μF 350 V D.C. WORKING
R1 — R8 20 K 7 W VOLTAGE SHARING RESISTOR
T1 15 A VARIAC
T2 250 V A.C. → 350-0-350 V A.C. 3·75 kVA

FIGURE 4-9

M.S. POWER SUPPLY CIRCUIT DIAGRAM

is better than 10%. A series resistor between the supply and the sputtering device helps reduce the effect of arcing, and approximates the supply to a constant current source. The series resistor is force cooled by air as considerable power may be dissipated.

CHAPTER FIVE

PROPERTIES OF METAL COATED FIBRES

5.1 INTRODUCTION

If an uncoated glass fibre is tested mechanically some time after it has been drawn, it is found to be more brittle and comparatively weak in tension compared to pristine fibre. It is also found[34] that the fibre environment, especially the humidity, affects the rate at which the fibre strength deteriorates - when an applied stress, lower than the critical failure stress, is applied in the presence of moisture, there is a time delay to failure, the time being dependent on the relative humidity. This phenomenon is known as stress corrosion.

The original aim of the project was to coat the fibre with metal at an elevated temperature, so that on cooling the glass would be prestressed in a state of compression due to the coefficients of thermal expansion and the fibre surface protected by the metal layer. Then the composite structure could be stretched or bent without the glass reaching its ultimate tensile stress. This chapter attempts to predict the effect of a coating of metal on the prestress and investigates candidate materials. Our coating process is limited to somewhat thin film thickness, however, and it is shown that such a film really does not provide significant fibre reinforcement, but simply an hermetic seal around the fibre. This would be an improvement over conventional 'plastic' coatings which tend eventually to allow water to seep through.

A correctly chosen hermetic metal coating will also allow optical fibres to be used in high temperature environments, (conventional plastic coatings breaking down in the region of $300^{o}C$), and will enable the fibre to be soldered directly for splicing and attachment to sources and detectors.

5.2 PRESTRESSING OF FIBRES

Consider a silica fibre of radius a. We require to find the stresses induced if a layer of metal is deposited such that the total radius is b, and the composite structure is reduced in temperature by ΔT, and that the bond between glass and metal does not allow slippage. The stresses in the region 1 (silica) and 2 (metal), (see figure 5.1), may be written

$$\sigma_{r1} = \sigma_{\theta 1} = A_1 \; ; \quad \sigma_{z1} = C_1$$

$$\sigma_{r2} = A_2 + \frac{B_2}{r^2} \; ; \quad \sigma_{\theta 2} = A_2 - \frac{B_2}{r^2} \quad \sigma_{z2} = C_2 \tag{5.2.1}$$

where we have made use of Lame's formulae (see Appendix).

Axial equilibrium gives us

$$C_1 a^2 + C_2 (b^2 - a^2) = 0 \tag{5.2.2}$$

Continuity of σ_r at r = a gives us

$$A_1 = A_2 + \frac{B_2}{a^2} \tag{5.2.3}$$

The condition that $\sigma_r = 0$ when r = b results in

$$A_2 + \frac{B_2}{b^2} = 0 \tag{5.2.4}$$

Equalising the strains in the axial and circumferential direction gives

$$\frac{C_1}{E_1} - 2\gamma_1 \frac{A_1}{E_1} - \alpha_1 \Delta T = \frac{C_2}{E_2} - 2\gamma_2 \frac{A_2}{E_2} - \alpha_2 \Delta T \tag{5.2.5}$$

and

$$\frac{A_1}{E_1} - \gamma_1 \frac{A_1}{E_1} - \gamma_1 \frac{C_1}{E_1} - \alpha_1 \Delta T = \frac{A_2 - \frac{B_2}{a^2}}{E_2} - \frac{\gamma_2 (A_2 + \frac{B_2}{a^2})}{E_2}$$

$$- \gamma_2 \frac{C_2}{E_2} - \alpha_2 \Delta T \tag{5.2.6}$$

where E is Young's Modulus, γ is Poisson's Ratio and α is the coefficient of linear expansion.

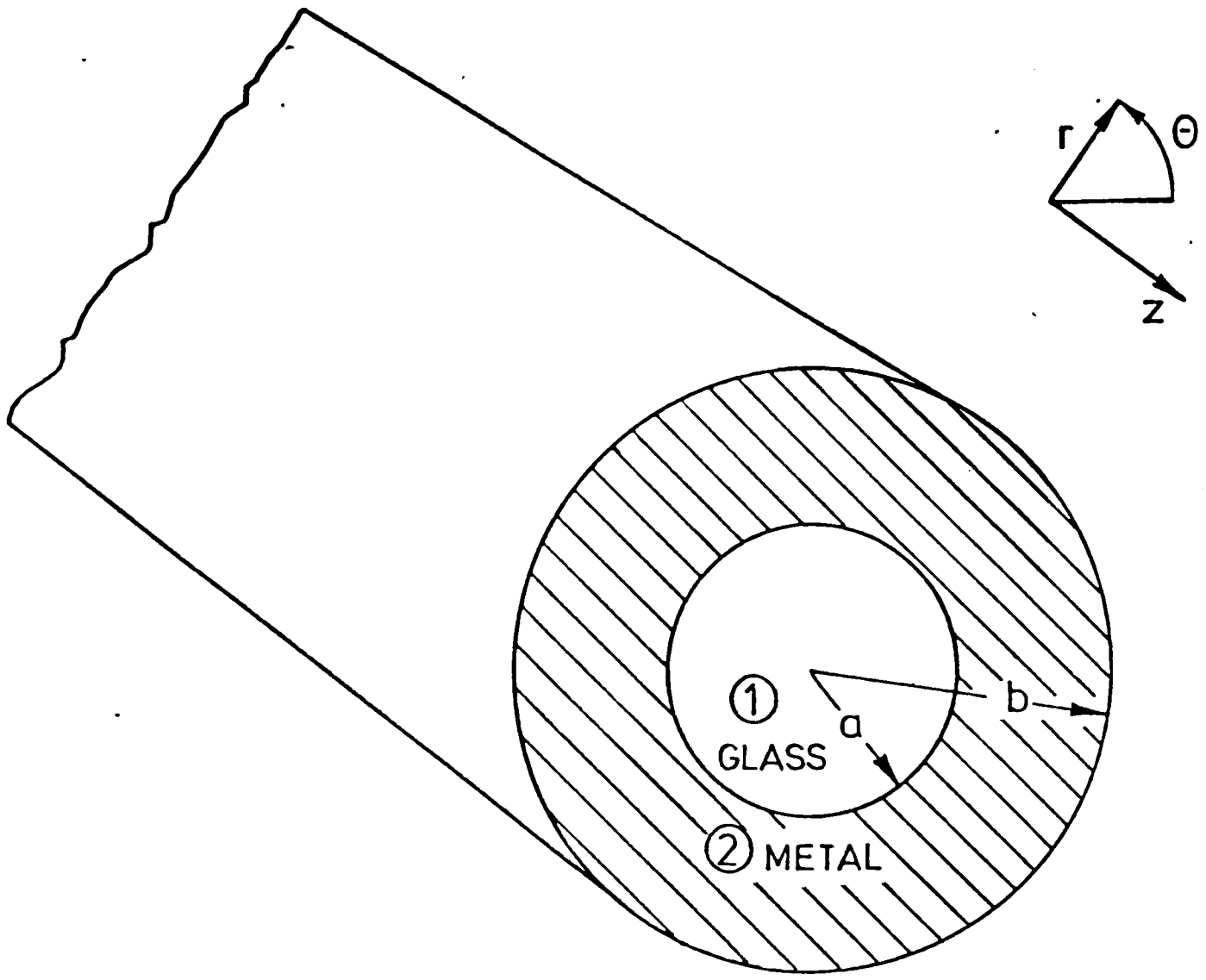


FIGURE 5-1

METAL COATED OPTICAL FIBRE

Substituting (5.2.2, (5.2.3) and (5.2.4) in (5.2.5) and (5.2.6), and writing

$$x = \frac{b^2 - a^2}{a^2} , \qquad \mu = \frac{E_1}{E_2} ,$$

we obtain two simultaneous equations for C_1, A_2:

$$(1 + \frac{\mu}{x})C_1 + 2[x\gamma_1 + \mu\gamma_2]A_2 = -(\alpha_2 - \alpha_1)E_1\Delta T \qquad (5.2.7)$$

$$(\gamma_1 + \frac{\mu\gamma_2}{x})C_1 + [x(1-\gamma_1) + \mu x(1 + \gamma_2) + 2\mu]A_2 = (\alpha_2 - \alpha_1)E_1\Delta T \qquad (5.2.8)$$

If we assume $\gamma_1 = \gamma_2$, it may be shown that the longitudinal stress in the glass may be written

$$\sigma_{z1} = -(\alpha_2 - \alpha_1)E_1 \frac{\Delta T x(Ax + B)}{(x+C)(Dx+F)} \qquad (5.2.9)$$

where A, B, C, D and F are material properties given by

$$A = 1 + \mu \qquad D = 1 + \mu - 2\gamma$$
$$B = 2\mu \qquad F = 2\mu(1 - \gamma) \qquad (5.2.10)$$
$$C = \mu$$

Taking, for example, $\mu = \frac{1}{4}$, $\gamma_1 = \gamma_2 = 0.3$, the stress may be calculated and is shown as a function of $t = \frac{b-a}{a}$ in figure 5.2.

We note that this curve has an asymptotic behaviour for very large or very small values of t. For small t,

$$t = \frac{x}{2} \qquad (5.2.11)$$

and hence

$$\sigma_{z1} \rightarrow -(\alpha_2 - \alpha_1)E_1 \frac{\Delta T\ 2t}{\mu(1-\gamma)} \qquad (5.2.12)$$

and is proportional to the thickness of the coating. For the values we are considering

$$\sigma_{z1} \rightarrow -(\alpha_2 - \alpha_1)E_1\ \Delta T x 11.43t \qquad (5.2.13)$$

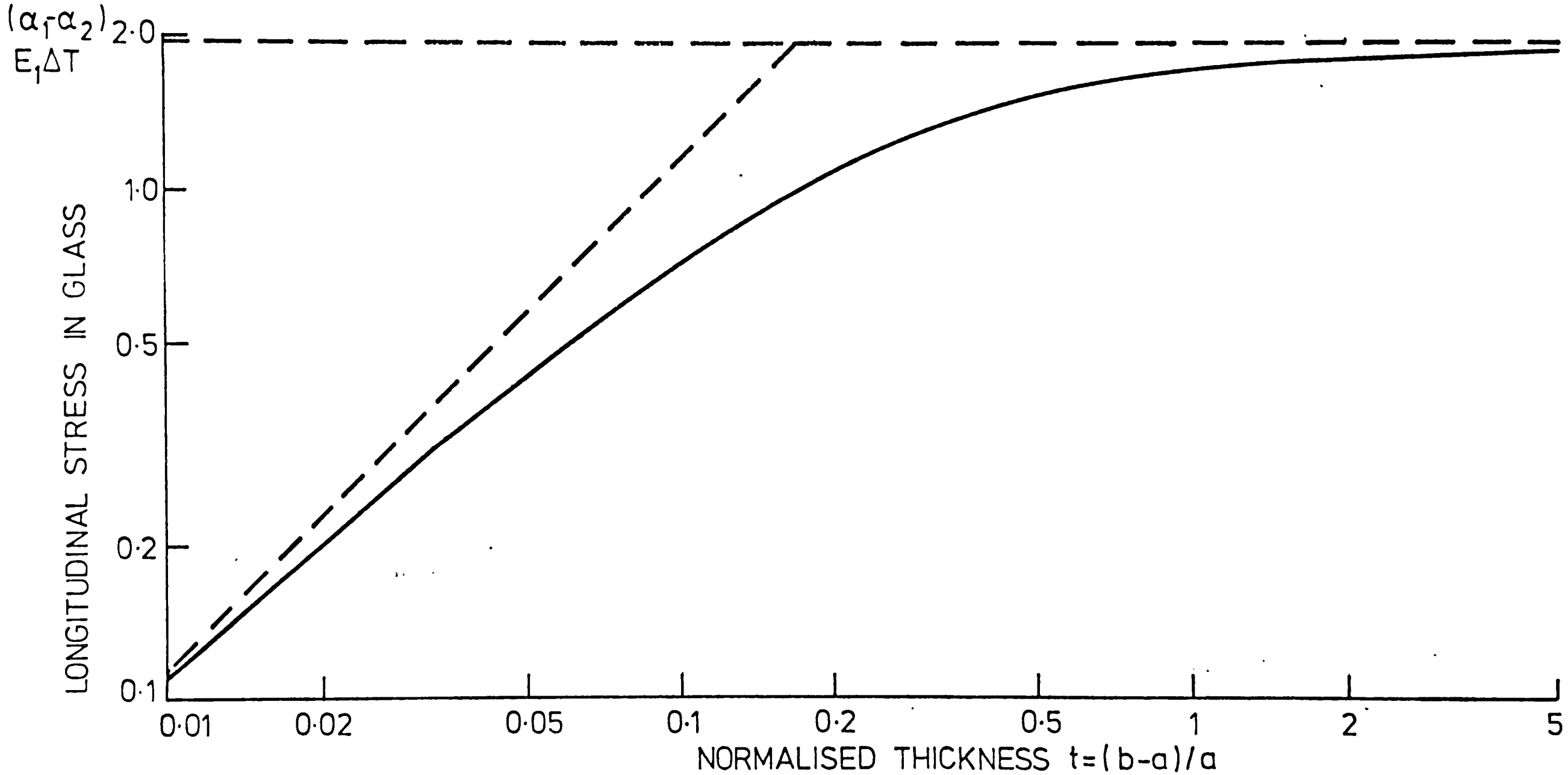


FIGURE 5-2
LONGITUDINAL PRESTRESS INDUCED IN A HYPOTHETICAL COATING AS A FUNCTION OF NORMALISED THICKNESS

For large t

$$\sigma_{z1} \rightarrow -(\alpha_2 - \alpha_1)E_1 \Delta T\left(\frac{1 + \mu}{1 + \mu - 2\gamma}\right) \tag{5.2.14}$$

that is, σ_{z1} tends to a value independent of coating thickness. For the given values

$$\sigma_{z1} \rightarrow -(\alpha_2 - \alpha_1)E_1 \Delta T \times 1.923 \tag{5.2.15}$$

Let us now consider the effect of the material properties of the coating. If $\gamma_1 \neq \gamma_2$ the algebra is more complicated. For small t we find that equation (5.2.12) still holds with the Poisson's Ratio that for the metal:

$$\sigma_{z1} = -(\alpha_2 - \alpha_1)E_1 \Delta T \frac{t}{\mu(1-\gamma_2)} \tag{5.2.16}$$

which may be written

$$\sigma_{z1} = -(\alpha_2 - \alpha_1)\, E_2 \frac{\Delta T\ 2t}{(1-\gamma_2)} \tag{5.2.17}$$

or for thin coatings the axial prestress in the glass is greatest for a coating material with the greatest value of $\frac{(\alpha_2-\alpha_1)E_2}{(1-\gamma_2)}$

For any value of t, σ_{z1} may be written

$$\sigma_{z1} = -(\alpha_2 - \alpha_1)E_1 \Delta T \frac{x\{(L+M)x + 2M\}}{Nx^2 + Px + Q} \tag{5.2.18}$$

where L, M, N, P and Q are constants for a given material defined by

$$\begin{aligned} L &= 1 + \gamma_1 \\ M &= \mu(1 + \gamma_2) \\ N &= (1-2\gamma_1)L+M \end{aligned} \qquad \begin{aligned} P &= \mu(3-\gamma_1 - 4\gamma_1\gamma_2 + M) \\ Q &= 2\mu M(1-\gamma_2) \end{aligned} \tag{5.2.19}$$

The other components of stress in the glass and metal may also be calculated from equations (5.2.1) to (5.2.8). These may be written:

$$\sigma_{r1} = \sigma_{\theta 1} = \sigma_{r2max} = -(\alpha_2-\alpha_1)E_1 \Delta T \frac{x(Lx + M)}{Nx^2 + Px + Q} \tag{5.2.20}$$

$$\sigma_{\theta 2max} = (\alpha_2-\alpha_1)E_1 \Delta T \frac{(x+2)(Lx+M)}{Nx^2 + Px + Q} \qquad (5.2.21)$$

$$\sigma_{z2} = (\alpha_2-\alpha_1)E_1 \Delta T \frac{(L+M)x + 2M}{Nx^2 + Px + Q} \qquad (5.2.22)$$

5.3 THE EFFECT OF AN AXIAL LOAD

If an axial tension $\pi a^2\sigma$ is applied to the fibre then calculation of the stresses produced in the glass and metal is similar to the calculation of prestressing. As the system is linear we may calculate the effect of load and then afterwards add this to the stresses produced by the temperature drop. Equations (4.5.1) then still apply where the new constants are now designated by primes. Axial equilibrium gives us

$$C_1' + xC_2' = \sigma \qquad (5.3.23)$$

Equality of axial strains results in the equation:

$$\frac{C_1'}{E_1} - 2\gamma_1 \frac{A_1'}{E_1} = \frac{C_2'}{E_2} - 2\gamma_2 \frac{A_2'}{E_2} \qquad (5.3.24)$$

and equality of circumferential strains:

$$\frac{A_1'}{E_1} - \gamma_1 \frac{A_1'}{E_1} - \gamma_1 \frac{C_1'}{E_1} = \frac{(A_2'-B_2'/a^2)}{E_2} - \gamma_2\frac{(A_2'+B_2'/a^2)}{E_2} - \gamma_2 \frac{C_2'}{E_2} \qquad (5.3.25)$$

Equations (5.2.3) and (5.2.4) still apply. Substituting as before we obtain:

$$C_1'(1 + \frac{\mu}{x}) + 2[\mu\gamma_2 + x\gamma_1]A_2' = \frac{\mu\sigma}{x} \qquad (5.3.26)$$

$$C_1'(\frac{\mu\gamma_2}{x} + \gamma_1) + [x(1-\gamma_1) + \mu x(1+\gamma_2) + 2\mu]A_2' = \frac{\mu\gamma_2\sigma}{x} \qquad (5.3.27)$$

The stresses are thus:

$$\sigma_{z1}' = \sigma \frac{\{(P-U)x + Q\}}{Nx^2 + Px + Q} \qquad (5.3.28)$$

where

$$U = 2(1 - \gamma_1\gamma_2) \tag{5.3.29}$$

$$\sigma_{z2}' = \frac{\sigma(Nx + U)}{Nx^2 + Px + Q} \tag{5.3.30}$$

and

$$\sigma_{2max}' = \mu\sigma \frac{(\gamma_2-\gamma_1)(2+x)}{Nx^2 + Px + Q} \tag{5.3.31}$$

It is seen that if $\gamma_1=\gamma_2$ the circumferential stress in the metal is zero, as would be expected.

Ideally we should arrange that the amount of prestressing is such that when the fibre is loaded, the silica reaches its maximum tensile stress σ_T when the metal reaches its yield stress Y.

If the yield stress in the metal is reached first in the circumferential direction, then this occurs when

$$x^2Y(L+M) + x(2MY + \sigma_T L) + \sigma_T M = \sigma M \tag{5.3.32}$$

Similarly, if the metal reaches its yield stress in an axial direction first, then

$$xY + \sigma_T = \sigma \tag{5.3.33}$$

This equation could be written down straight away from equilibrium considerations. It is seen that for all positive values of σ_T, equation (5.3.32) predicts a higher value of σ than equation (5.3.33). Hence the metal will in fact reach its yield stress firstly in an axial direction and equation (5.3.33) applies.

If we require that no tensile stress appears in the glass, $\sigma_T = 0$ and hence the applied tensile force is

$$T = \pi a^2 xY \tag{5.3.34}$$

and is proportional to the cross-sectional area of metal. The axial

stress in the metal for zero axial stress in the glass is given by

$$\sigma_{z2_{TOTAL}} = (\alpha_2 - \alpha_1)E_1\Delta T\left\{\frac{(L+M)x + 2M}{(P-U)x + Q}\right\} \qquad (5.3.35)$$

The temperature drop needed to give the correct amount of prestressing may be calculated by putting $\sigma_{z2_{TOTAL}}$ equal to Y, the yield stress of the glass.

If the maximum tensile stress permitted in the glass is σ_T, then the maximum load

$$T = \pi a^2(xY + \sigma_T) \qquad (5.3.36)$$

or

$$T/T_o = 1 + \frac{xY}{\sigma T} \qquad (5.3.37)$$

where T_o is the load permitted for uncoated fibre. The temperature drop needed to give this amount of prestressing is given by

$$(\alpha_1 - \alpha_2)E_1\Delta T = \frac{\{(P-U)Y - N\sigma_T\}x + (QY-U\sigma_T)}{(L+M)x + 2M} \qquad (5.3.38)$$

If $\sigma_T << Y$ and $x << 1$,

$$(\alpha_2 - \alpha_1)E_1\Delta T = \mu(1 - \gamma_2)Y \qquad (5.3.39)$$

and in fact for nickel this is approximately true for all x - see next section.

To give the greatest possible tensile strength for a given permitted tensile stress in the glass, the only important coating material property is thus the yield stress.

The axial strain for a given applied stress may be calculated from equation (5.3.24) by substituting into the solutions of (5.3.26) and (5.3.27). We obtain

$$\varepsilon = \frac{\sigma}{E_1}\left(\frac{\mu Nx + Q}{Nx^2 + Px + Q}\right) \qquad (5.3.40)$$

and from this we may calculate an effective stiffness

$$\frac{E_{eff}}{E_1} = 1 + \frac{x}{\mu} + \frac{2\mu x\, \gamma_{12}^2}{\mu\, Nx + Q}, \qquad (5.3.41)$$

where

$$\gamma_{12}^2 = (\gamma_1 - \gamma_2)^2 \qquad (5.3.42)$$

The third term of the equation is small compared with the other two. Equation (5.3.41) is the same as that developed by Muskhelishvili[36].

Using Muskhelishvili's treatment we may also calculate the effective bending stiffness. This is given by

$$\frac{(EI)_{eff}}{(EI)_1} = 1 + \frac{x(x+2)}{\mu} + \frac{4\,\gamma_{12}^2\, x(x+2)}{Vx(x+2)+2M} \qquad (5.3.43)$$

where

$$V = (3-4\gamma_1)(1+\gamma_1) + M \qquad (5.3.44)$$

It is found again that the third term is small compared with the other two.

5.4 CANDIDATE MATERIALS

It was thought desirable to restrict the preliminary analysis of candidate materials to those commonly available and commonly used in engineering and physics, if for no other reasons than practicality and cost. Table 5.1 lists those chosen, with physical data, and may be loosely categorised as 'soft', 'medium' and 'hard' metals:

Soft: Aluminium, Copper, Gold, Silver

Medium: Iron, Nickel, Nickel-Silver, Cupronickel

Hard: Chromium, Molybdenum, Tungsten

It will be noted that two alloys were selected, for reasons which will be discussed later, and also that the physical constants for silica are included for comparison.

For use in the following analysis, the desired physical parameters

MATERIAL 20%C	E $GN\ m^{-2}$	γ	$\alpha \times 10^6$ K^{-1}	$\alpha_2 - \alpha_1$ $\times 10^6\ k^{-1}$	$\mu = \frac{E_1}{E_2}$	$(\alpha_2-\alpha_1)E_2$ $Nmm^{-2}\ K^{-1}$	σ_{yield} (2) Nmm^{-2}
ALUMINIUM	70.3	0.345	23.0	22.55	1.040	1.648	$\simeq$ 30-140 (Δ)
CHROMIUM	279.1	0.21	7.0	6.55	0.262	0.479	$\simeq$ 360 (*)
COPPER	129.8	0.343	16.7	16.25	0.563	1.188	$\simeq$ 47-320 (Δ)
GOLD	78.0	0.44	14.0	13.55	0.937	0.991	0-210 (Δ)
IRON	211.4	0.293	11.7	11.25	0.346	0.822	$\simeq$ 160 (Δ)
MOLYBDENUM*	324	0.293	5.44	4.99	0.226	0.365	$\simeq$ 345-550 (×)
NICKEL	199.5	0.312	12.8	12.35	0.366	0.903	140-660 (×)
SILVER	82.7	0.367	19.0	18.55	0.884	1.356	55-300 (Δ)
TUNGSTEN	411.0	0.28	4.5	4.05	0.178	0.296	$\simeq$ 550 (×)
†NICKEL SILVER	132.5	0.333	18	17.55	0.552	1.283	124-618 (×)
§CUPRONICKEL	163	0.327	16	15.55	0.449	1.137	200-500 (×)
SILICA	73.1	0.170	0.45				$\simeq$ 3500

† Approximate % composition Cu55 Ni18 Zn27
§ 'Constantan' approximate composition Cu55 Ni45
* Date from Goodfellows Metal Catalogue No.5
+ Approximate pessimistic values - limit of elastic region
Δ Data from H.L.T.
× Data from Smithells 'Metals Reference Book' 5th Ed., Butterworths

TABLE 5.1
PHYSICAL CONSTANTS OF CANDIDATE COATING METALS

L, M, N, P, Q, U, V and $(\gamma_{12})^2$ are listed in table 5.2.

From equations (5.2.18), (5.2.20), (5.2.21) and (5.2.22) graphs of σ_{z1}, $\sigma_{r1}(= \sigma_{\theta 1} = \sigma_{r2max})$, $\sigma_{\theta 2max}$ and σ_{z2} versus normalised coating thickness are plotted (figures 5.3, 5.4, 5.5 and 5.6 respectively). It should be noted that (for σ_{z1}) although values for E_2 vary by a factor of six; for thin coating the axial prestress in the fibre varies by only a factor of two.

Let us assume a nominal fibre diameter of 100μm, then for a coating thickness of 0.05μm, t = 0.001. For gold, the 'worst' material of figure 5.3, the curves give an actual fibre prestress of (only) $0.0052 Nmm^{-2}$ per degree centigrade temperature drop, and for nickel the 'best' material, $0.0065 Nmm^{-2}$ per degree centrigrade. This indicates a coating application at a temperature of the order of $1000^{o}C$ (impossible for gold, which melts at $1064^{o}C$, and impractical for nickel) to provide an appreciable compressive prestress. For t=1 (50μm on a fibre 100μm in diameter), the prestress for Tungsten, now the 'worst' material, is $0.113 Nmm^{-2} K^{-1}$ and for Aluminium $2.55 Nmm^{-2} K^{-1}$ - an appreciable change from the thin coating case.

It is interesting to review the work conducted by Pinnow et al., reported in their recent publication[36]. In their experiments, 15-20μm of aluminium was deposited on fibre diameter 110μm by the freeze coating technique. This corresponds to a t of approximately 0.36, giving a glass axial prestress of $1.65 Nmm^{-2} K^{-1}$. The melting point of aluminium is approximately $660^{o}C$, and if we assume that the temperature drop is to ambient ($\sim 20^{o}C$), the total axial prestress should be approximately $1 KNmm^{-2}$, significant compared to the reported failure stress of pristine silica fibres, $\sim 6\text{-}10 KNmm^{-2}$.

In this respect Pinnow's results are somewhat disappointing. Although isolated data points from his experiments do indicate fibre of high strength ($\simeq$ 900,000 psi = $6.2 KN/mm^2$), the mean strengths are somewhat lower than the best published results. This suggests that

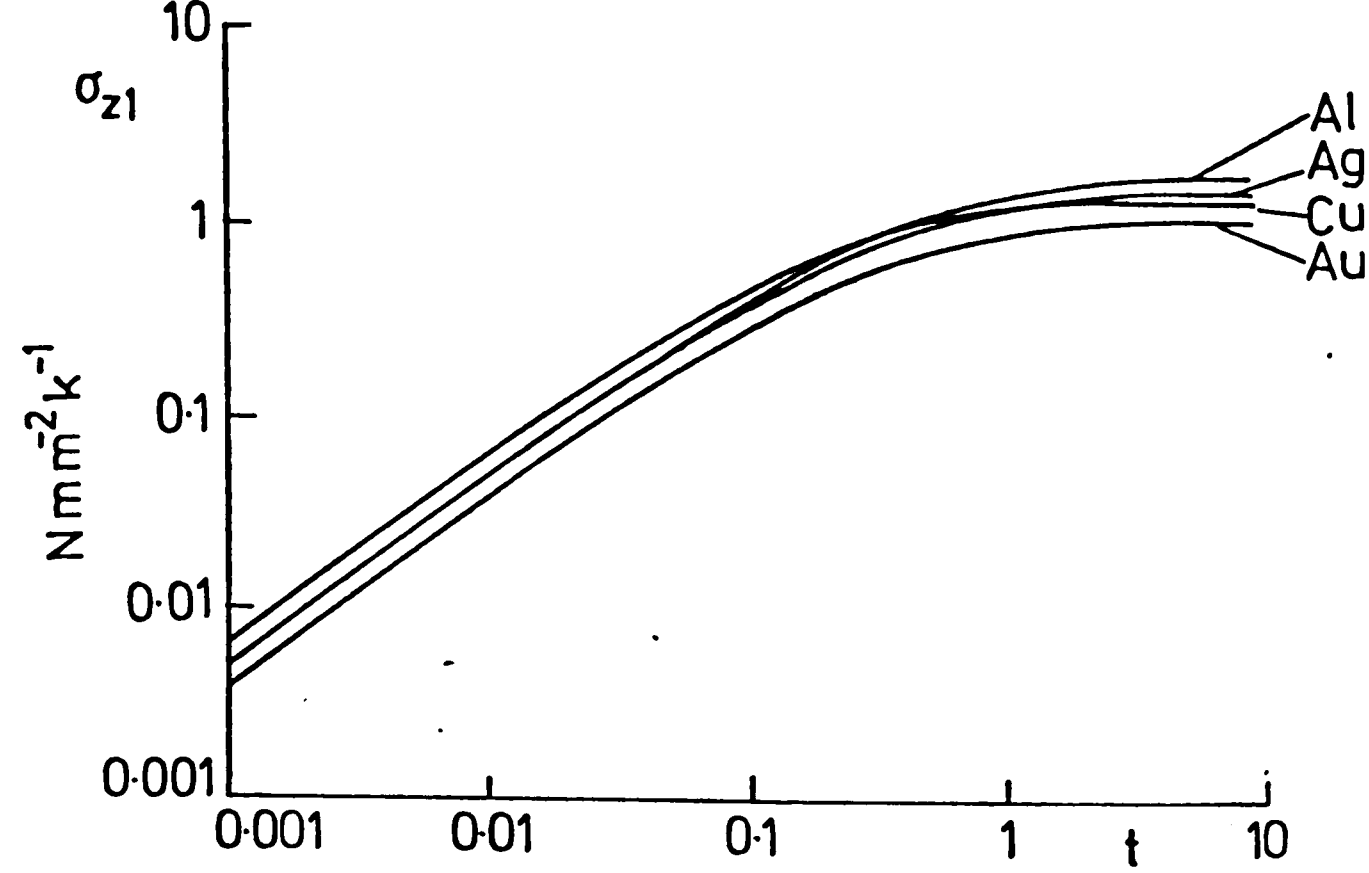
MATERIAL	L $(1+\gamma_1)$	M $\mu(1+\gamma_2)$	N $(1-2\gamma_1)L+M$	P $\mu(3-\gamma_1-4\gamma_1\gamma_2+M)$	Q $2\mu M(1-\gamma_2)$	U $2\mu(1-\gamma_1\gamma_2)$	V $(3-4\gamma_1)L+M$	γ^2 $(\gamma_1{}^1-\gamma_2{}^2)^2$
Al	1.17	1.399	2.171	4.154	1.906	1.957	4.113	0.0306
Cr	1.17	0.317	1.089	0.787	0.1312	0.505	3.031	0.0016
Cu	1.17	0.756	1.528	1.888	0.5592	1.061	3.470	0.0299
Au	1.17	1.349	2.121	3.636	1.416	1.734	4.063	0.0729
Fe	1.17	0.447	1.219	1.065	0.2187	0.657	3.161	0.0151
Mo	1.17	0.292	1.064	0.661	0.0933	0.429	3.006	0.0151
Ni	1.17	0.480	1.252	1.134	0.242	0.693	3.194	0.0202
Ag	1.17	1.208	1.980	3.349	1.352	1.658	3.922	0.0388
Wf	1.17	0.228	1.000	0.511	0.0584	0.339	3.942	0.0121
[+]Ni/Cu	1.17	0.736	1.508	1.844	0.5419	1.041	3.450	0.0266
[§]Cu/Ni	1.17	0.596	1.368	1.439	0.3602	0.848	3.310	0.0246

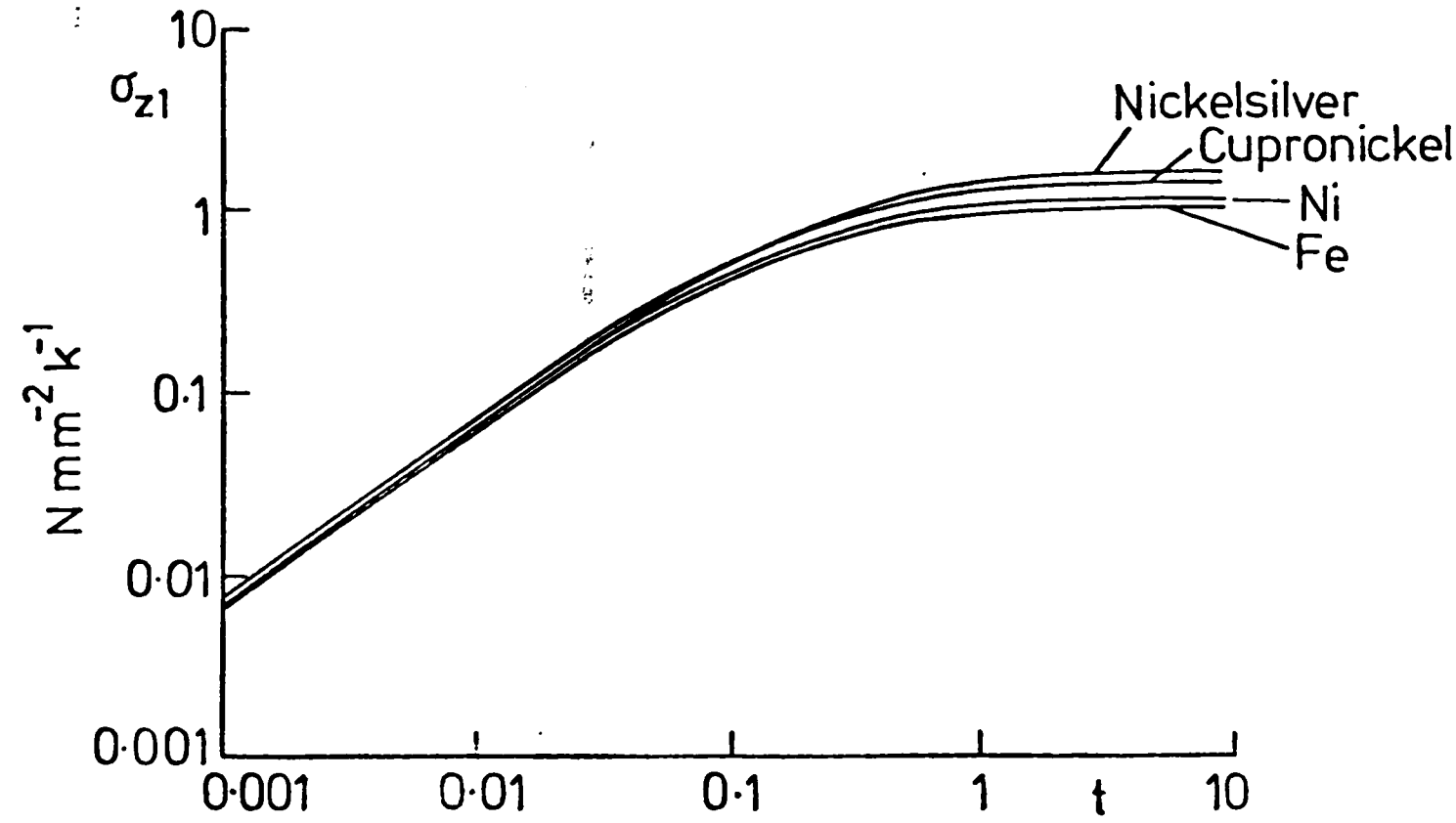
[+] Nickel/Silver

[§] 'Constantan' Cupronickel

TABLE 5.2

DERIVED PHYSICAL PARAMETERS OF COATING MATERIALS





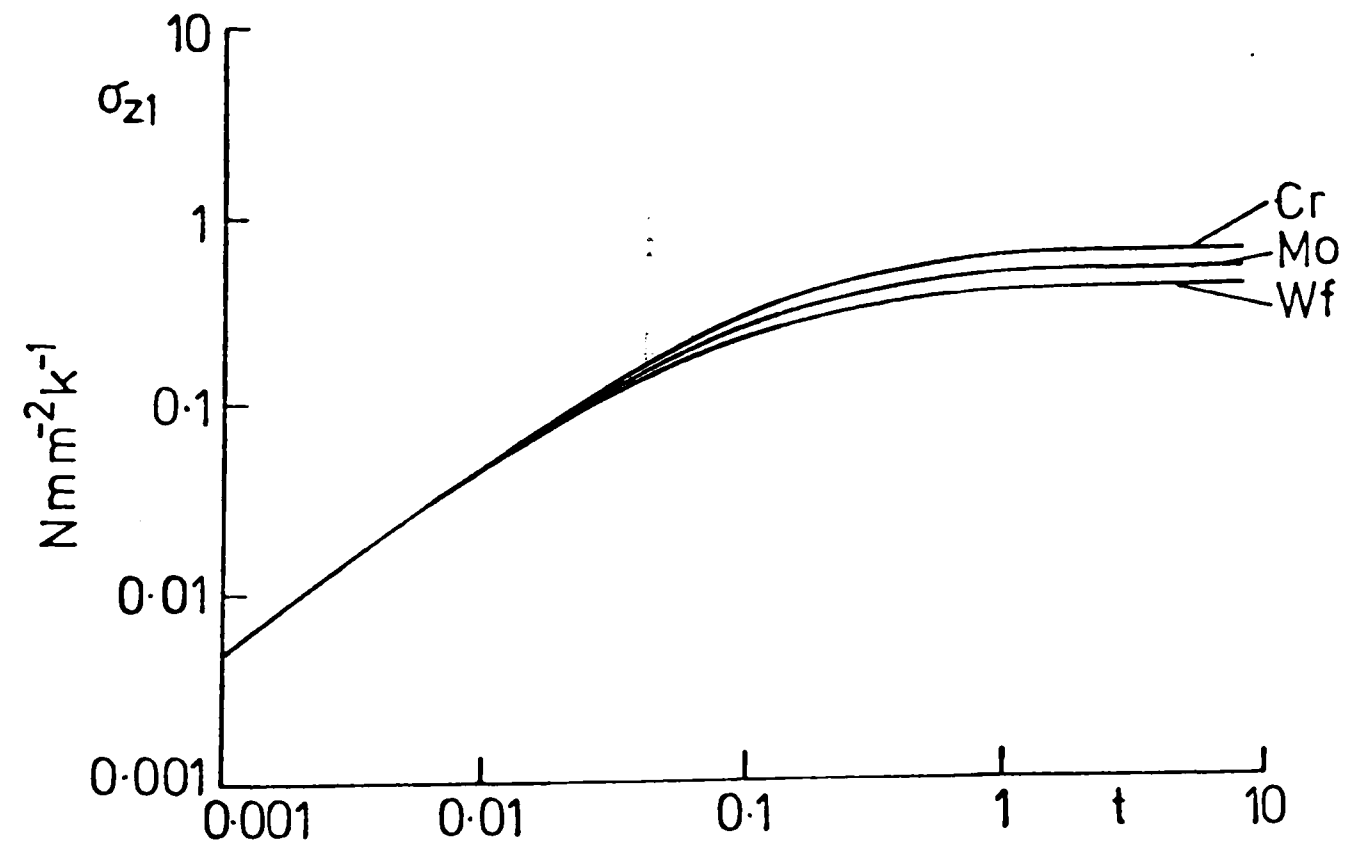
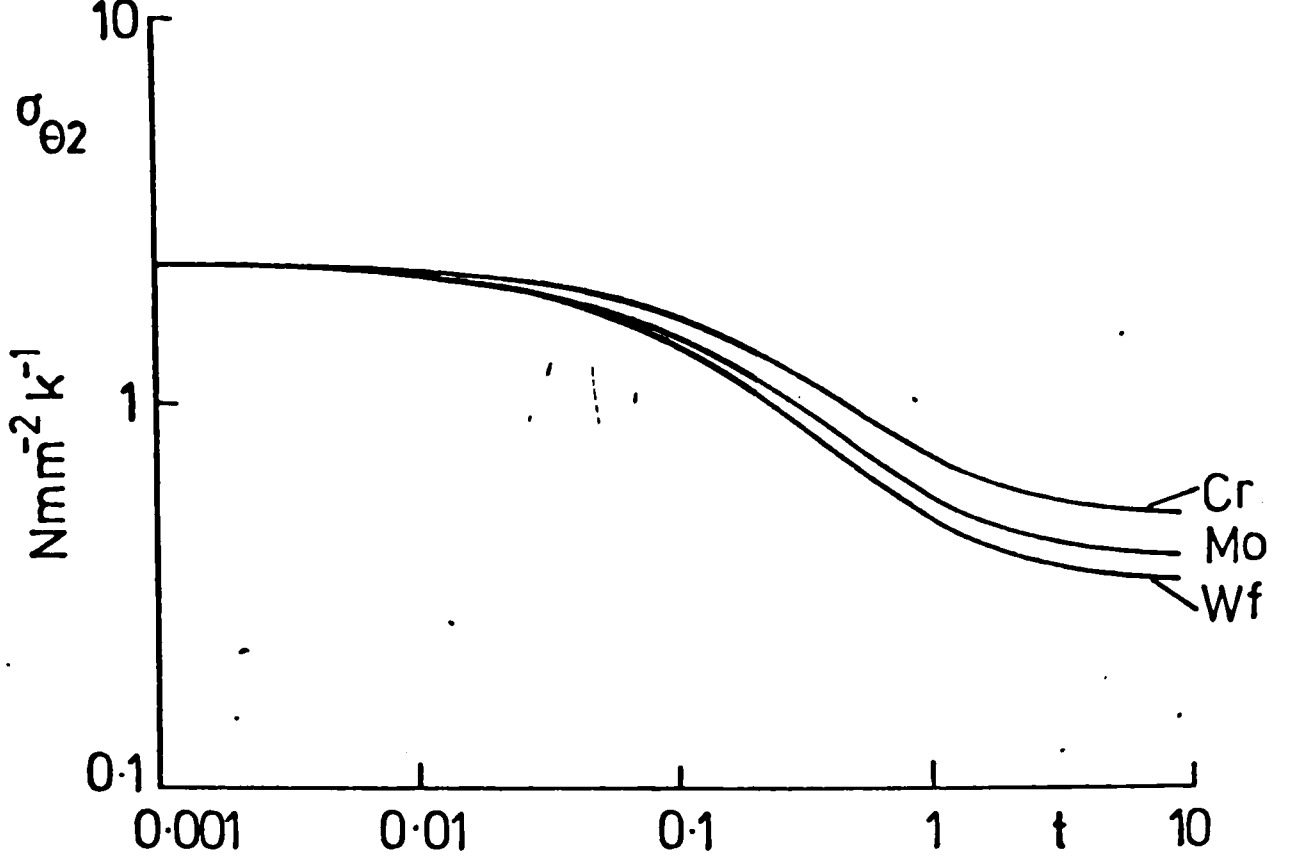


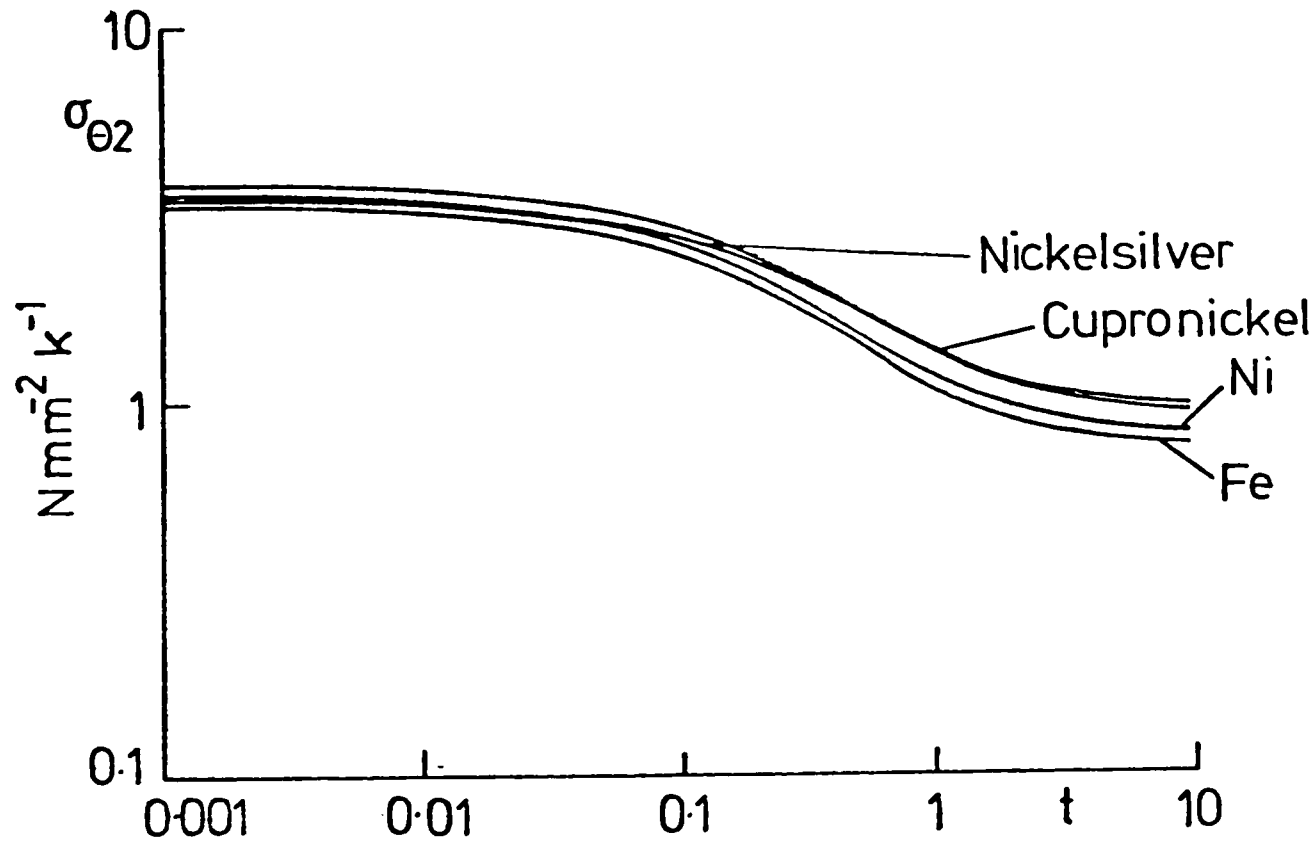
FIGURE 5-3

LONGITUDINAL PRESTRESS IN FIBRE VERSUS NORMALISED COATING THICKNESS (σ_{z1} at)

FIGURE 5-4

RADIAL PRESTRESS IN FIBRE VERSUS NORMALISED COATING THICKNESS ($\sigma_{r1} \alpha t$)





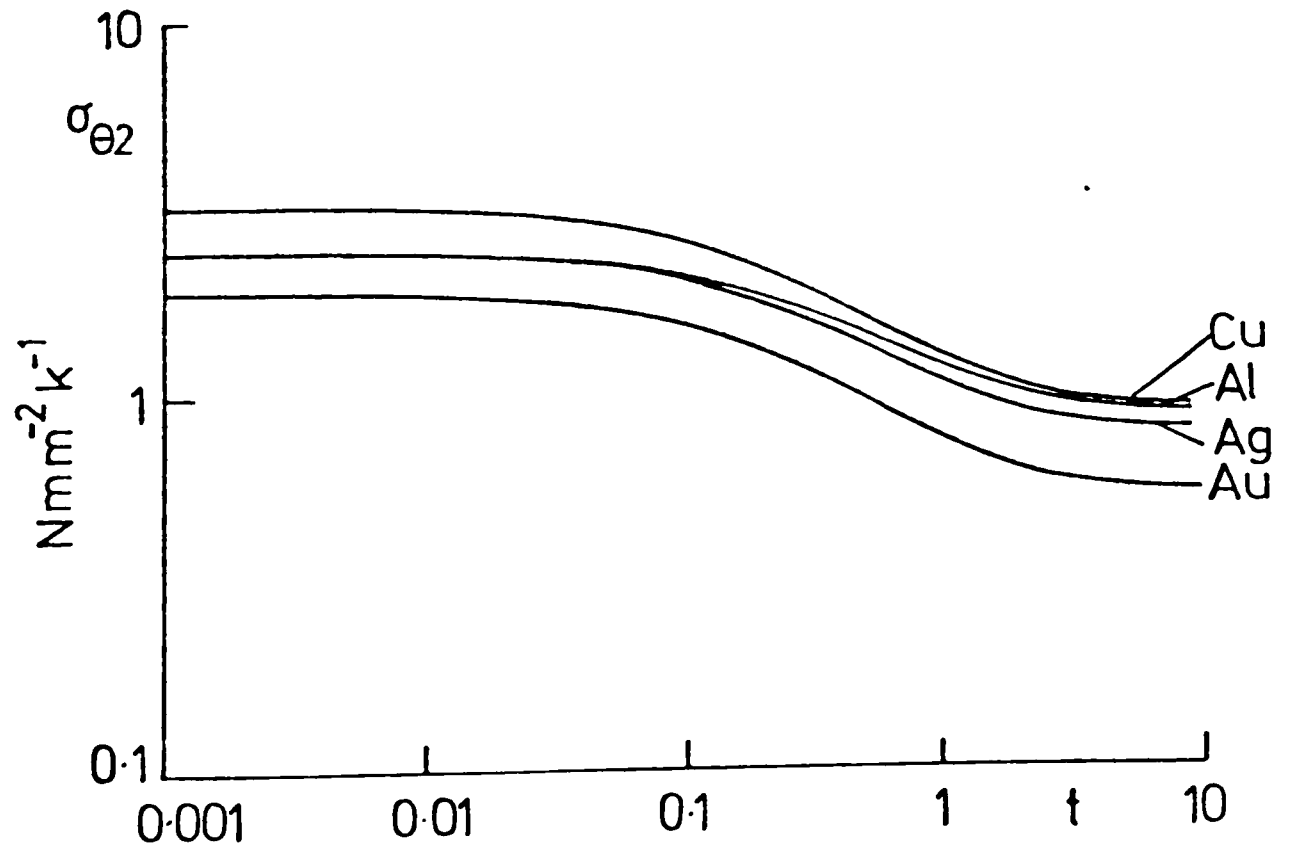
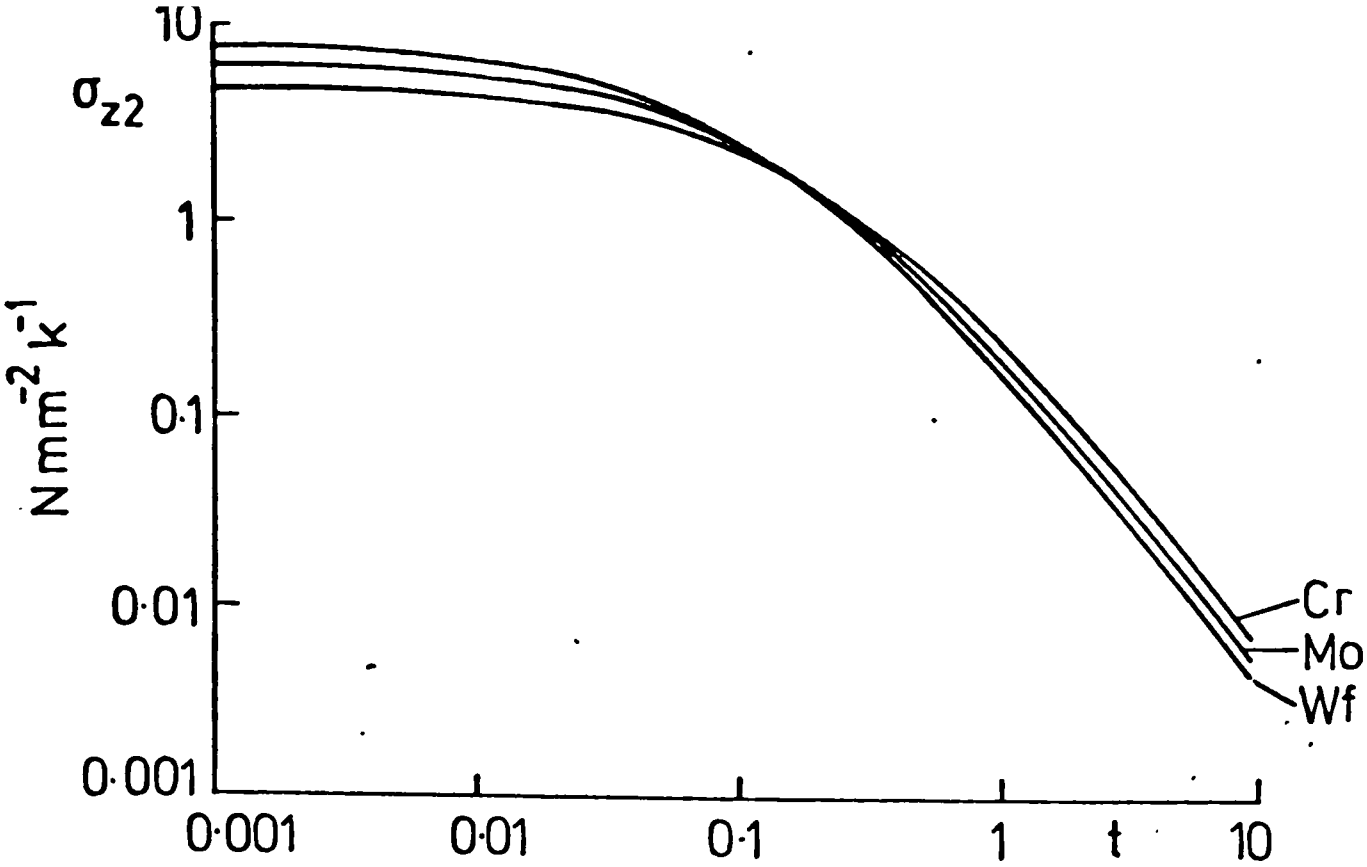
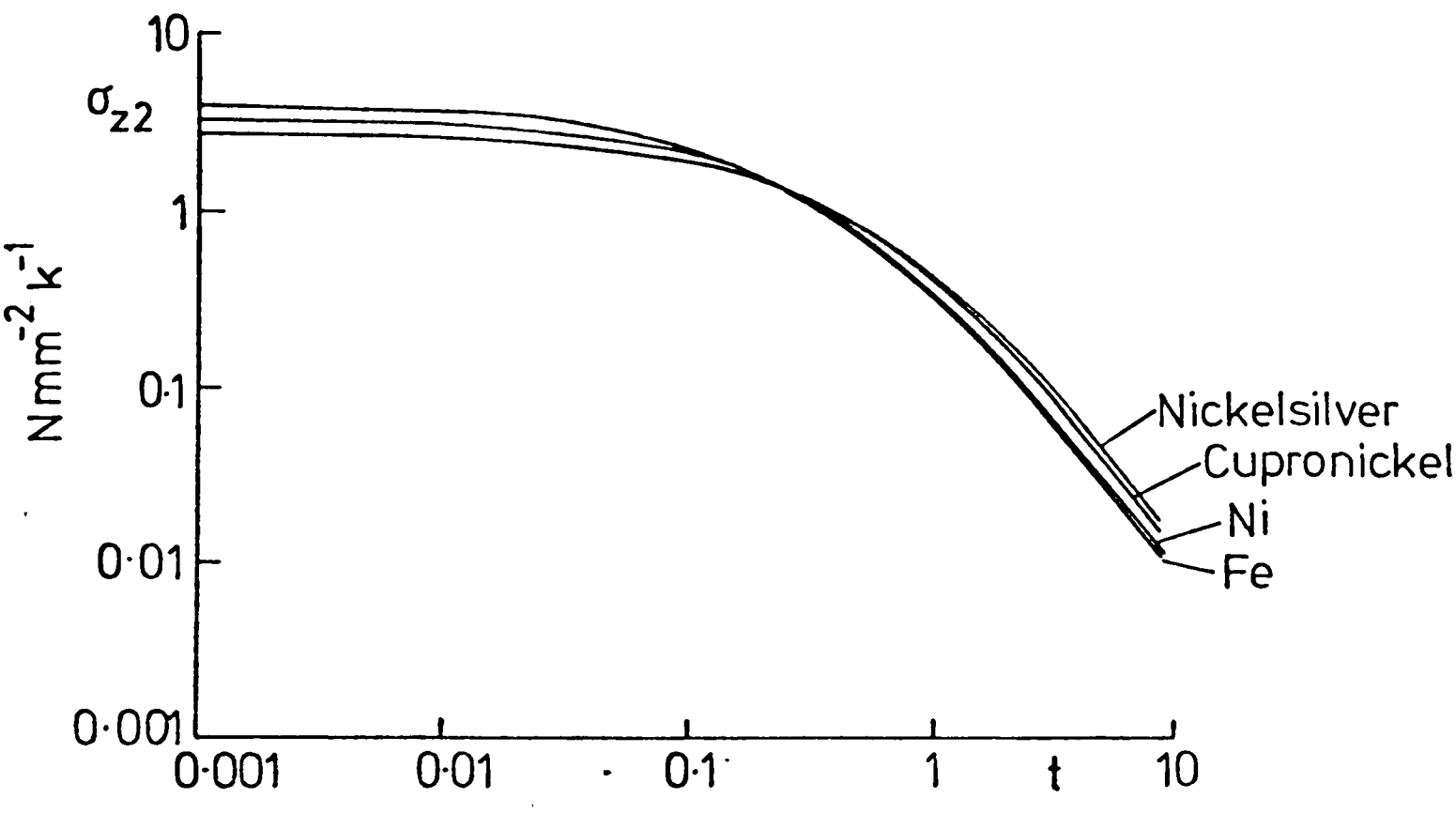


FIGURE 5-5

CIRCUMFERETIAL PRESTRESS IN METAL VERSUS NORMALISED COATING THICKNESS ($\sigma_{\theta 2} \alpha t$)





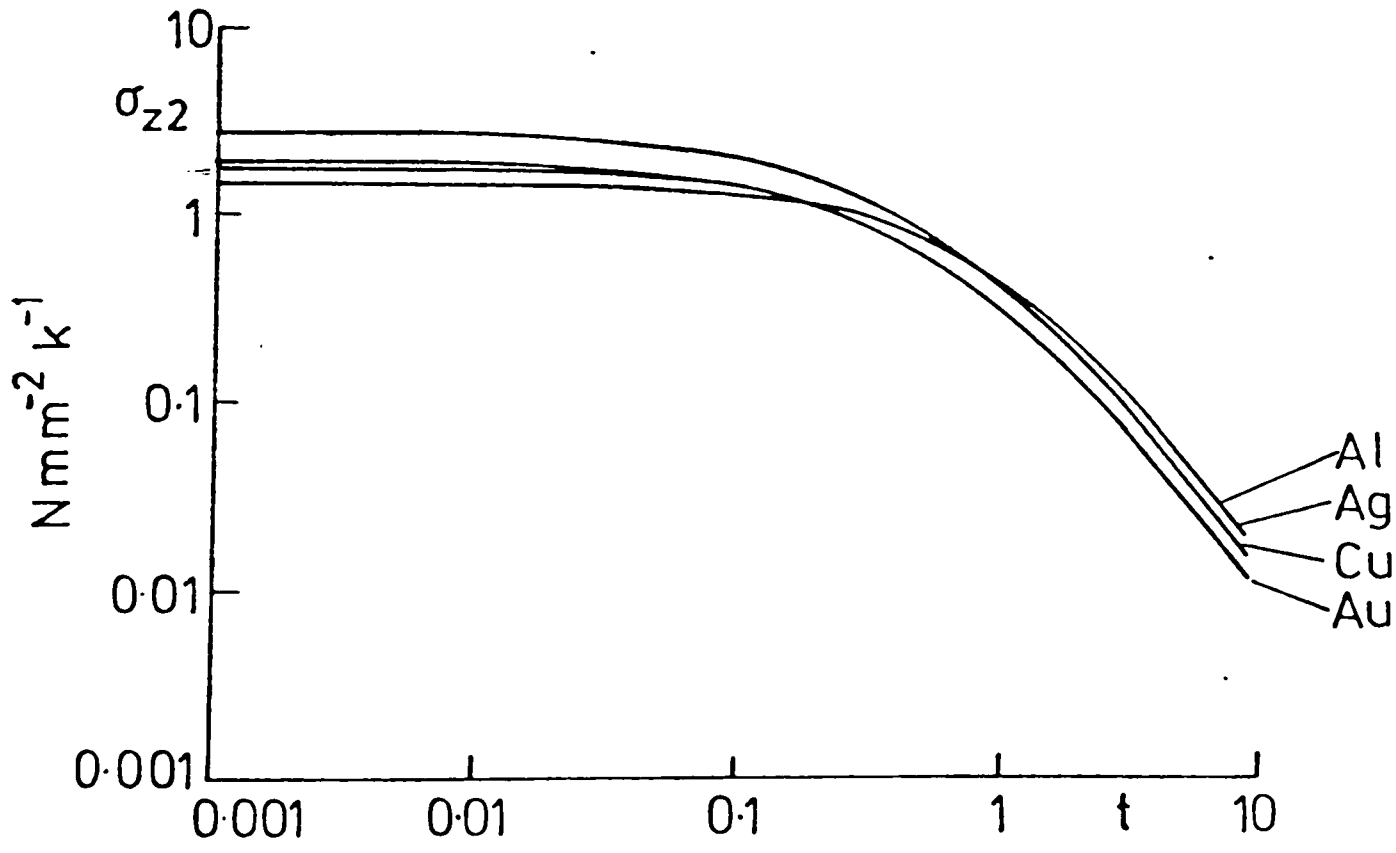


FIGURE 5-6

LONGITUDINAL PRESTRESS IN METAL VERSUS NORMALISED COATING THICKNESS ($\sigma_{z2}\alpha t$)

the 'freeze coating' technique does deteriorate the fibre surface, but the static fatigue results obtained indicate that stress corrosion is inhibited by the process.

As can be seen from figures 5.3 to 5.6, the curves are similar in form, and the remaining analysis will be mainly restricted to nickel to avoid confusion. For providing an axial prestress within the fibre, nickel appears to be a promising candidate material over a wide range of coating thicknesses. Figure 5.7 summarises the stresses induced in a silica fibre and nickel coating as a function of coating thickness. As is expected, all of the stresses within the metal fall with increasing coating thickness.

If the temperature drop is too great, the stress in the metal will reach its yield stress. The greatest stress in the metal is in the circumferential direction, and the ratio

$$\left|\frac{\sigma_{z1}}{\sigma_{\theta 2max}}\right| = \frac{(L+M)x + 2M}{(x+2)(Lx+M)} \qquad (5.4.45)$$

is plotted for various materials in figure 5.8. By referring to material tables of yield stress, these curves can be used in conjunction with figure 5.5 to define an upper temperature limit for a predetermined axial prestress and coating thickness.

Different criteria may be applied when establishing a desired temperature drop and associated coating thickness. As suggested before, we should ideally arrange for the fibre to reach its maximum tensile stress when the metal coating reaches its yield stress, Y. Equation (5.3.37),

$$\frac{T}{T_o} = 1 + \frac{xY}{\sigma_T},$$

where σ_T is the maximum tensile stress allowed in the fibre, is plotted in figure 5.9 for various values of Y assuming that σ_T is $30 Nmm^{-2}$. Equation (5.3.39) is used to define the required temperature drop for these curves.

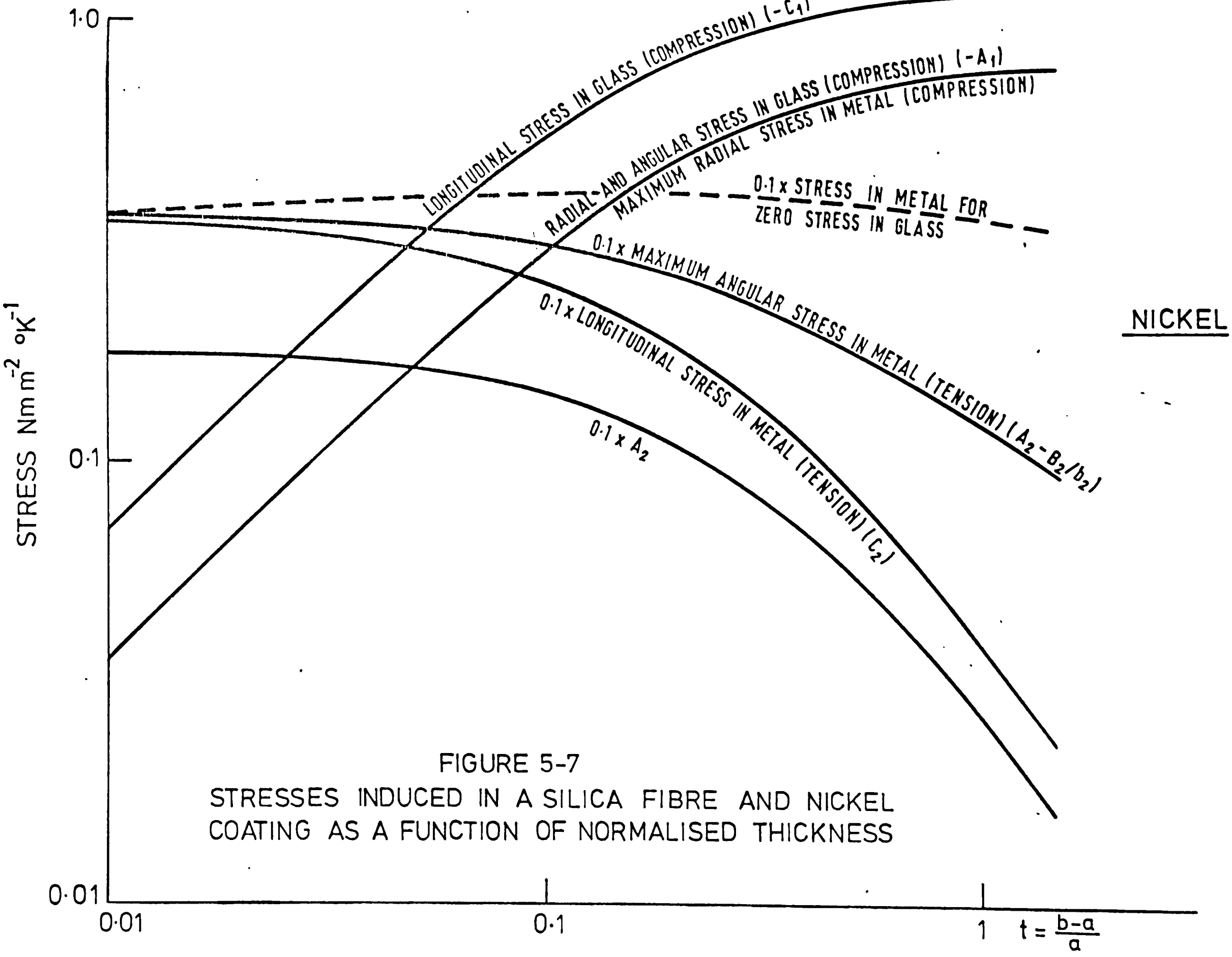


FIGURE 5-7
STRESSES INDUCED IN A SILICA FIBRE AND NICKEL COATING AS A FUNCTION OF NORMALISED THICKNESS

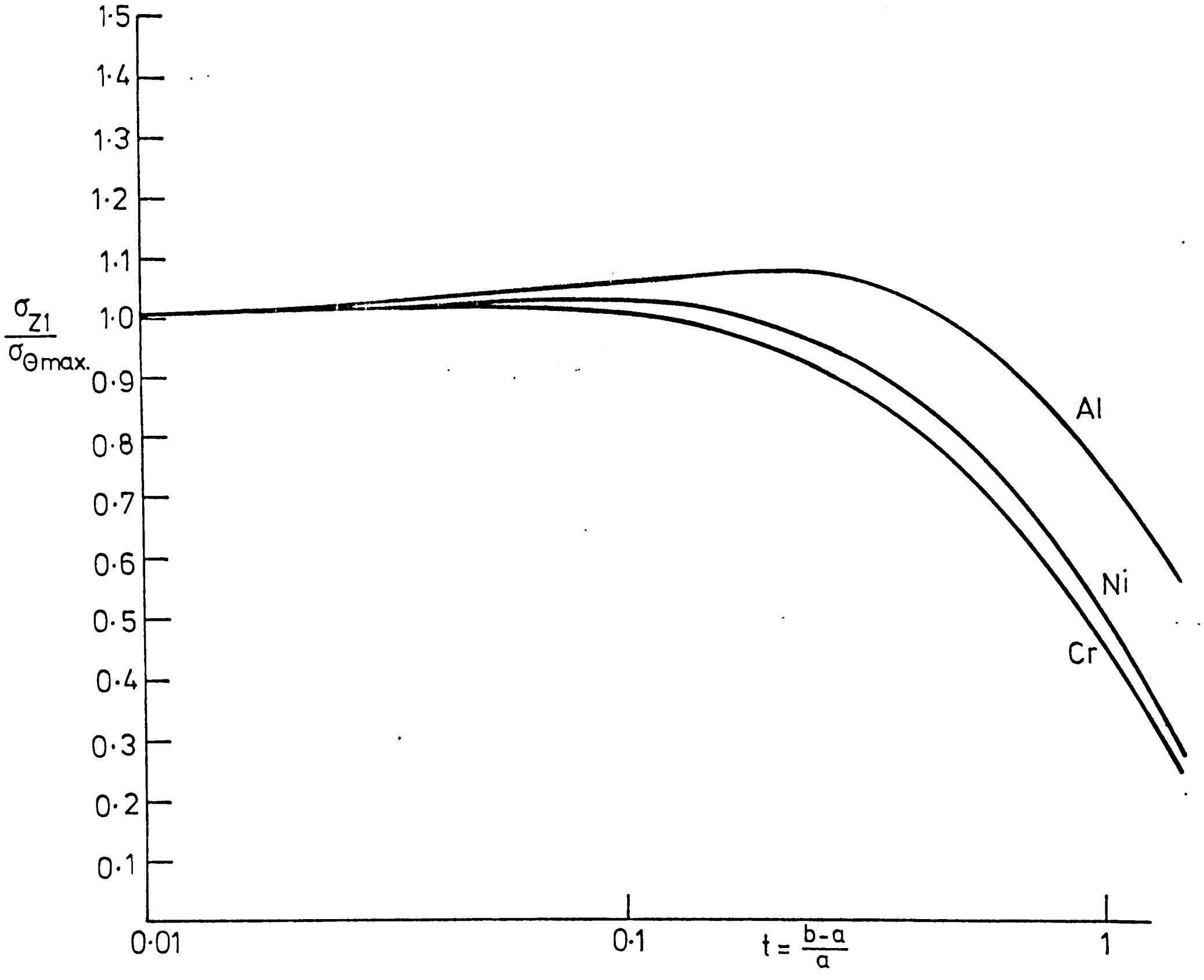


FIGURE 5-8 $\frac{\sigma_{Z1}}{\sigma_{\theta max.}}$ FOR ALUMINIUM, NICKEL, & CHROMIUM

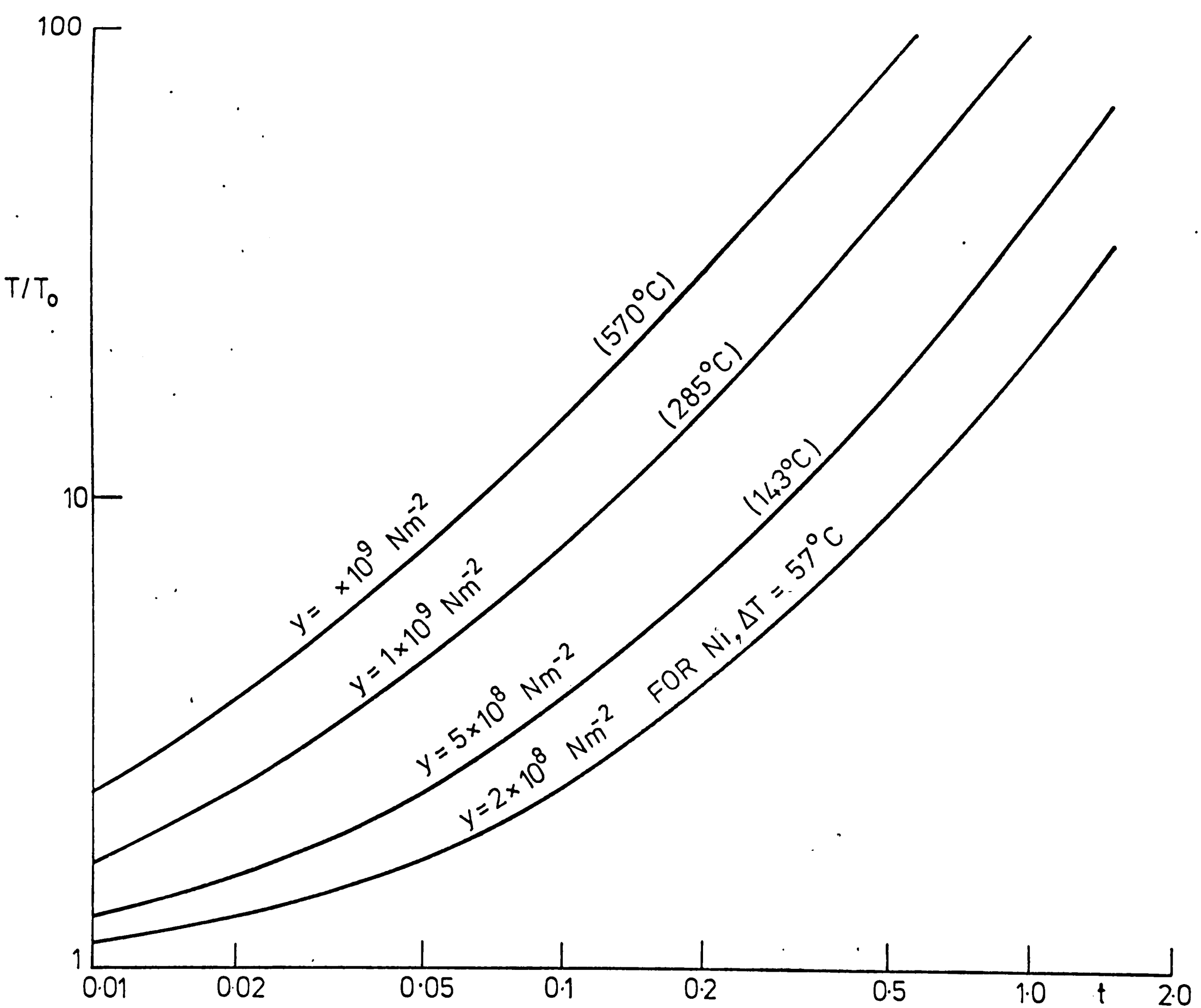


FIGURE 5-9 NORMALISED MAXIMUM TENSILE LOAD OF A COATED FIBRE AS A FUNCTION OF NORMALISED COATING THICKNESS ($\sigma_T = 30\ Nmm^2$)

Alternatively, should we require the metal to fail when there is zero axial stress in the fibre, we may use equation (5.3.35), plotted with a dotted line in figure 5.6. The required temperature drop may be calculated directly from this curve assuming a particular metal yield stress.

Finally, we may calculate the effective tensile or bending stiffnesses (modulii) of the composite by employing equations (5.3.41) and (5.3.42). Figure 5.10 plots these normalised stiffnesses versus coating thickness for nickel. It should be noted that the stiffnesses are independent of temperature drop.

5.5 IMPLICATIONS

Whilst it may appear to be short-sighted to restrict the analysis to nickel, it may be seen from figures 5.3 to 5.7, that for a thin metal coating of the order of $t = 0.002$, the prestress added by the coating is negligible compared to the tensile strength of pristine fibres. As our apparatus is limited to providing coatings of this order, the choice of coating is not effectively determined by which material will give the greatest prestress, unless the deposited layer can be subsequently thickened up to give a prestress in both the fibre and 'primary' metal layer. It may be possible to combine the magnetron sputtering process with the 'freeze coating' method, the sputtered layer isolating the fibre from chemical attack by the molten aluminium used for freeze coating. At this stage of work, however, utilizing both techniques is merely a suggestion.

From the stress corrosion aspect, we should primarily seek an hermetic seal, which implies the utilisation of a material which sputters quickly. This begs the question - what thickness of material constitutes an hermetic seal? Certainly a continuous stable film is required, the actual thickness being dependent mainly upon substrate

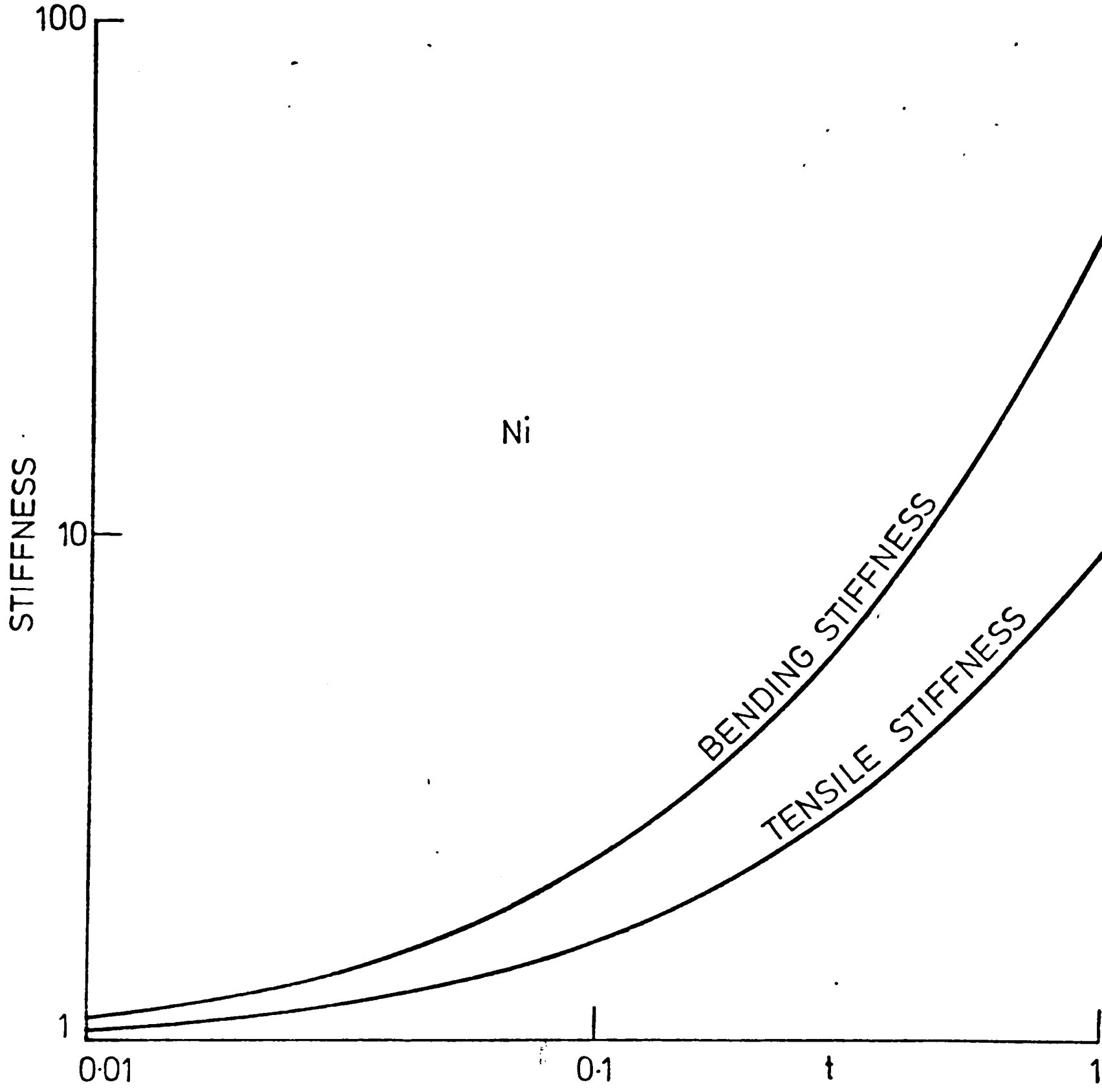


FIGURE 5-10

NORMALISED STIFFNESS IN TENSION AND BENDING FOR A NICKEL COATED FIBRE VERSUS NORMALISED COATING THICKNESS.

temperature, deposition rate, material, and method of deposition. A film thickness of at least 0.05μm is desirable, thinner films of most metals generally being unstable[38].

The nature of the adherence of the metal to the fibre substrate is also an important factor. As mentioned previously, Pinnow, using a reactive metal, aluminium, has achieved good stress corrosion results, but the ultimate strength of the fibre appears to be affected. Whether this is a function of the drawing operation or the coating process, is undetermined. Other experiments using a very similar coating method certainly experienced a vigorous silica-aluminium reaction which was difficult to control completely, and which damaged the fibre surface. Whether or not a vigorous chemical bond is required is not yet known.

Of importance to our coating technique is the requirement for a fast-sputtering material in order to produce a film of the required minimum thickness. Table 5.3 lists the yield in atoms per ion and deposition rates for a planar magnetron source[39]. It is evident that silver, gold, copper, palladium and platinum are preferred candidates from this aspect.

A final requirement for the coating is that it should be resistant to chemical, especially atmospheric attack. The specific choice of material will be dependent on the environment in which the fibre is to be used.

5.6 CONCLUSIONS

The analysis of section 5.2 suggests that a thick metal coating can substantially reinforce a silica fibre, and can relieve the fibre of an applied stress. If the coating is applied according to an established criterion (e.g. equations (5.3.37) and (5.3.38)) it can be made to fail in tension at a desired loading. Also apparent is that for a thick coating, the choice of metal, and the application temperature are important.

A thin metal coating, on the other hand (t < 0.05) will achieve little reinforcement, and the choice of metal is governed by other constraints, primarily the coating process, and desired mechanical properties.

Element	Yield Atoms/Ion @ 600V	Average Å/min† (Cu = 18,000)
Ag	3.4	21,200
Al	1.2	6,000
Au	2.8	17,000
Co	1.4	3,000
Cr	1.3	8,000
Cu	2.3	14,000
Fe	1.3	(*)
Mo	0.9	5,500
Ni	1.5	3,000
Pd	2.4	14,500
Pt	1.6	10,000
Si	0.5	3,200
Ta	0.6	3,500
Ti	0.6	3,500
W	0.6	3,500

† High rate Planar Magnetron deposition rates for 5 x 12 inch cathodes using 6A D.C.

* Magnetic materials may not be deposited except with thin cathodes using special magnetics

TABLE 5.3

Planar Magnetron Deposition Rates(39)

CHAPTER SIX

EXPERIMENTAL PROCEDURES AND RESULTS

6.1 INTRODUCTION

This chapter details the methods by which fibres are manufactured, and outlines the properties of fibres thus produced as far as they have been ascertained. As the apparatus is novel, much experimental procedural detail is included as a guide for future work and operation of the fibre drawing machine. The conditions under which the fibre is drawn, as far as they can be determined, are stated for the experiments which have been conducted.

Some five or six kilometres of metal coated fibre have been produced, with coatings of a variety of metals. This is not really sufficient to produce accurate, quantitative results for fibre strength and stress corrosion resistance, but certain properties can already be inferred. The later sections of the chapter discuss the preliminary results of the investigation into the mechanical qualities of the fibre. For these initial experiments, poor quality (i.e. cheap) silica rods with many internal flaws were drawn down into fibre - the flaws, mainly internal voids, are present within the fibre and tend to somewhat limit the validity of conclusions made.

6.2 OPERATION OF THE FIBRE DRAWING APPARATUS

To produce fibre from a fresh rod or preform, several steps are necessary. The list below outlines these procedures, which are then detailed in steps.

A) Introduction of new rod into the system

B) Pumpdown procedure to produce vacuum

C) Furnace warm up to melt rod

D) 'Blob' formation to initiate fibre draw-off

E) Drawing and coating fibre

F) Removal of fibre from apparatus

A) Introduction of new rod into the system

1) Select rod and corresponding 'O' ring seal. Check rod diameter at both ends with micrometer to ensure against undersize or taper. Mount rod within seal and tighten.

2) Drive moving crosshead and chuck to upper limit.

3) Insert rod through furnace top plate hole, and with seal in central position, clamp seal to furnace top plate.

4) Lower moving crosshead and tighten chuck onto rod.

5) Align chuck to ensure rod is vertical.

B) Pumpdown

1) Close electrical isolator on wall.

2) Open water valve for diffusion pump - minimum flow 1.6 L/min.

3) Ensure all vacuum valves shut.

4) Close main console contactor, switch on power to vacuum control.

5) Start rotary pump, open backing line valve.

6) Start diffusion pump; wait until backing line pressure reaches 0.04 Torr (5 minutes).

7) Close backing line valve.

8) Open roughing line valve; wait until system pressure reaches 0.15 Torr (15 minutes).

9) Close roughing line valve.

10) Open backing line valve.

11) Open quarter swing valve; wait until system pressure reaches 2×10^{-6} Torr (20 minutes to 2 hours, dependent upon outgassing).

C) Furnace Operation

1) Check vacuum - 2×10^{-6} Torr for 'blob' formation,

2×10^{-3} Torr (Argon) for pulling run with coating.

Argon is admitted to the system via a bleed valve on the winding drum chamber. Allow argon to flow for 5 minutes to eliminate air which may have been trapped in pipework.

2) Open water valve for furnace cooling - minimum flow 3.2 L/min.

3) Switch on power to controller electronics.

4) Check controller function switches:

Switch	Position
Auto./Man.	Man.
Temperature range	L
Power range	300 W
Reset	Press
Power limit control	Zero

5) Close thyristor stack contactor (power distribution panel).

6) Press 'GO' button.

7) Set desired power - the power to the furnace will ramp up to this desired power and maintain this constant power input level.

C) 'Automatic' Mode of Operation

1) Wait until indicated temperature reaches changeover temperature ($1100^{o}C$).

2) Set desired temperature.

3) Set desired power limit.

4) Adjust 'integral' and 'differential' time to zero.

5) Press and hold integrator reset button.

6) Adjust 'gain' control for zero transfer error, swith to 'AUTO'.

7) Trim 'integral', 'differential' and 'gain' controls to optimal values indicated on panel.

8) Controller automatically reaches and maintains desired temperature $\pm 5^{o}C$ (indicated).

D) Blob Formation

1) Lower 150mm of rod into the furnace using feed motor.
2) With furnace in manual mode ramp to required power level 7.4 (element temperature 2080°C, axis temperature 1800°C, actual power 3.8kW).
3) Wait until 'blob' (excess rod plus fibre) falls through coating chamber to winding drum.
4) Reduce 'power limit' control to zero and switch off controller.

E) Fibre Drawing and Coating Procedure

Note: Omit asterisked steps for production of uncoated fibre.

1) Allow furnace to cool (20 minutes).
2) Isolate main vacuum system (close quarter swing valve) and bring system to atmospheric pressure using bleed valve.
3) Support lower end of coating chamber and swing winding drum forward to expose fibre and 'blob'.
4) Cut off 'blob'. Araldite thin copper wire to end of fibre and attach wire to drum with 6BA bolt.
5) Swing winding drum back to close vacuum system.
6) Pumpdown to 2×10^{-6} Torr.
*7) Bleed argon into system to 2×10^{-3} Torr.
8) Operate furnace to desired temperature/power.
9) Set desired feed, winding and traverse speeds.
10) Start feed motor and then winding and traverse motors.
*11) When drawing is initiated, switch on power to sputtering D.C. supply, with variac at minimum. Open water valve for cathode cooling (3.2 L/min).
*12) Increase sputtering supply voltage and initiate plasma (approximately 650 Volts, dependent on target material).
*13) Gradually increase sputtering current to desired value. Occasional current surges occur until the target is 'clean'.

14) To terminate experiment:

- * Reduce sputtering powersupply voltage to zero and switch off.
- Switch off feed, winding and traverse motors.
- Reduce furnace power to zero and switch off.
- Allow furnace to cool (20 minutes).

F) Removal of Fibre from Apparatus

1) Isolate main vacuum system and bring system to atmospheric pressure.
2) Support lower end of coating chamber and swing winding drum forwards to expose fibre.
3) Cut fibre.
4) Position wind-off apparatus over winding drum chamber flange (photograph figure 2.3).
5) Reverse direction of winding drum motor, switch on at low speed to withdraw enough fibre to reach off-wind spool.
6) Attach fibre to off-wind spool with plastic insulating tape.
7) Apply sufficient power to wind-off motor (using variac) to just tension fibre.
8) Start winding drum motor and increase speed to a maximum of 2m/min. No transverse motion is necessary.

The concept of 'blob' formation may strike the reader as quite odd. When the apparatus was first completed the greatest difficulty envisaged was that of actually starting a pulling operation from a fresh rod. However, during preliminary trials of furnace performance, it was noted that the rod melting process was very well controlled, and that when excess rod was within the furnace, a neck was produced when the rod softened. This feature has been utilised in a modified form to initiate fibre draw off. The difference between this apparatus and conventional machines is that there is no easy access to the

bottom of the furnace; in conventional machines fibre initiation and draw off is usually completed in one operation. The extra time needed to actually draw a fibre in an evacuated chamber may be an eventual limitation to an industrial process. However, the author is confident that the apparatus could be modified to accomplish 'blob formation' and fibre draw off in one operation. In our research, we do not consider this to be a drawback; if nothing else the delay enables the operators to gather their thoughts.

6.3 PERFORMANCE OF THE FIBRE DRAWING APPARATUS

6.3.1 Temperature

The temperature of the draw-down zone cannot be measured during an experiment, but an estimate can be extrapolated from furnace performance curves. Figure 3.5 plots indicated element temperature versus actual element temperature as measured by a disappearing filament optical pyrometer viewing through the furnace observation port. By using figure 3.5, the axis temperature may be estimated for each fibre drawing run.

A further complication to temperature estimation became evident after initial experiments. The thermocouples used proved to be somewhat unreliable due to their fragility, and several of them went open-circuit at high temperatures. This results in the furnace shutting itself down and the subsequent loss of fibre. Consequently experiments have generally been conducted at a constant power level. Preliminary calibration has shown that operating at constant power produces an indicated temperature repeatable to within $15^{o}C$, and which varies during an experiment by a maximum of $10^{o}C$. The power limit versus indicated temperature calibration is periodically checked to ensure repeatable experimental conditions as the furnace element ages. Figure 6.1 plots indicated temperature and power versus power

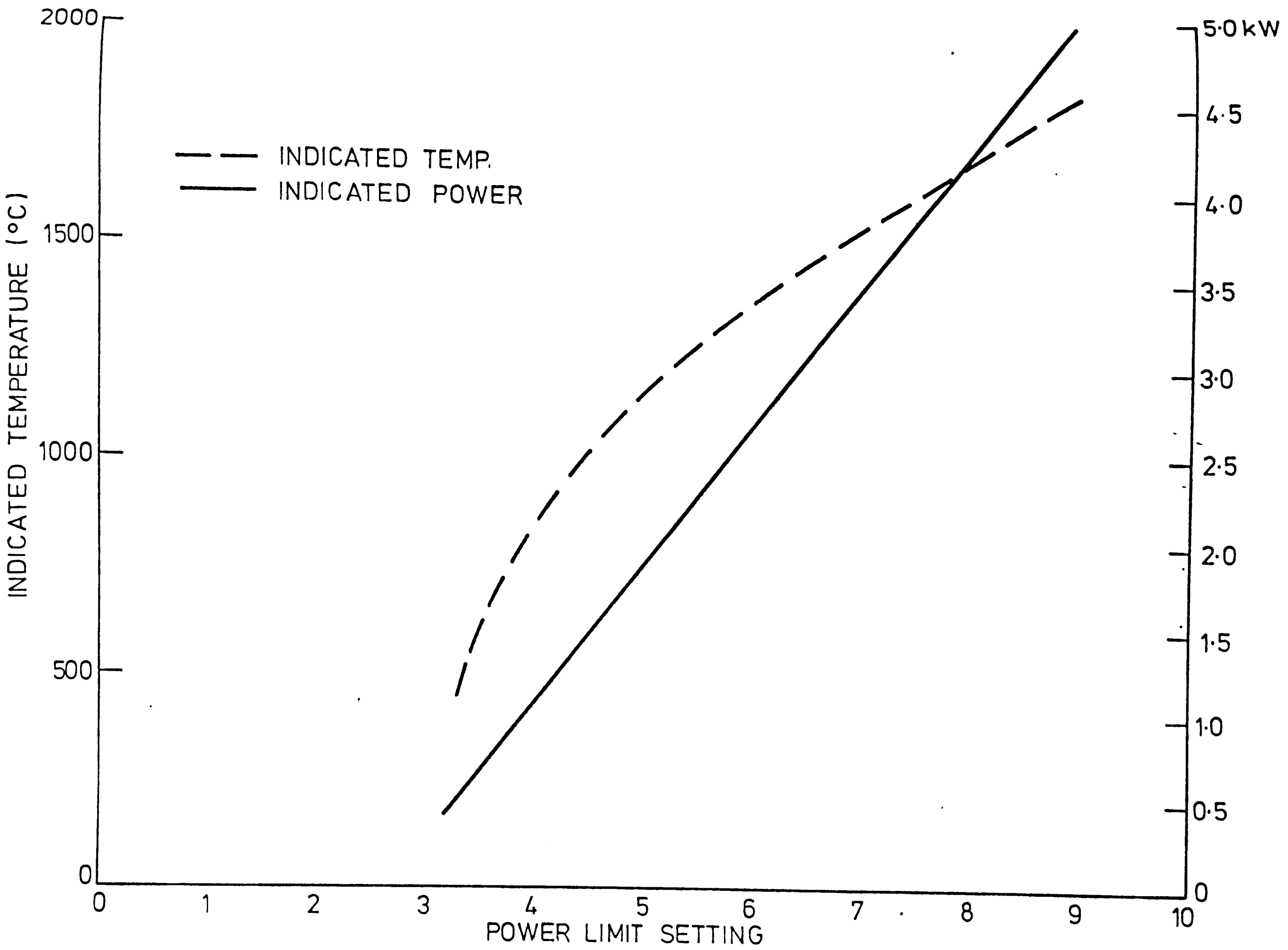


FIGURE 6-1 INDICATED TEMPERATURE AND POWER VERSUS POWER LIMIT SETTING (MANUAL MODE)

limit setting, from which the element and subsequently the axis temperature may be determined, again by consulting figure 3.5.

Figure 6.2 plots indicated furnace power versus actual furnace power, the actual furnace power being measured using an ammeter and voltmeter directly attached to the furnace power lines. A correction has been applied to allow for a slight phase lag. These measurements were achieved by powering the element step-down transformer via a variac, thereby avoiding the problem of peculiar wave shape (and difficulty in measuring R.M.S. values) which would have been present using the furnace controller phase-fired thyristors. As the furnace controller power measurement circuit multiplies together instantaneous values of current and voltage, the peculiar wave-shape should still produce consistent readings of power with the phase firing circuit. The curve of figure 6.2 is somewhat limited by non-availability of equipment to read more than 300A but is consistently repeatable.

An initial experiment with the apparatus was to draw fibre whilst gradually reducing the furnace power. Qualitatively, the strength of the fibre produced was fairly consistent above a power limit setting of 6.8, corresponding to an axis temperature of 1730^{o}C. Since this experiment, we have used a power limit setting of 7.1 (axis temperature 1765^{o}C) for all subsequent experiments in an attempt to produce fibre under consistent conditions.

Below an axis temperature of 1760^{o}C, the viscosity of the silica at the draw-down neck increases, and a higher tension is required to pull off fibre from the neck. There is then a danger of introducing fibre flaws by overstressing the fibre whilst in a semi-molten state, which would account for the strength reduction observations. (On the other hand, fibre diameter control improves). The actual pulling tension has been estimated by weighing the 'blob' formed when initiating the fibre; this weighs between 4-5 grams. The blob falls under its own weight at a speed comparable to that of a fibre drawing and coating experiment, of the order of 3m/min.

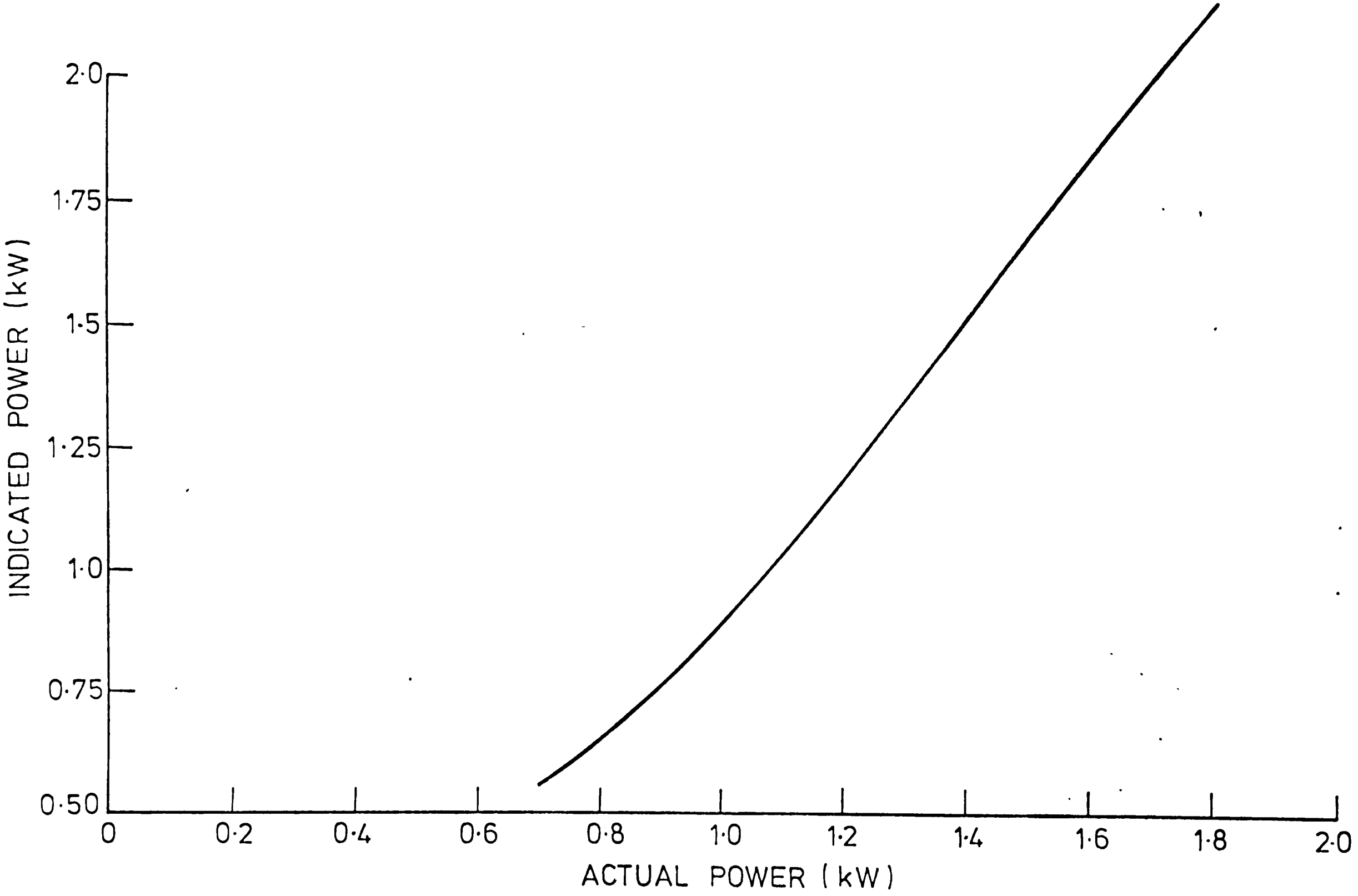


FIGURE 6-2

INDICATED FURNACE POWER VERSUS ACTUAL POWER

6.3.2 Fibre Diameter Stability

Due to the comparatively long hot zone of the tungsten mesh furnace compared to heat sources used with conventional fibre drawing machines, and the slow drawing speed needed to deposit a substantial amount of metal, it was thought that fibre diameter control may have been a problem. Both the aforementioned characteristics tend to encourage re-melting of the fibre immediately beneath the draw-down region. The low drawing speed also denied the use of an optical diameter measuring device to servo-control the drawing speed, as it would tend to be unstable and limit cycle unless very carefully designed to overcome the time lag between measurement and correction. As it turns out, the use of constant feed speed and constant drawing or winding speed produces acceptable results, as is shown below.

Figure 6.3 shows a plot of fibre length versus diameter of an early experiment, during which the apparatus was stopped, cooled, and restarted twice (indicated on the graph). The fibre diameter was measured using a micrometer at 0.4m intervals, and the base rod was visually inspected and deemed flaw-free before the experiment. The drawing speed was 3m/min, and the feed speed selected to produce a fibre with diameter 170μ (2.5mm/min) from a rod 6mm in diameter. After about 70m of fibre has been drawn the process can be seen to have stabilised, with a diameter 184.5 ± 7.5μm (± 4.06%). The system response can be seen to be rather underdamped, with about 20% initial overshoot, with short term fluctuations observable after the apparatus has stabilised; the cause of the short term fluctuations (approximately every 6m) is not at present understood. After each stop, the fibre diameter in each case overshoots the final settled value.

In order to investigate the settling length of a drawing experiment, a similar experiment to the last was carried out (with the feed and drawing speeds recalibrated) without stopping and restarting. Figure 6.4 plots the results.

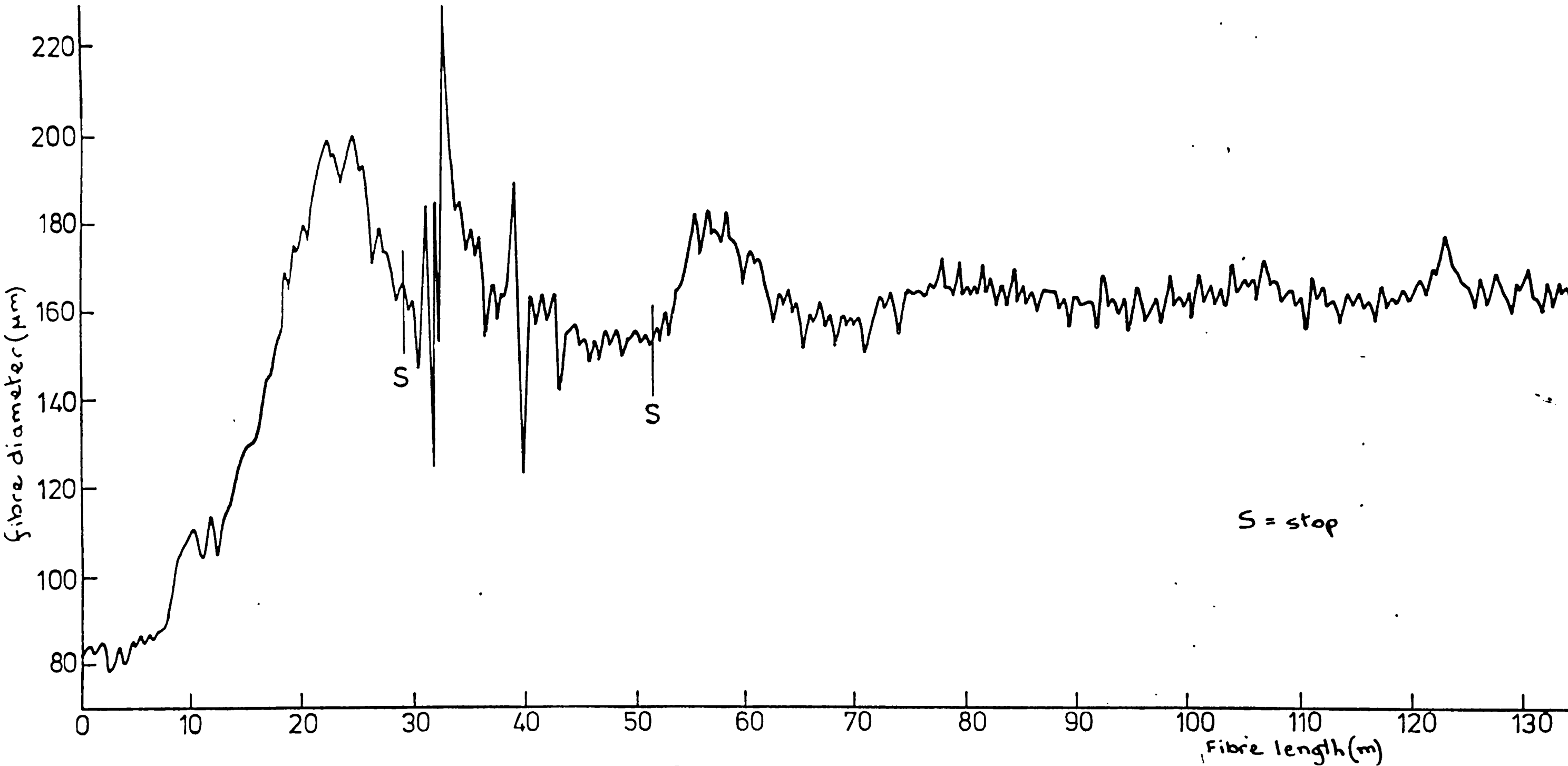


FIGURE 6-3
EARLY PLOT OF FIBRE DIAMETER VERSUS LENGTH (expt. No. SR7)

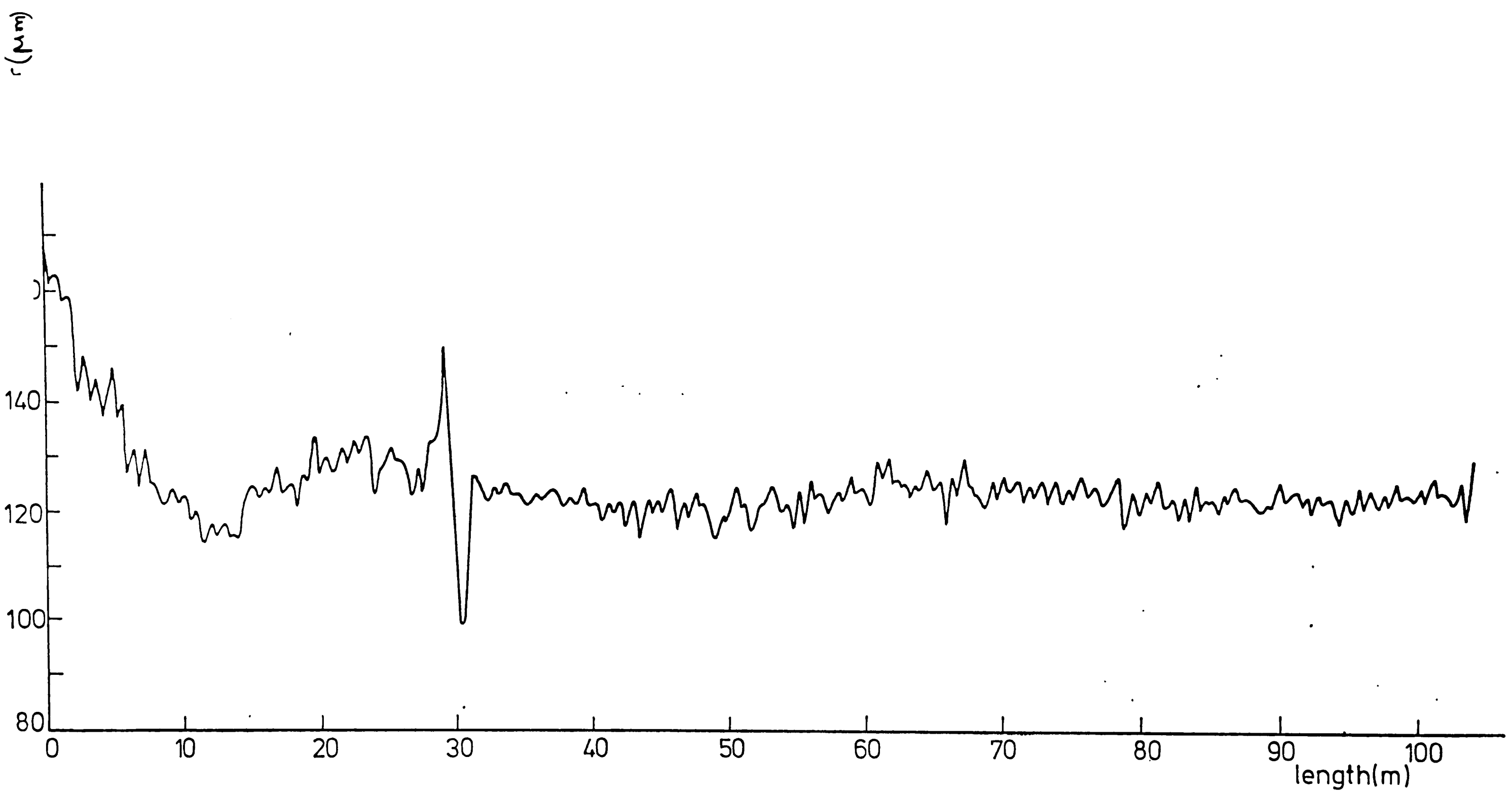


FIGURE 6-4

PLOT OF FIBRE DIAMETER VERSUS LENGTH (expt. No. SR11)

Again, overshoot is present (the first few metres of fibre were lost), and the process can be seen to have settled after a distance of 31 metres - this is now used as the basis for stability; the first 40 metres of fibre drawn from an experiment is now discarded, allowing a safety margin of 25%. The feed speed in this case was 1.28mm/min, and the drawing speed 3m/min, which gives for the 6mm rod used, a calculated fibre thickness of 124μm; the actual thickness after settling is 123μm ± 7μm (5.7%, standard deviation 2.425). The wild diameter fluctuation at 30m is due to a small flaw within the rod, which produced hollow fibre at this point.

Figure 6.5 shows the inadvisability of

(i) using rods with flaws, and

(ii) changing feed and winding speeds during an experiment.

The feed and drawing speeds were chosen to produce a fibre diameter of 124μm from a 6mm rod, the initial drawing speed being 3m/min. The initial part of the plot (to a fibre length of 86m) shows the effect of a major internal flaw - wide fluctuation of fibre diameter. At 86m, the feed and drawing speeds were both doubled, and again the fibre diameter fluctuates wildly, with the diameter beginning to stabilise to 124μm at a length of 120m. The feed and drawing speeds were doubled again at 124m, the drawing speed now being 12m/min, and the fibre diameter did not settle at all up to a pulled length of 170m, when the original drawing conditions were reselected. It can be seen that at the end of the experiment, the fibre diameter was increasing towards the desired 124μm. From these results it is evident that to change pulling speeds during an experiment is undesirable as much fibre is wasted during the re-stabilising period.

Figures 6.6 show cross sections of a silica rod and the fibre drawn from the rod. The ellipticity of the fibre (ratio of minor axis length to major axis length) is 0.976, whereas that of the rod is 0.993. Because of the nature of the furnace, the hot zone is not

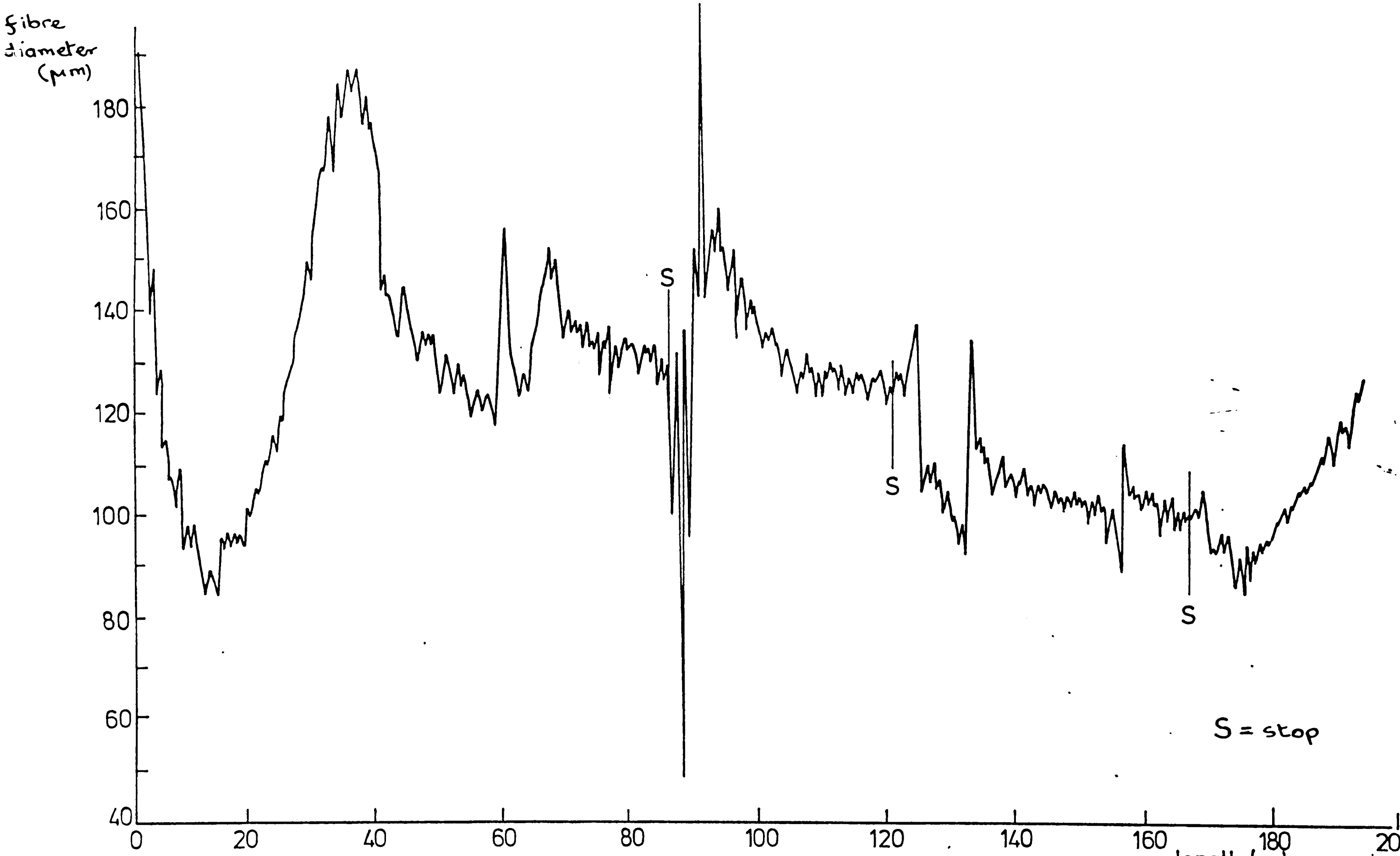
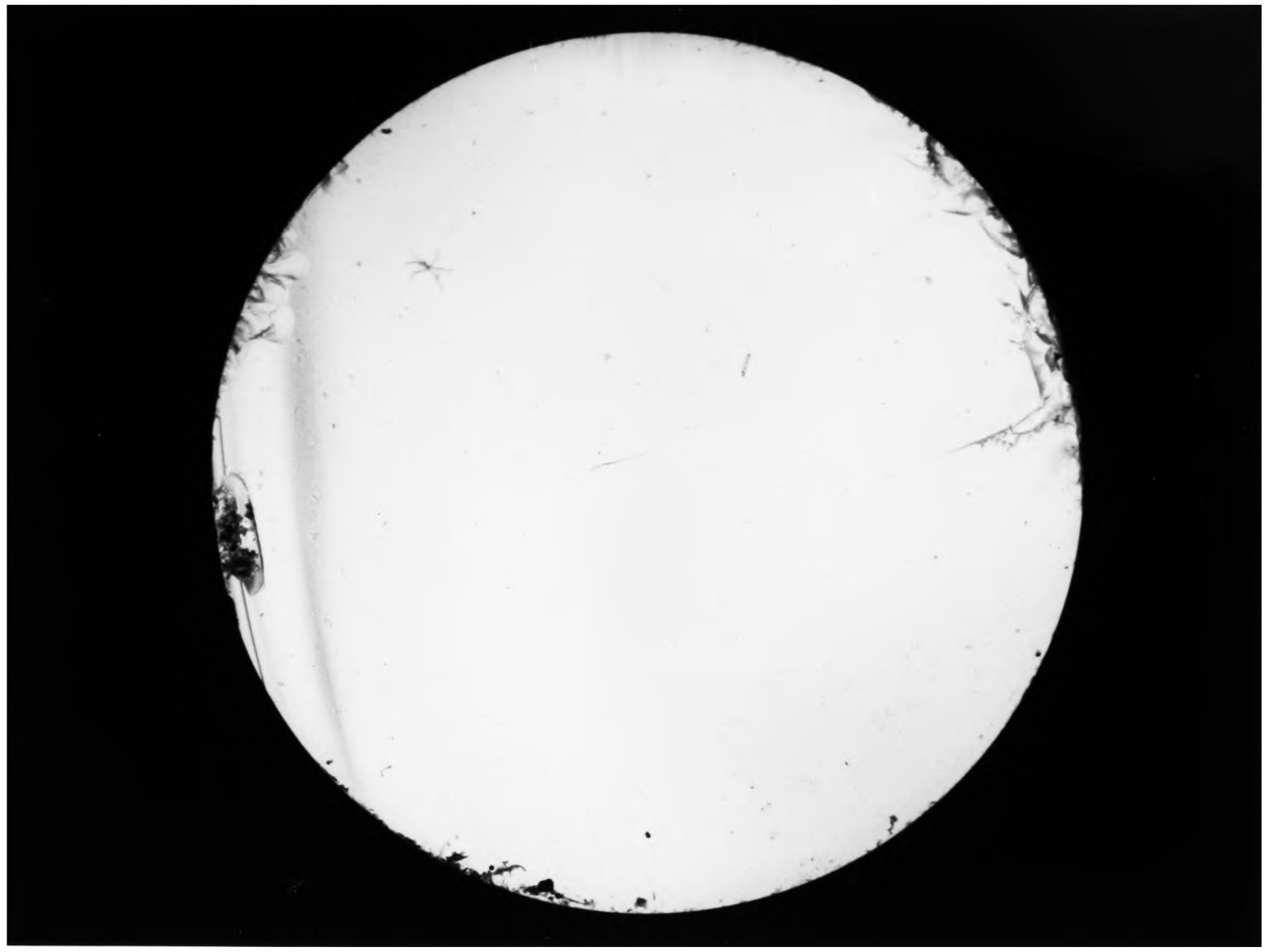


FIGURE 6-5
PLOT OF FIBRE DIAMETER VERSUS LENGTH (expt. SRIQ)

(i)



(ii)

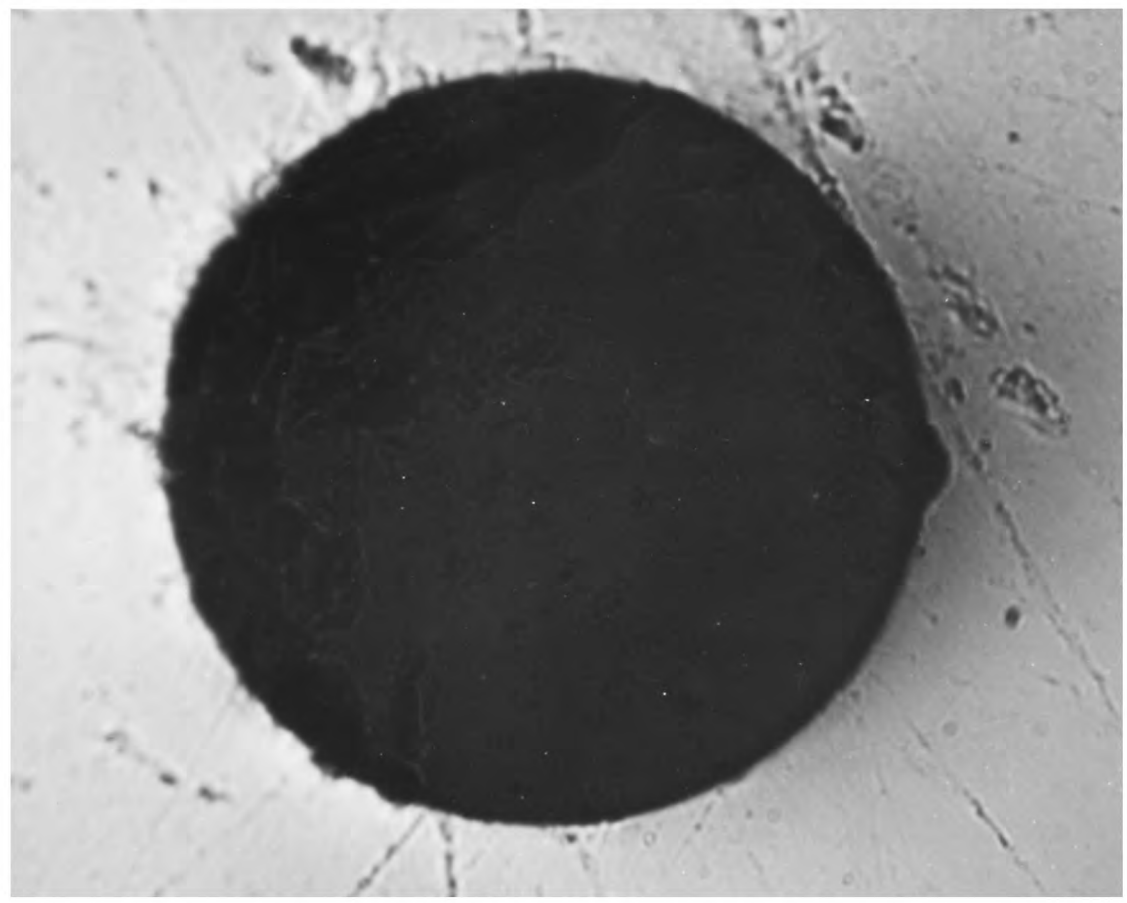


Figure 6.6 Photographs of Cross Sections of (i) Rod (ϕ=6mm)
(ii) Fibre drawn from Rod
($\phi \simeq 120\mu m$)

strictly cylindrically symmetrical but this can be seen to produce no major fibre ellipticity.

6.3.3 Characteristics of Uncoated Silica Fibre

At present, only qualitative assessments of the fibre produced can be made, although preliminary tensile strength measurements have been made. This is primarily because the apparatus has up to this point been used to determine its own characteristics, and to prove that fibres can indeed be produced within a vacuum. Consequently, cheap base material has been used, and to conduct exhaustive mechanical tests on fibre produced from silica of dubious characteristics would produce largely meaningless results. Preliminary results are presented here, but work is now in progress with high purity flaw-free rods which are necessary to produce high strength and repeatability.

The fibre strength measurements were made using an Instron 1026 tensile testing machine, with the following test conditions:

Material: Vibrisil

Gauge Length: 100mm

Crosshead Speed: 10mm/min (i.e. strain rate 10%/min)

Jaws: pneumatic action, rubber faced; clamping pressure 45 p.s.i.

At the time of the tests, the uncoated fibres were four weeks old, having been wound on a 150mm diameter plastic drum immediately after production, and stored in the normal laboratory atmosphere. The nominal diameter of the fibre was 163μm, and the diameter at break was measured using a calibrated graticule within a conventional optical microscope. The results of fifty tests are expressed on a Weibull plot in figure 6.7

The results show a fairly large spread of ultimate strengths, varying from 0.29 GN/m^2 to 0.83 GN/m^2, and well below figures reported for freshly drawn fibres. This suggests the existence of flaws, produced by the drawing technique, the poor quality rod, or stress

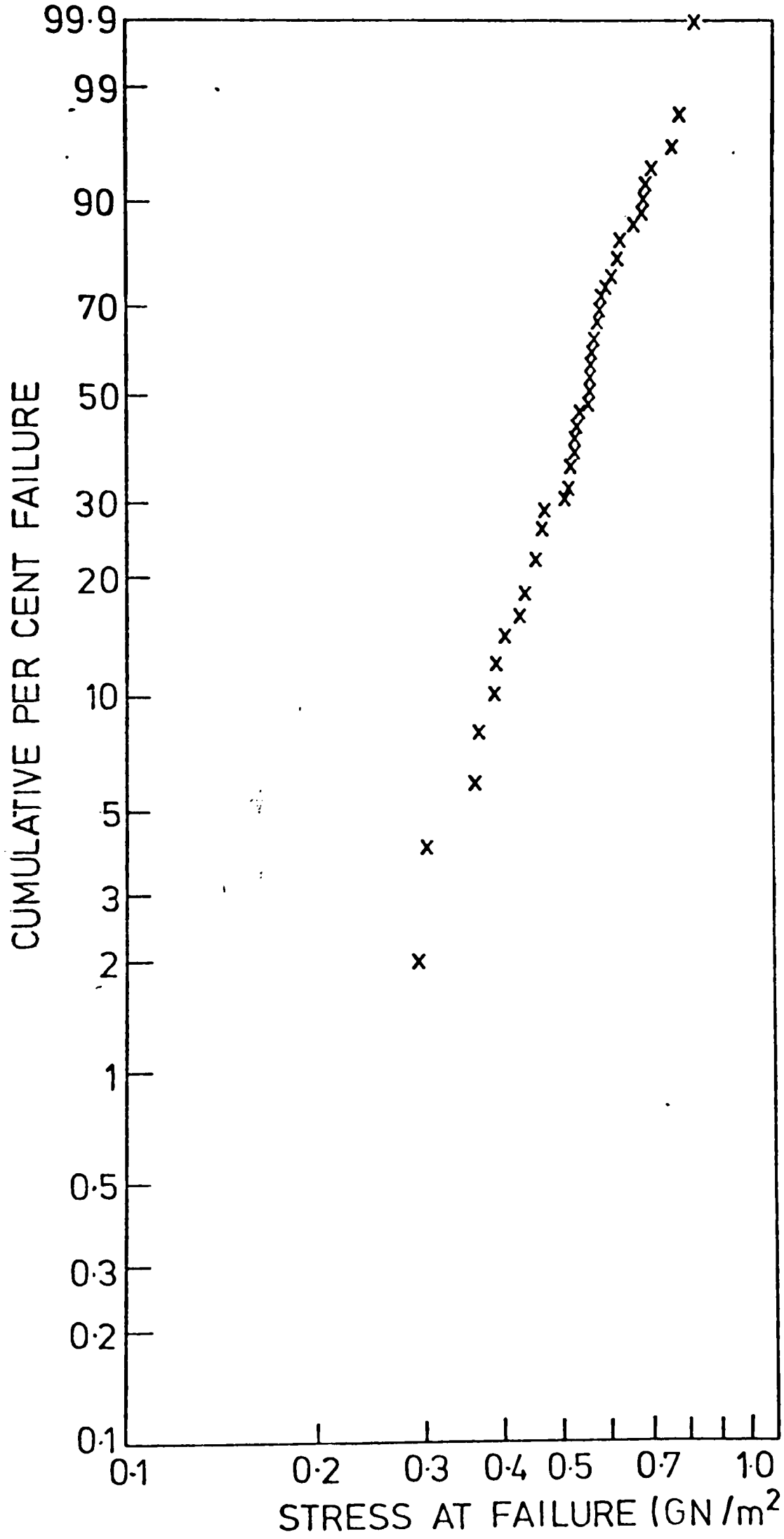


FIGURE 6-7

WEIBULL PLOT OF FIBRE STRENGTH RESULTS (Exp't. No. FMIII)

corrosion. Qualitative 'bend' tests have shown that freshly drawn fibre can be bent into a much tighter radius before fracture than old fibre which has been wound on a drum and exposed to the atmosphere, indicating that stress corrosion is at least partly responsible for the weakness. Unfortunately, due to the distance between the drawing apparatus and the tensile testing machine, no strength data is available for our freshly drawn fibre. The results are at least comparable with bare fibre of the same age produced conventionally.

There are a number of reasons why fibre produced from this apparatus may have different mechanical characteristics to that drawn with conventional machines, namely:

- degradation of the rod through the furnace entry seal. There is evidence that surface rod flaws may be reproduced on the fibre after the drawing process[27], and certainly flame polished preforms or rods are generally known to produce stronger fibre. Any damage caused by the rod entry seal will be removed when the bellows unit is used, and flame polished rod may then also be employed to effect.
- The overall effect of the vacuum/argon atmosphere is not known fully. Qualitative results indicate no difference between fibre drawn at 3×10^{-6} Torr and 2×10^{-3} Torr (Argon), the condition under which metal coated fibre is produced.
- The fact that our fibre must be re-wound to enable it to be removed from the vacuum system could be a source of fibre damage not normally encountered with conventional apparatus.
- A tungsten mesh furnace has not been used before for fibre drawing, and quite what effect this may have is not yet known. Certainly, inspection of the rod just above the draw-down region shows a very thin metal film to have been deposited.
- Drawing fibre in a vacuum tends to accentuate voids within a rod or preform, although it is observed that good quality silica rods are void free.

This section has served to outline the preliminary observations into the qualities of fibre pulled in a vacuum. This thesis is primarily about the techniques used to produce the fibre, and more quantitative results will be produced later.

6.3.4 Characteristics of Metal Coated Silica Fibre

The first experiments to be conducted were to ensure that the apparatus performed as designed; that is to prove that the draw-down process was compatible with the magnetron sputtering operation. Trial experiments were conducted with a nickel target, the only one then available, with a drawing speed of 3m/min.

The first attempt started successfully, with a sputtering current of 2A. After two or three minutes one of the furnace safety circuits tripped, but some three to four metres of fibre were successfully coated. The fibre produced had a diameter of 270μm - somewhat thick - and the coating had a resistance of approximately 100Ω/mm, corresponding to a calculated thickness of 10Å, assuming the resistivity of nickel to be that of the bulk material (6.2×10^{-8} Ωm). This figure is difficult to believe, as the coating could be clearly seen, and it was suspected that pinholes or non-continuity of the sputtered film were the cause of the result. The metal surface had a mirror-like finish, and the fibre looked like nickel wire. However, under a low power microscope, a few pinholes could indeed be seen, but in general the coating was impressive in its smoothness. No mechanical tests were conducted on this preliminary run as too little fibre was produced to lead to meaningful results. In fact, most of the fibre produced to date has been made from rod of dubious quality, and only qualitative strength measurements have been made until very recently.

Further drawing operations under the same conditions were carried out and some 150 metres of coated fibre were produced. This fibre had a nominal diameter of 150μm and could be bent to a radius

of 2.5mm before rupture, corresponding to a strain of about 1½%. Preliminary tensile tests suggested this figure to be fairly accurate.

During the latter part of a drawing operation, the furnace temperature was reduced to below a power level setting of 7.1 (primarily in an attempt to reduce fibre diameter fluctuations) but the fibre produced was very brittle, and broke at a touch.

After a week, the fibre was re-examined and was found to have mechanically degraded, indicating a non-continuous film as predicted by the resistance measurements. Also, by cleaning a section of the fibre and illuminating a cleaved end with a Helium-Neon laser, it was apparent that the coating was very thin in places, and tended to form in lands - light could be seen emerging radially from the fibre. This type of land formation is a common feature of thin evaporated nickel films on glass/silica, and is due to migration of atoms on the substrate, it being energetically perferable to form aggregates. Considerable material may have to be deposited before electrical continuity is established[38].

In order to investigate the difference between an adhering and non-adhering film, molybdenum and cupronickel targets were prepared, and coated fibre produced with each target under essentially the same experimental conditions. Molybdenum was chosen because of its use in the semiconductor industry as a good bond with silicon. The results were as follows (drawing speed 3m/min, sputtering current 3A, fibre diameter 125μm):

a) Molybdenum Microscope inspection of the surface indicated a continuous mirror-like film (figure 6.8) and firing a Helium-Neon laser down the fibre showed no light leakage. The film thickness was measured, using the resistance technique, and found to be approximately 70Å. The scratch resistance of the coated fibre (measured when trying to cleave the fibre by rubbing with the edge of a microscope slide) was markedly improved with respect to bare fibre, but

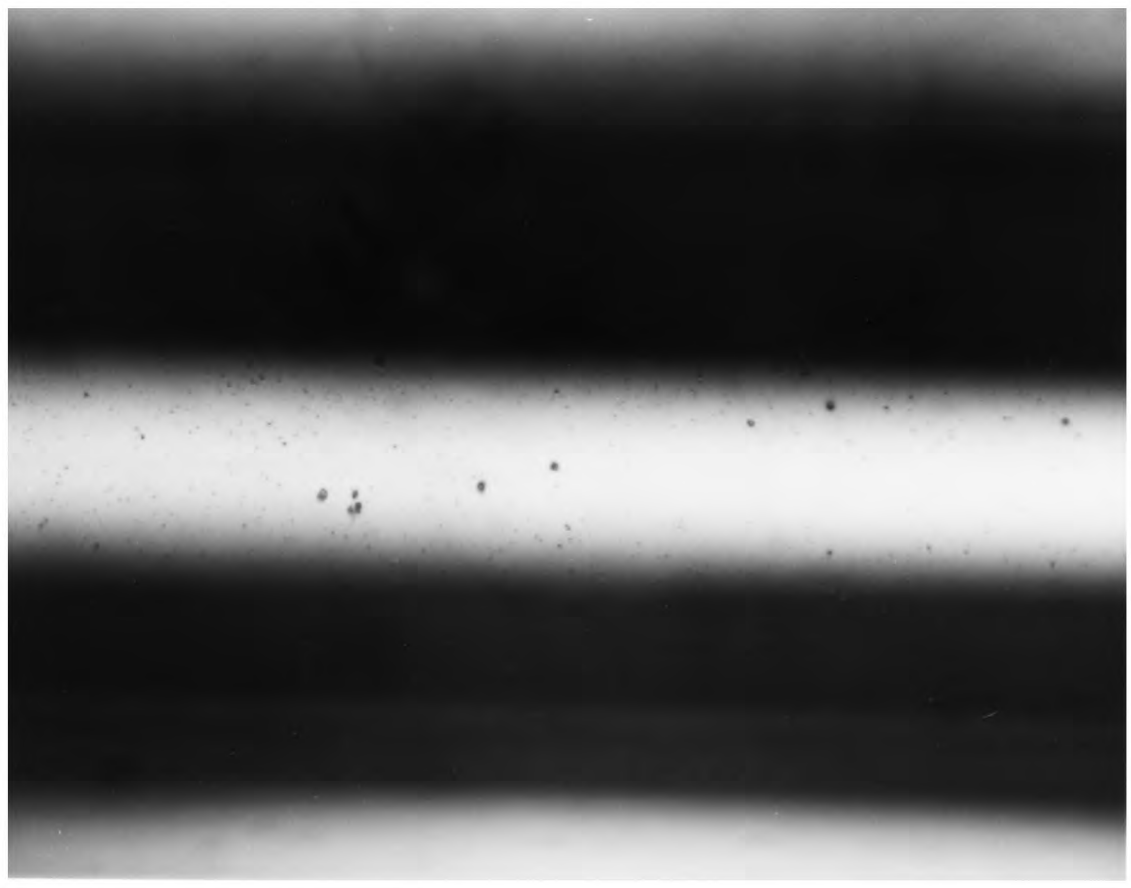


Figure 6.8 Micrograph of Moly -coated Fibre

the brittleness had increased.

b) Cupronickel (Ni67/Cu33) Again a continuous film of about 70Å was produced, but the fibre was still more brittle than uncoated fibre produced during the same run, the degradation being less marked than that produced by molybdenum. The scratch resistance was improved.

Some mechanism inherent in the sputtering system suggested itself as the cause of fibre weakening and four mechanisms were initally considered;

(i) the fibre temperature whilst being sputtered is still high enough to make the surface reactive,

(ii) the sputtered metal atoms have sufficient energy to degrade the fibre surface,

(iii) electron bombardment,

(iv) the metal atoms reacting chemically with the silica surface.

To investigate (ii) and (iii) an experiment was conducted with the cupronickel target at different drawing speeds (whilst maintaining a constant fibre diameter) and different sputtering currents, comparing the fibre thus produced with uncoated fibre produced at the latter stage of the experiment. No qualitative difference in brittleness could be detected between the fibres under the different conditions, which suggested that (ii) is not a dominant mechanism, but as the sputtering unit is essentially a constant voltage device, cause (iii) could not be discounted.

Electron bombardment could be caused by untrapped electrons between the magnetic flux paths being accelerated directly towards the single anode[40]; electrons diametrically opposite the anode could thus be impinging upon the fibre with some considerable energy, the anode being at 400-500V with respect to the target. In the trial sputtering devices, multiple anodes were used, the fibre then being out of a direct path between target and closest anode, and little, if any, fibre damage was detected (albeit with lower current density,

but with approximately the same anode potential) even with protracted sputtering times approaching one hour. To eliminate such effects with the on-line device, a multiple anode system (three equispaced anodes) has now been employed, with some effect.

With regard to cause (iv) it is to be noted that less fibre damage was caused with cupronickel than molybdenum as a target, indicating that a metal known better for its non-adherence to silica is perhaps in some respects a better coating material.

Finally, to investigate (i) sputtering with molybdenum was carried out with a stationary, cooled fibre within the coating column. This was rather inconclusive because after sputtering for ten minutes at 3A the fibre ruptured, and on inspection the ends of the fibre appeared charred. It cannot be ascertained, however, whether or not the fibre was on the axis of the coating column; if not, and the fibre was slack, a portion would have been in one of the plasma rings and would consequently have been heated. Rupture would then occur as the fibre melted, and the hot fibre ends would touch the hot target and charring may have occurred.

If cause (i) has any effect on fibre damage, little or no control can be exercised over it. In conventional fibre drawing machines, it is known that in an atmosphere, the fibre cools very quickly, and can be handled only a few inches below the draw-down region, but in vacuo we have no means of knowing the fibre temperature through the sputtering column, save that it is cool enough to be wound on the take-up drum. The only means of fibre cooling in vacuo is by radiation, and the only means by which the cooling period can be increased is by reducing the drawing speed further, with the inherent difficulties of diameter control.

With the previous points in mind, the recent drawing results seem quite promising. The 'three anode' system was used with a copper target, copper being relatively inert, not being renowned

for a good bond with silica. Using good quality silica rod producing again 125μm diameter fibre with a drawing speed of 3m/min, sputtering was conducted at 1.5A when the sputtering column had stabilised. 70% of the coated fibre achieved a strength of $3.6GN/m^2$, with a maximum fibre strength of $4.2GN/m^2$. The strength was measured by bending the fibre in a semicircular arc, and observing the diameter at break (sample size 50). In a similar way, uncoated fibre produced during the same experiment, although having a similar maximum strength, has a much greater spread of strengths, 70% of the fibre breaking below $2.4GN/m^2$. Fibre coated whilst the sputtering column was stabilising showed a similar spread of breaking stresses to the uncoated fibre. It must be emphasised that these results are purely comparative, one against the other, but the suggestion is that metal coating is now doing something positive towards fibre strength, certainly within the limitations of the apparatus.

CHAPTER SEVEN

CONCLUSIONS AND DIRECTION OF FURTHER WORK

This thesis is mainly concerned with the methods and techniques used for producing metal coated optical fibres employing magnetron sputtering - a process still in its infancy. Much work has still to be done to characterise the process and assess the merits of the fibres thus produced.

The feasibility of drawing optical fibres hundreds of metres long *in vacuo* has been shown, and the limitations of the process have been realised. The experimental apparatus has not produced fibres with as consistent a diameter as commercial machines - mainly due to the author's inexperience at the outset of the project - but for the purposes of research this is not a serious disadvantage. Commercial fibre has typically a diameter variation of better than ±1% over lengths greater than one kilometre whereas the apparatus has to date produced no better than ±6%. This, as mentioned before, is mainly due to the low drawing speed which is necessary causing instabilities at the draw-down region, and also to the lack of closed-loop diameter control commonly used with conventional systems. The fluctuation encountered is tolerable, as the main purpose of the work is an investigation into the mechanical properties of fibres, and merely necessitates fibre diameter measurements when determining stresses. In other respects, the apparatus shows similar characteristics to conventional machines, producing more brittle fibre with decreasing furnace tempreature (but decreased diameter fluctuations), and improving diameter control with increasing drawing speed.

The apparatus is less convenient to use than conventional machines, the major difference being lack of access to the underside

of the furnace. This means that fibre initiation is a separate process to fibre drawing, thereby increasing the time taken to produce a batch of fibre - this may be a major drawback to commercial use of the process, but a means of automatically attaching the 'blob' to the winding drum would overcome the problem. The other features of the process which make it unattractive commercially are the pump-down time, and the necessity to off-wind the fibre from the permanently mounted take-up drum. This latter feature could be overcome by making the drum removable through a port.

Vacuum drawing may offer commercial advantages which existing machines lack, especially for production of low water vapour content fibres. By using careful procedures O-H absorption bands can be virtually eliminated from attenuation curves; this entails the use of time consuming and expensive clean room techniques when drawing. A vacuum environment could effectively relax this necessity, especially if primary (metal?) coating were conducted on-line before the fibre reached the atmosphere.

The use of a tungsten-mesh furnace for fibre production has been demonstrated (which has, to the author's knowledge, never hitherto been attempted). Whether or not this is advantageous has yet to be ascertained. There is some evidence of metal evaporation onto the rod or preform immediately above the draw-down region, but the metal coating tends to mask this effect on the fibre itself. Should it be a disadvantage a different furnace could easily be substituted, an R.F. induction furnace as used elsewhere[41] appearing an attractive candidate immediately compatible with the existing apparatus. Another source of contamination, silicone grease used with the rod entry seal has been eliminated with the bellows unit, which also enables fire polished rods to be used sensibly leading hopefully, to more consistent strength measurements.

The metal coating experiments have yielded interesting results.

Although coating thicknesses have not been as high as was calculated it appears from the latest measurements that fibre protection can be achieved. The degradation effect which some metals cause can be controlled by selecting the metal used, and the degradation mechanism itself has been identified as a reaction between metal and silica, and not due to the sputtering process itself. The nature of the reaction, physical or chemical, has not been ascertained. For commercial use, the coating process would have to be speeded up to make it economical. This could be achieved by increasing the length of the coating chamber and current capability of the power supply, thereby allowing a higher drawing speed and enabling a greater coating thickness to be attained. Once a protective layer has been nucleated, the coating could be thickened (by electroplating, or perhaps by freeze coating) or a plastic coating could subsequently be applied if desired.

As suggested at the beginning of this chapter, the apparatus in its present form allows a vast amount of work to be carried out, both characterising precisely the nature of fibre drawing, and improving the quality and extent of protection of the coating. In particular, the following directions are of immediate interest.

1) The temperature of the fibre whilst being coated is at present unknown. If too high, the metal on cooling may be taken above its failure stress and cracking may occur. It is difficult to envisage how to measure precisely the fibre temperature within the coating column but coating may be conducted at lower temperatures by moving the coating column further away from the furnace, thus allowing more time for the fibre to cool. Alternatively, the drawing speed could be further reduced, which would also allow a thicker coating to be applied should this be desired.

2) It has been suggested that flaws in conventional fibre may be due to silica dust impinging onto the fibre surface within the furnace region at the draw-down neck. If they become attached to the

fibre they may be subsequently broken off (perhaps during the primary coating phase) and cause minute surface stress raising voids. The contactless metal coating process may trap such 'spikes' and enable them to be observed with an electron microscope. In a similar manner it would be experimentally interesting to deliberately produce brittle fibre by drawing at a reduced temperature, metal coat, and again investigate the fibre surface for flaws. The idea is quite speculative as it is not known whether the metal film will be evenly spread or will tend to agglomerate in cracks. (Uncoated fibre is difficult to examine successfully with an S.E.M. because being an insulator it tends to charge up under the electron beam and an intense spot is seen on the display screen with very little detail.)

Microscopic optical observation of the silica surface after removal of the metal by chemical etching will show whether or not the coating procedure causes major surface flaws; if the surface is not mirror-like it would suggest that a chemical reaction takes place. Care will be needed with the choice of etchant to ensure that the silica itself is not attacked.

3) During preliminary trials of the equipment, low cost plain silica rods have generally been used to avoid possible wastage of expensive preforms. Arrangements have been made to obtain a fibre preform, half of which will be drawn on this apparatus, and half on a production machine, to produce fibre with the same overall diameter. Optical and mechanical tests are to be conducted to compare the fibre attenuation, bandwidth and strength, in order to see whether vacuum drawing introduces unforeseen contamination (due, perhaps, to absorption of tungsten from the element or molybdenum from the radiation shields) and consequent fibre degradation. If any serious differences exist between the fibres, they will be investigated. Part of the fibre drawn in the vacuum equipment will be left uncoated, and again optical comparisons will be made.

4) The range of metals to be used for coating are to be expanded, and quantitative comparisons of strength conducted to seek an optimum coating. Of importance in these experiments will be time-to-failure strength measurements with differing static loadings. Stress corrosion effects will be identified if the fibre ages due to loading; an hermetic seal will effectively eliminate such static fatigue effects by not allowing water to attack and increase the size of any flaws.

5) A technique which is being used increasingly commonly in the glass industry to increase the strength of formed glassware (e.g. milk bottles) is to chemically diffuse molecules of larger size than the glass into the surface. This effectively maintains the glass surface in a compressive state of stress, and prevents flaws growing. (Milk bottles made of such 'titanised' glass may be dropped onto hard surfaces, and instead of shattering, simply bounce.) This technique may be achieved with optical fibres, by depositing the relevant material on to the fibre surface on-line by magnetron sputtering, and the subsequent chemical heat treatment would diffuse the material into the fibre.

The basis of this process is attractive but somewhat speculative and is at present in the 'idea' stage, but may prove of use in the future.

6) Of a more mundane nature is the necessity to achieve an accurate means to measure the thickness of the films produced by the coating technique. The resistive method so far adopted is not regarded as precise for two reasons. Firstly, the resistivity of the sputtered film may be different to that of the bulk material, and secondly it was noticed that with a nickel coating the film was not strictly continuous, causing errors in measurement.

CHAPTER EIGHT

AN APPLICATION OF METAL COATED OPTICAL FIBRE A MECHANICAL OPTICAL FIBRE SWITCH

8.1 INTRODUCTION

In future optical fibre systems for communication and computing, a need for connecting and disconnecting signal paths at speeds measured in milliseconds rather than nanoseconds may arise. For the ultrafast switches, or modulators, technologies have been developed, many based on integrated optics, which use a variety of physical phenomena such as the Kerr effect, the Pöckels effect, or Faraday rotation in magneto-optically active transparent materials. None of these methods can be used directly with fibres, at least with fibres that will carry information over distances of practical interest; moreover, one has to employ a variety of transition devices to couple the fibres to the switches and back again.

For low switching speeds one can make use of the fact that fibres have very small cross-sections, the core diameter being less than 100μm in the multimode case. One can therefore accomplish switching by a relatively small motion between the ends of the two fibres one wishes to connect or disconnect. It has been observed[42] that a lateral displacement by one core diameter, the ends being a few micrometres apart, reduces the power transfer to a few percent of the maximum when the fibres are exactly in line. An additional displacement of an equal amount can reduce the power transfer to an amount so small as to be negligible. It is thus possible to construct a switch out of fibres in which the maximum power transfer is obtained when the fibre ends are aligned (or coaxial) and in which (approximately) zero power transfer is obtained when their ends are displaced with respect to each other by several core diameters.

To suffer minimum loss of signal in the 'connect' position, it is essential to have as good an alignment of the two fibres as possible. This can be accomplished by placing the fibres inside a square cross-section tube, as has been done successfully for the purpose of splicing fibres[43]. Provided that the two fibres have the same outside diameter and the cores are in the centre of the fibres, when they are pressed into the same corner of the square tube they will be in line, and, if an index matching liquid is used, it has been found that the power transfer loss can be as low as 0.05dB, and typically is around 0.07dB.

This way of aligning fibres can be used in constructing a mechanically operated fibre switch[44,45] shown in figure 8.1. Two fibres of identical cross-sections (circular core and cladding), labelled A and B, are pressed into opposite corners of the square tube, their ends being in one plane. A third fibre, labelled C, is introduced at the other end of the square tube and placed so that its ends is a few micrometres away from the ends of fibres A and B. When C is moved into the opposite corner, connection will be established between B and C, and A is now disconnected.

Practical fibre switches have been made with fibres of accurately uniform outside diameter with a concentric core, and with a square glass tube of reasonably uniform cross-section for accurate positioning of the fibres. The motion is achieved by magnetic forces acting on the fibre, fibre C being ferromagnetically coated. The magnetic field is generated by electromagnets as in the conventional kind of telephone switching relay.

8.2 CONSTRUCTION OF SWITCHES

8.2.1 Fabrication of Clean Fibre Ends

To enable efficient transfer of power between two distinct optical

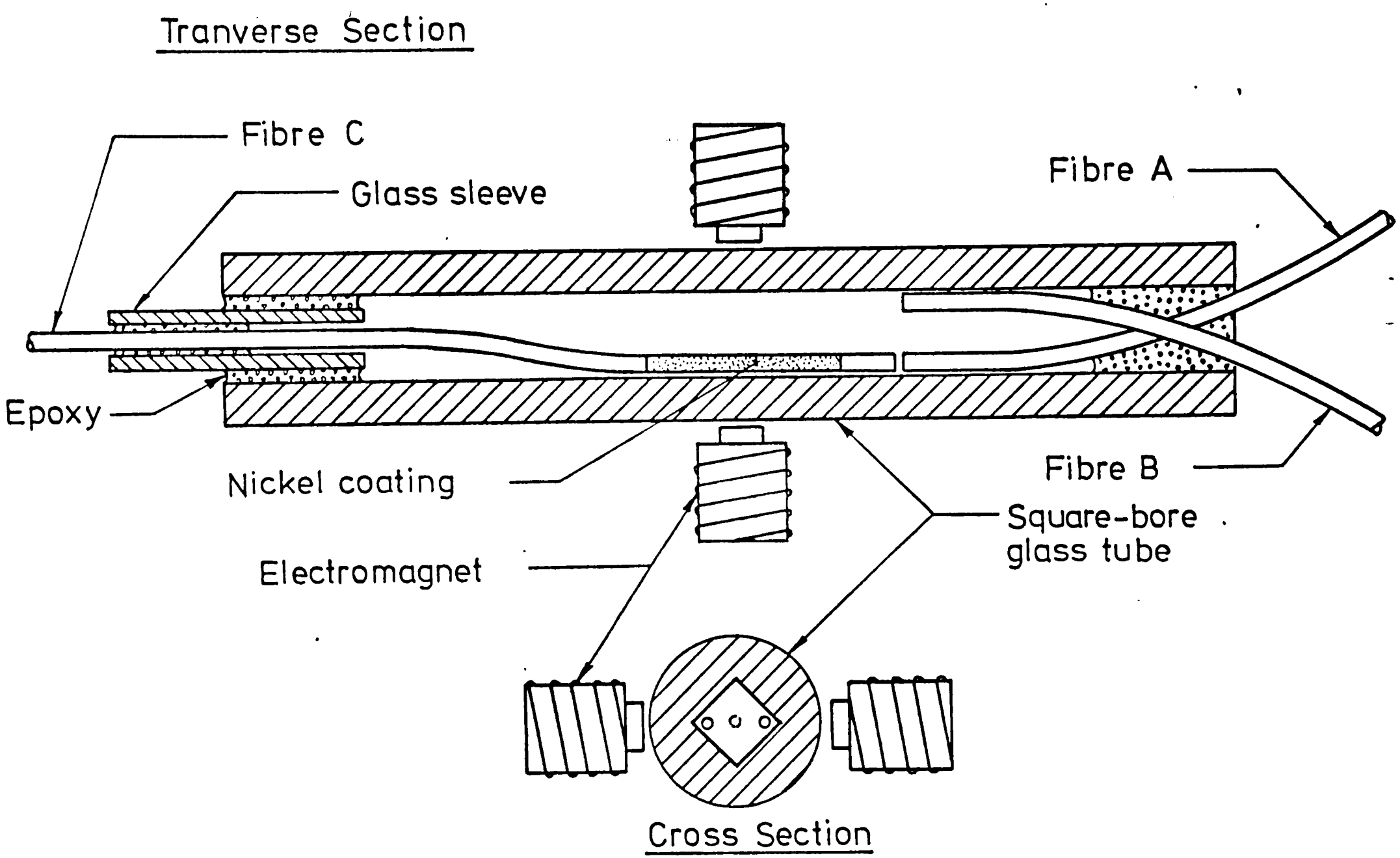


FIGURE 8-1

CROSS SECTION OF A MECHANICAL OPTICAL FIBRE SWITCH

fibres, it is necessary to manufacture clean, square end faces, otherwise energy will not be transferred effectively from one fibre core to the other. A simple method[46] for cleaving fibres to produce such 'good' fibre ends has been adopted, which involves scoring the fibres whilst in tension over a low friction curvedsurface. A fibre cleaving machine using this principle has been constructed and consistent clean, mirror-like fibre ends are achieved of a quality consistent with that needed for a splice or switch.

8.2.2 Ferromagnetic Coating of Optical Fibre

Nickel was chosen for the ferromagnetic coating as it exhibits good corrosion resistance. It was initially envisaged that a sufficient thickness of nickel could be achieved by sputtering alone. Indeed, 2-3μm nickel films so deposited with a static magnetron sputtering head (the first trial device discussed in Chapter 4, Section 4.3) did exhibit ferromagnetic properties, but only weakly, and further coating was deemed necessary. Switches with such thin coatings have been constructed but have operated erratically and need a laborious amount of precise alignment. The easiest solution was to increase the thickness of the deposited film, and thereby increase the 'pull' from a given electromagnet. Two methods to increase the film thickness were available; electroplating and electro-less plating. The latter produced only a very weak magnetic coating and was thus dismissed, but a bright nickel plating solution achieved consistent, thick, strongly magnetic films.

The technique used to produce such films is as follows. Firstly a conducting film is nucleated on a clean fibre surface (having first removed any protective coating) by using the cylindrical magnetron sputtering device. This produces a 2μm film of molybdenum, chosen for its high sputtering rate, and, after investigation, its good adherence to silica. The coated part of the fibre is now immersed

in an electroplating solution consisting of 300gm Nickel Sulphate, 30gm Sodium Chloride and 40gm Boric Acid, dissolved in 1 litre distilled water. A cathode connection to the fibre is made by attaching a copper wire with Silver Dag. A nickel anode is placed in the solution and current passed to maintain 20A/ft^2 of surface area to be coated. In practice this means a current of 8-12mA for a single fibre 50mm immersed length. The coating bath is maintained at 40-50^{o}C whilst plating. Current is supplied for 50-60 minutes to obtain a uniform coating approximately 20μm thick. A coated fibre produced in this manner can be made to switch without centering accurately within the tube.

Such a thick coating does not allow the fibres to align axially within the tube and 10mm are stripped by immersing the fibre end in a solution of ferric chloride for 15 minutes, which removes both nickel and molybdenum to leave a mirror-like surface finish. The tilt angle caused by the remaining coating is less than 0.12^o.

8.2.3 Switch Assembly

For switch assembly, the square-bore glass tube (internal cross-section 500 x 500 μm, length 25mm), and all three fibres must be held rigidly to enable the fibres to be sealed into the tube, and, prior to sealing, all threefibres must be manipulated accurately into their respective positions.

Referring to figure 8.2, the glass tube is cleaned thoroughly and then clamped on to a micro-manipulator enabling it to be moved along its axis. The square bore is positioned such that its diagonals are in horizontal and vertical planes. Fibres A and B are inserted into the tube and then clamped into similar manipulators positioned adjacent to one end of the tube, and side by side. When inserted into the tube, the fibres are pushed into opposite corners, and the micro-manipulators allow each to move axially to facilitate

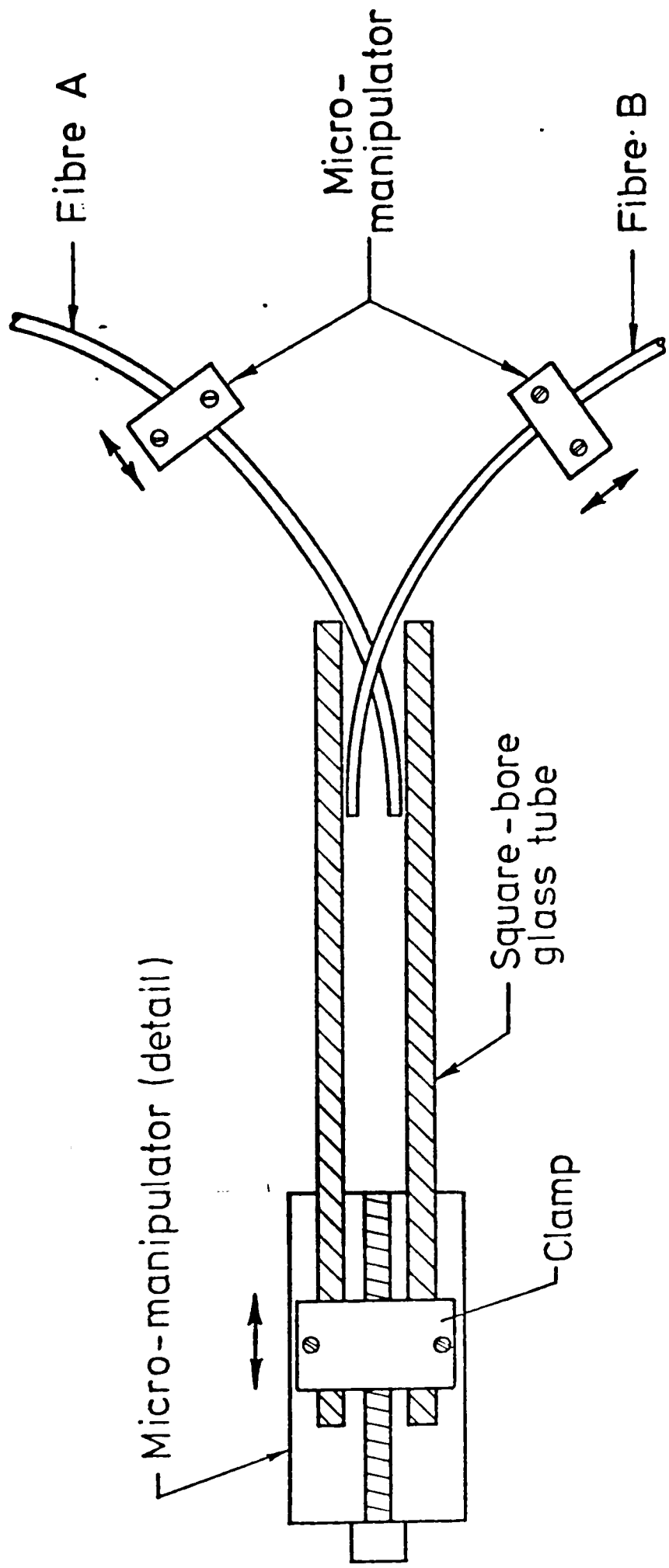


FIGURE 8-2
INSERTION OF UNCOATED FIBRES INTO TUBE

alignment. The fibre ends are inserted into the tube to a depth of approximately 5-6mm, and with the aid of a low power binocular microscope, are aligned such that their end faces are in the same plane as accurately as possible. The tube is then moved 2-3mm away from the fibres, a small amount of rapid curing epoxy resin is applied to the fibres at the entrance to the tube, and the tube moved back towards the fibres. The epoxy is thus worked until a good seal is obtained. Before the epoxy sets final adjustment is made to the fibres to ensure accurate alignment.

A slightly different technique was evolved for the mounting of the coated fibre C within the tube, as its position on the axis of the tube must be maintained to enable reliable switching. It was found that by using a short glass sleeve which fits snugly around the fibre and within the tube, the fibre movement is restricted to a very small area at the centre of the tube and makes accurate assembly much easier (figure 8.3). The fibre is otherwise epoxied into position in a similar manner to the uncoated fibres, but using an axial micromanipulator for positioning, as illustrated in the figure. To ensure consistent switching, the end of fibre C not within the tube is illuminated with the He-Ne laser, the fibre positioned whilst the electromagnets are actuated alternately, and the light output from fibres A and B monitored. When consistent switching is achieved, fibre C is epoxied in position.

8.2.4 Selection of Electromagnets

Various electromagnet/tube geometries were suggested and tried, but it was decided to opt for a simple design with two similar electromagnets on opposite sides of the tube, with their poles adjacent to the appropriate corners of the tube bore as illustrated in figures 8.1 and 8.4. This design was favoured for its simplicity and convenience over alternatives including the fibre as part of the magnetic circuit.

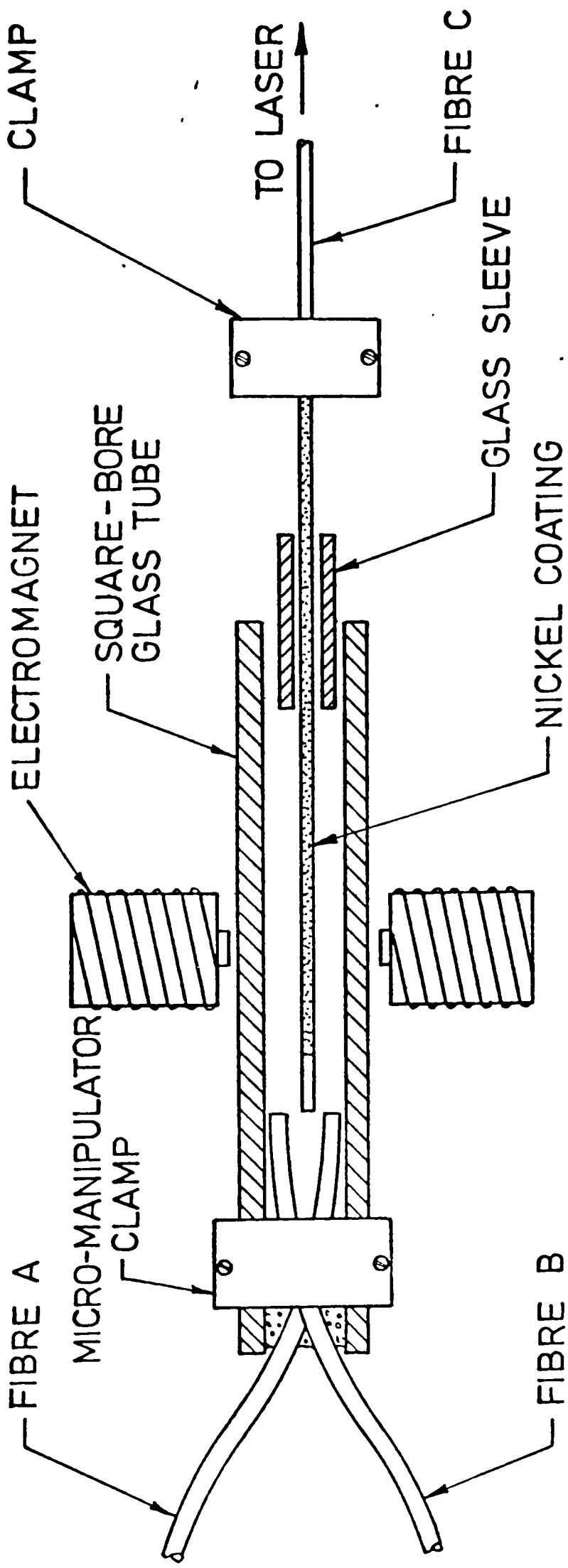


FIGURE 8-3
INSERTION OF COATED FIBRE INTO TUBE

In practice, the reluctance of even a short length of coated fibre negates attempts to include it in any closed magnetic path due to the tortuous nature of the path, and the simple design utilised switches easily and effectively.

The electromagnets used were selected by trial and error, it being difficult, if not impossible, to calculate exactly what flux would be needed. Initially the coils were wound in the laboratory, but it was found that electromagnets stripped from miniature relays worked better, and were used for convenience. Each electromagnet consumes 12mW of power. By experiment it was found that the fibre needs a force of approximately 23mgf (= 22.6 x 10^{-4}N) to deflect it to a corner of the tube.

8.2.5 Switch Format

The prototype switches so far produced have been mounted on 0.1in matrix Veroboard, 50 x 50 mm square, with solder pin connections to the electromagnets. The electromagnets have been screwed to the board, and the tube epoxied to a stand-off post between the electromagnets to ensure its position between the two polepieces. Fibre pigtails approximately 0.5m long have been left with each of the three fibres. This format is convenient for a prototype, but is not envisaged as a commercial package. Figure 8.4 shows a photograph of a completed switch.

8.3 PERFORMANCE

The prototype devices so far constructed have not been optimised for switching speed, but have been made to convenient dimensions with materials generally available within the laboratory to demonstrate the operating principle.

The upper limit to switching speed of the device is determined

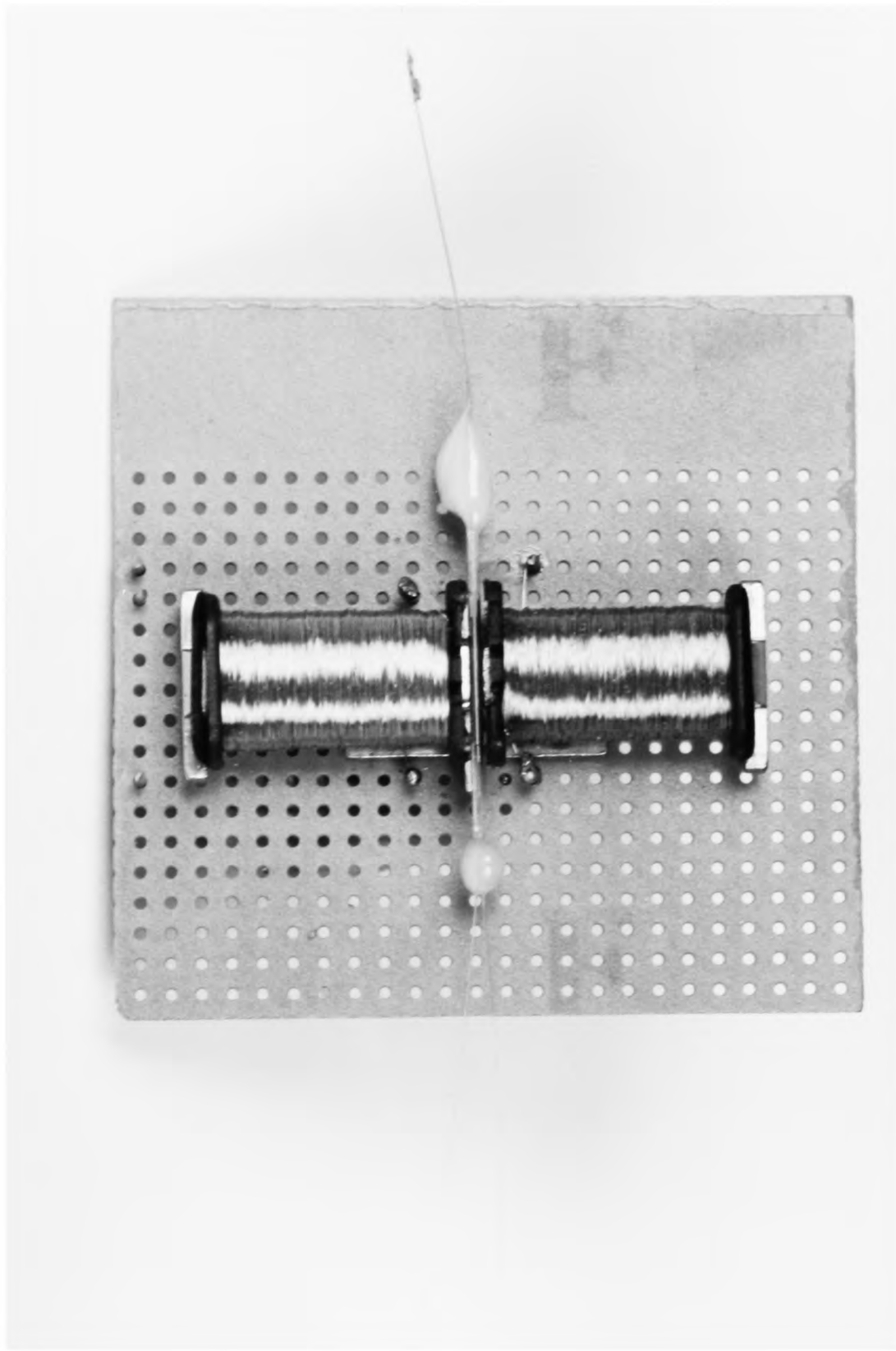


Figure 8.4 View of Prototype Switch

by the physical characteristics of the coated fibre, assuming the fibre to be a cantilever. The resonant frequency of such a system can be shown to be

$$f_{res} = \frac{1}{2\pi} \frac{420\ EI}{33\ M\ell^3} \quad Hz, \qquad (8.3.1)$$

by using simple structural analysis. For the case of a 125μm diameter silica fibre coated with 20μm of nickel, with a cantilever length of 20mm, the resonant frequency is approximately 560Hz, indicating a switching time of about 0.9mS. The devices so far constructed have not been as fast as this, with a switching time from one 'on' position to the other of about 10mS. This is due to inaccuracies in centering the fibre within the tube bore, with consequent rubbing of the fibre against the tube wall, and imperfect switching techniques when energising one coil and de-energising the other.

The insertion loss of the switches has been rather greater than the losses reported for a splice made with a similar technique. For recent completed switches, the insertion loss has been between 2 and 5dB, with channel balance between 1 and 2.5dB. There is a negligible amount of crosstalk between input and unused fibre being less than 30dB and beyond the resolution of the measuring apparatus. Loss measurements are rather rudimentary, precise apparatus being unavailable. The insertion loss is due to a number of factors:

(i) No index matching fluid is used, thus causing unavoidable interface reflection.

(ii) The fibre cleaving machine is not perfect, the cleave end generally being a degree or so from right angles to the fibre axis.

(iii) A small gap between entrance and exit fibres has been found necessary to compensate for the differences in the temperature coefficients of expansion of the components used in the switch. Early switches with a minimal gap tended to jam after about 30 minutes operation, due to the heat generated by the electromagnets.

Fatigue life of the switch has yet to be ascertained, but several switches have achieved 100,000 operations without failure.

Further investigation of the transmission properties of the prototype switches has not been attempted, as it is beyond the scope of the equipment in the laboratory. The technique has been demonstrated to work, quite simply and effectively.

8.4 CONCLUSIONS

Some forty switches described have now been completed and are undergoing evaluation in a separate laboratory, the intention being to use them in a switching matrix to couple a number of sources to different receivers. The insertion loss of the prototype switches may be a limitation to the number of channels which may be coupled and it would be desirable to be able to switch between more than two fibres. By utilising the two remaining corners of the tube for further exit fibres, the number of switches needed in such a matrix would be reduced, but this is at present beyond the technology of the laboratory.

The device is a relatively cheap method of switching between fibres, but needs to be developed further if it is to be used commercially. Each device has taken about 4-5 hours of construction time, and material costs are about £12 per unit, inclusive of fibre costs for 0.5m pigtails. This compares quite favourably with the cost of integrated-optic devices which are, however, somewhat more rapid in operation.

The use of the 'corner' technique has been demonstrated successfully for switching purposes; if to be used commercially, further work is necessary to make the devices more consistent in quality. The development of production techniques is beyond the sphere of work done within the laboratory. The merits of this type of switch are

simplicity of construction, using few component parts, and a minimum amount of precision alignment and precision parts. Many other mechanical or pseudo-mechanical switches have been described (e.g. references (47) - (52)), which are generally more complicated and expensive in design, and have comparable performance.

APPENDIX

DERIVATION OF LAMÉ SOLUTION FOR CYLINDRICAL TUBE UNDER INTERNAL AND EXTERNAL PRESSURE

By considering the field equations of linearized isotropic isothermal elasticity (equations of motion, Hooke's Law equations, and geometrical equations), the Navier displacement equation is obtained:

$$(\lambda+\mu)\nabla(\nabla.\underline{u}) + \mu\nabla^2\underline{u} + \rho\underline{b} = \rho\frac{\partial^2\underline{u}}{\partial t^2} \qquad \text{(I)}$$

where λ and μ are the Lamé elastic constants, $\underline{u}$ is the relative displacement vector, ρ is the material density and $\underline{b}$ is the body force per unit mass.

In cylindrical polar co-ordinates, equation (I) becomes

$$\left.\begin{aligned}
(\lambda+2G)\frac{\partial e}{\partial r} - \frac{2G}{r}\frac{\partial \omega_z}{\partial \theta} + 2G\frac{\partial \omega_\theta}{\partial z} + \rho b_r &= \rho\frac{\partial^2 u_r}{\partial t_2} \\
(\lambda+2G)\frac{1}{r}\frac{\partial e}{\partial \theta} - 2G\frac{\partial \omega_r}{\partial z} + 2G\frac{\partial \omega_z}{\partial r} + \rho b_\theta &= \rho\frac{\partial^2 u_\theta}{\partial t^2} \\
(\lambda+2G)\frac{\partial e}{\partial z} - \frac{2G}{r}\frac{\partial}{\partial r}(r\omega_\theta) + 2G\frac{\partial \omega_r}{\partial \theta} + \rho b_z &= \rho\frac{\partial^2 u_z}{\partial t^2}
\end{aligned}\right\} \qquad \text{(II)}$$

where

$$e = \frac{1}{r}\frac{\partial}{\partial r}(ru_r) + \frac{1}{r}\frac{\partial u_\theta}{\partial \theta} + \frac{\partial u_z}{\partial z} \qquad \text{(III)}$$

and

$$\left.\begin{aligned}
\omega_r &= \frac{1}{2}\left(\frac{1}{r}\frac{\partial u_z}{\partial \theta} - \frac{\partial u_\theta}{\partial z}\right) \\
\omega_\theta &= \frac{1}{2}\left(\frac{\partial u_r}{\partial z} - \frac{\partial u_z}{\partial r}\right) \\
\omega_z &= \frac{1}{2}\left(\frac{1}{r}\frac{\partial}{\partial r}(ru_\theta) - \frac{1}{r}\frac{\partial u_r}{\partial \theta}\right)
\end{aligned}\right\} \qquad \text{(IV)}$$

Consider a tube long in the z-direction, loaded by an internal pressure p_i and an external pressure p_o, with negligible body forces, and assume plane deformation with radial symmetry, independent of z and θ in the plane region $a \leq r \leq b$. Equations (II) then become, with $u_\theta = u_z = 0$, $u_r = u$:

$$(\lambda+2G)\,\frac{\partial e}{\partial r} = 0 \qquad \text{(V)}$$

where now

$$e = \frac{1}{r}\,\frac{d}{dr}\,(ru) \qquad \text{(VI)}$$

whence the Navier equation is satisfied if

$$\frac{d}{dr}\left|\frac{1}{r}\,\frac{d}{dr}\,(ru)\right| = 0, \qquad \text{(VII)}$$

which, upon two integrations, becomes

$$u = Ar + \frac{B}{r} \qquad \text{(VIII)}$$

where A and B are arbitrary constants.

Now,

$$\left.\begin{aligned} \varepsilon_r &= \frac{\partial u_r}{\partial r} = A - \frac{B}{r^2} \\ \varepsilon_\theta &= \frac{u_r}{r} = A + \frac{B}{r^2} \\ \varepsilon_{r\theta} &= 0 \end{aligned}\right\} \qquad \text{(IX)}$$

whence Hooke's law gives

$$\begin{aligned} \sigma_r &= \lambda(\varepsilon_r + \varepsilon_\theta) + 2G\,\varepsilon_r \\ &= 2A\lambda + 2GA - \frac{2GB}{r^2} \\ &= A' + \frac{B'}{r^2} \end{aligned} \qquad \text{(X)}$$

$$\sigma_\theta = \lambda(\varepsilon_r + \varepsilon_\theta) + 2G\,\varepsilon_\theta$$

$$= 2A\lambda + 2GA + \frac{2GB}{r^2}$$

$$= A' - \frac{B'}{r^2} \qquad \text{(XI)}$$

$$\tau_{r\theta} = 2G\varepsilon_{r\theta}$$

$$= 0 \qquad \text{(XII)}$$

$$\sigma_z = \nu(\sigma_r + \sigma_\theta)$$

$$= 4A\gamma(\lambda+G)$$

$$= C' \qquad \text{(XIII)}$$

where G is the shear modulus, γ is Poisson's ratio, and A', B' and C' are new constants.

The preceding derivation can be found more fully in reference 35.

REFERENCES

1. Kao, C.K. and Hockham, G.A.: 'Dielectric-fibre surface waveguides for optical frequencies', Proc.IEE, 1966, 113, (7), pp.1151-1158.

2. Foord, S.G., Poole, L.J. and Ramsay, M.M.: 'Installation of fibre optic cables in post office ducts', IEE Colloquium on Optical Fibre Cable, May 1977.

3. Brace, D.J., Cameron, K.H., Malyon, D.J., Midwinter, J.E., Nelson, B.P. and Stern, J.R.: 'The Installation of 20km of optical fibre cable into operational ducts in the vicinity of the Post Office Research Centre, Martlesham Heath, Suffolk', IEE Colloquium on Optical Fibre Cable, May 1977.

4. B.S.T.J., 1978, 57, (6), Part 1 of 2, entire issue.

5. Gloge, D.: 'Weakly guiding fibres', App.Opt., 1971, 10, pp.2252-2258.

6. Unger, H.-G.: 'Planar optical waveguides and fibres', O.U.P., 1977.

7. Stern, J.R. and Dyott, R.B.: 'Off-axis launching into a fibre-optical waveguide', Electron.Lett., 1971, 7, (2), pp.52-53.

8. Day, C.R., Beales, K.J., Midwinter, J.E. and Newns, G.R.: 'The development of optical fibre using sodium borosilicate glasses and the double crucible technique', 1st European Conference on optical fibre communication, IEE, London, 1975, pp.33-35.

9. Black, P.W. and Irven, J.: 'The development of high silica optical fibre waveguides', proceedings of electro-optical system design conference, Brighton, 1974.

10. Kaye, G.W.C. and Laby, T.H.: 'Tables of Physical and Chemical Constants', Longman, 1975.

11. Griffith, A.A.: 'The phenomena of rupture and flaws in solids', Phil.Trans.Roy.Soc., London, 1920, 221A, pp.163-198.

12. Hilling, W.B.: 'Strength of bulk fused quartz', J.Appl.Phys., 1961, 32, p.741.

13. Morlay, J.G.: 'Strong fibres and fibre reinforced metals', Proc. Roy.Soc., 1964, A282, 43ff.

14. Morley et al., Phys. and Chemical Glasses, 1964, 5, 1.

15. Kelly, A. .: 'Strong Solids', Clarendon Press, 1973.

16. Pascoe, K.J.: 'An introduction to the properties of engineering materials', Van Nostrand, 1972.

17. Unger, H.-G., ibid, p.569-575.

18. Pinnow, D.A., Wysocki, J.A. and Robertson, G.D.: 'Hermetically sealed high strength fiber optical waveguides', I.O.O.C., 1977, B9.5.

19. Gloge, D.: 'Optical-fiber packaging and its influence on fiber straightness and loss', B.S.T.J., 1975, 54, No.2, pp.245-262.

20. Black, P.W. and Cook, A.: 'Properties of optical fibre in cabling', First European Conference on Optical Fibre Communication, IEE, 1975.

21. Isomura, A., Yamamoto, Y. and Yamanishi, T.: 'Plastic coating of optical glass fiber', First European Conference on Optical Fibre Communication, London 1975.

22. Arridge, R.G.C., Baker, A.A. and Cratchley, D.: 'Metal coated fibres and fibre reinforced metals', J.Sci.Instrum., 1964, 41, pp.259-261.

23. Standage, A.E. and Gani, M.S.: 'Reaction between vitreous silica and molten aluminium', J.Am.Cer.Soc., 1967, Vol.50, No.2, pp.101-105.

24. Arridge, R.G.C. and Heywood, D.: 'The freeze coating of filaments', Brit.J.Appl.Phys., 1967, 18, pp.447-457.

25. Waits, R.K.: 'Planar magnetron sputtering', J.Vac.Sci.Technol., 15, No.2, March/April 1978, pp.179-187.

26. Hoffman, V.: 'High rate magnetron sputtering for metallizing semiconductor devices', Solid State Technology, December 1976, pp.57-66.

27. Ramsay, M.M., private communication.

28. GÜnthershulze, A., Z.Phys., 38, 1926, p.575.

29. Penning, F.M. and Moubis, J.H.A., Proc.K.Ned.Akad.Wetenoch., 43, 1940, p.41.

30. Holland, L.: 'Vacuum Deposition of Thin Films', Chapman and Hall, 1960.

31. Vossen, J.L. and Kern, W. (Editors),: 'Thin Film Processes', Academic Press (USA), 1978.

32. Thornton, J.A.: 'Magnetron sputtering', J.Vac.Sci.Technol., 15, No.2, 1978, pp.171-177.

33. Waits, R.K.: 'Planar magnetron sputtering', J.Vac.Sci.Technol, 15, No.2, 1978, pp.179-187.

34. Kao, C.K., to be published.

35. Malvern, L.E.: 'Introduction to the mechanics of a continuous medium', Prentice Hall, 1969, p.532.

36. Muskhelishvili, N.I., 'Some basic problems of the mathematical theory of elasticity', Noordhoff, 1953, p.647.

37. Pinnow, D.A., Robertson, G.D. and Wysocki, J.A.: 'Reductions in static fatigue of silica fibres by hermetic jacketing', Appl. Phys.Lett., 34, (1), January 1979, pp.17-19.

38. Bond, W.L.: 'Notes on solution of problems in odd job vapour coating', J.Opt.Soc.Am., 44, No.6, 1954, pp.429-437.

39. Van Vorous, T.: 'Planar magnetron sputtering; a new industrial coating technique', Solid State Technology, December 1976, pp.62-66.

40. Reference 25, pp.183-184.

41. Checcacci, P.F., Sheggi, A.M. and Brenci, M.: 'R.F. Induction furnace for silica fibre drawing', El.Lett., 12, No.11, 1976.

42. Bisbee, D.L.: 'Measurements of loss due to offsets and end separations of optical fibres', Bell Syst.Tech.J., 50, 1971, p.3159.

43. Miller, C.M.: 'Losse tube splices for optical fibers, Bell Syst. Tech.J., 54, 1975, p.1215.

44. Hale, P.G. and Kompfner, R.: 'Mechanical optical-fibre switch', Electron.Lett., 1976, 12, p.388.

45. U.K.Prov.Pat. No.16796/76.

46. Gloge et al.: 'Optical fibre end preparation for low loss splices', Bell.Syst.Tech.J., 52, 1973, pp.1579-1588.

47. Ohmori,Y. and Ogiwara, H.: 'Optical fiber switch driven by PZT bimorph', Appl.Opt., 1978, 17, pp.3531-3532.

48. Nunoshita, M., Nomura, Y., Matsui, T. and Nakayama, T.: 'Optical switch for multimode optical-fiber systems', Opt.Lett., 1979, 4, pp.27-28.

49. Shimizu, M. and Moki, T.: 'Optical fiber switches and their applications', Conference on laser and electro-optical systems, digest of technical papers, 1978, pp.54-55.

50. Yamamoto, H. and Ogiwara, H.: 'Moving optical-fiber switch experiment', Appl.Opt., 1978, 17, pp.3675-3678.

51. Mito, I. and Matsushita, S.: 'Electrically driven rotating mirror type multichannel optical switch', Electronic Communication Society national conference, 1978, Paper 860, (in Japanese).

52. Tomlinson, W.J., Wagner, R.E., Strnad, A.R. and Dunn, F.A.:
'Multiposition optical fibre switch', Electron.Lett., 1979,
15, pp.192-194.